Structure and properties of norbornene-ethylene copolymers

Struktura i własności kopolimerów norbornenu i etylenu

Mariusz Błochowiak

Max Planck Institute for Polymer Research, Mainz, Germany

Topas Advanced Polymers, Frankfurt/M, Germany

Department of Molecular Physics, Faculty of Chemistry,
Technical University of Łódź, Poland

2006

„For what is a man profited,
if he shall gain the whole world,
and lose his own soul?
or what shall a man give
in exchange for his soul?”
Jesus Christ

to my parents

1. Introduction – Motivation

Cycloolefin copolymers (COCs) of ethylene (E) and norbornene (NB) (with the trade name Topas®) are based on linear and cyclic olefins, respectively (Fig. 1.1).

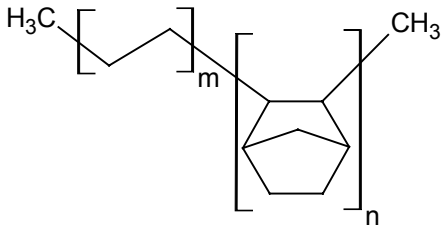

Fig. 1.1 Chemical structure of cycloolefin copolymer of ethylene and norbornene.

These materials have recently attracted both academic and industrial interest due to their useful combination of properties, including very high transparency, low density, very low water absorption, excellent water-vapor barrier capabilities and low birefringence. These properties, together with the unique mechanical characteristics, such as high rigidity, strength and hardness, and the excellent resistance to polar organic chemicals, make them well-suited to applications in the medical device, drug-delivery, optical, pharmaceutical and packaging sectors.[1] The properties of the COCs, especially their glass transition temperature, T_g, can be varied over a wide range; the bulky norbornene comonomer stiffens the chain, thus increasing the norbornene content results in copolymers with higher T_g.

The statistics and the stereoselectivity of the norbornene insertion can be controlled by selected use of catalysts.[2, 3] Studies carried out by Ruchatz et al.,[4] have shown that the microstructure of COCs is dominated by the metallocene, or more aptly by the metallocene symmetry or the ligand type; the metallocene substituents and symmetry dictate the tacticity[5, 6] and sequential distributions (blocky, random or alternating) of the ethylene-norbornene sequences in the copolymer backbone. Examples of the different metallocenic catalysts used in the copolymerization of the COCs are illustrated in Figure 1.2. Metallocene catalysts *rac*-Et(Ind)$_2$ZrCl$_2$ (A), *rac*-Me$_2$Si(Ind)$_2$ZrCl$_2$ (B), *rac*-Me$_2$Si(B-[e]-Ind)$_2$ZrCl$_2$ (C), *rac*-Me$_2$Si(2-Me-B-[e]-Ind)$_2$ZrCl$_2$ (D), *rac*-Me$_2$Si(2-Me-Ind)$_2$ZrCl$_2$ (E), all have C_2 symmetry whereas Me$_2$C-(Flu)(Cp)ZrCl$_2$ (F) is C_S symmetric. The monomers of Topas® are copolymerized with metallocene catalysts as well (the exact structure, however, is unknown) in a solution process and the amount of ethylene can be varied very easily by changing the ethylene pressure applied during the polymerization.[7]

The exact microstructure of cycloolefin copolymers was investigated with NMR. The microstructure was found to depend strongly on the catalyst systems employed during synthesis. Rische et al.[8] characterized the COC prepared according to the methods described in ref [9] within a wide compositional range (35.6 to 79 mol % of norbornene). This preparation method resulted in a linear T_g dependence on NB content. The cycloolefin copolymers[8] showed two distinctive chain structures depending on composition; copolymers with a NB content of less than 50 mol % consisted mainly of

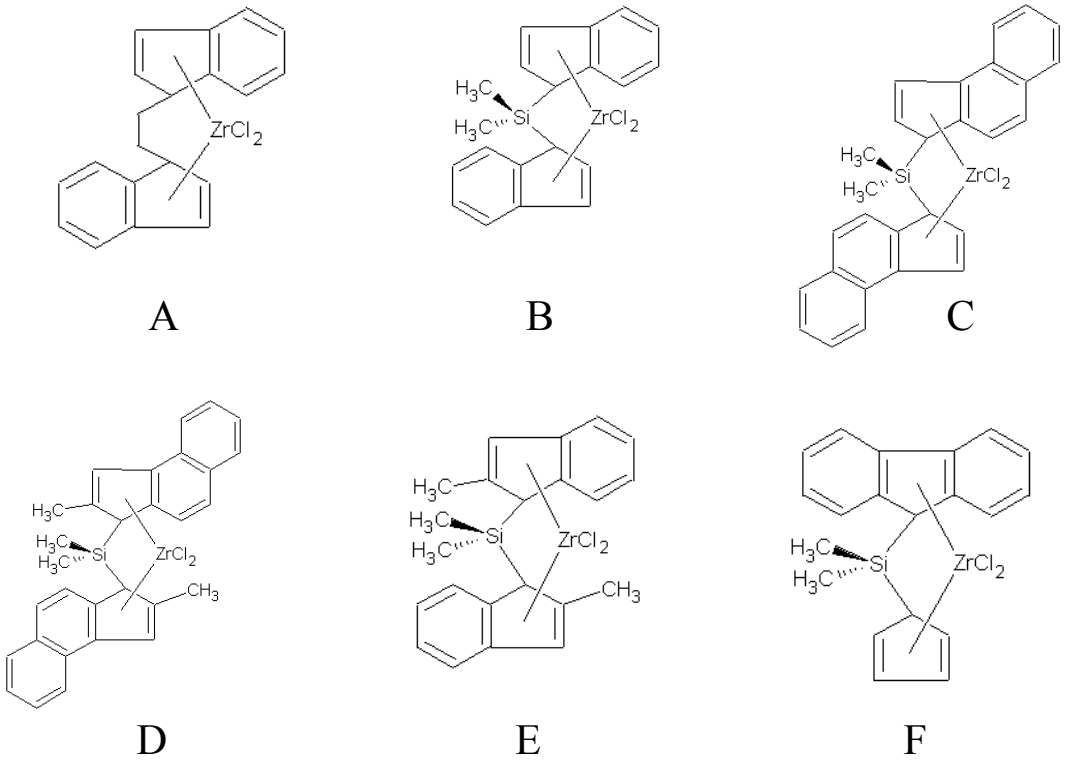

Fig. 1.2 The different metallocenic catalysts used in the synthesis of cycloolefin copolymers (see text) (after J. Forsyth et al., Macromol. Chem. Phys. 2001, 202, 614-620).

alternating norbornene/ethylene sequences and the stereoregularity of polymer chains was relatively high. In contrast, copolymers with NB content higher than 50 mol % consisted of blocks of norbornene of varying lengths, as well as alternating sequences. Because the NB units can be linked in both stereogenic positions in such blocks, the stereoregularity of chains was low. Such a microstructural heterogeneity as presented by Rische and co-workers[8] is expected to have direct consequences on the dynamics. However, this has never been tested until now.

Earlier studies on ethylene/norbornene copolymers reported on the thermal properties,[8, 10-14] the morphology,[8, 10, 11, 13] some mechanical properties,[10, 11, 13] and on the copolymer microstructure.[6, 8, 15-18] The thermal properties resulted in conflicting reports on the glass temperatures as a function of norbornene content. In most cases a linear increase of the single copolymer glass temperature on NB content was found[8, 11, 19] whereas another study[12] indicated a decreasing T_g with increasing NB content. In the latter, Forsyth et al.[12] synthesized and investigated cycloolefin copolymers with various metallocenic catalysts (see Fig. 1.2). The results of this study showed that the microstructure of the COCs is extremely catalyst sensitive. In the case of copolymers made up of predominantly alternating/isolated norbornene, the measured T_g was relatively low. This was attributed to the increased flexibility in the polymer backbone. On the other hand, polymers where longer NB sequences predominated had higher T_g's due to the increased backbone stiffness. Forsyth and co-workers found that not only the presence of a type of sequence but also the stereoregularity of the different chain

segments had an affect on the glass temperature. Harrington et al.[14] studied two copolymers with different microstructures, random and stereoregular/alternating. The results showed that COCs with similar NB content had significantly different glass transition temperatures. The stereospecific, alternating copolymers were found to be semicrystalline with a T_g approximately 30°C lower than their random counterparts. COCs with identical NB content, but synthesized using different methylaluminoxane (MAO) cocatalysts by Wang et al.,[20] exhibited significantly different glass transition temperatures. The reason was quoted as being the result of differences in the copolymer microstructure. Bergström et al.,[18, 21] hypothesized that the presence of blocks of norbornene along with alternating norbornene monomers results in higher glass temperatures due to an increased backbone stiffness. From the above it is concluded that the thermal properties of COCs are a strong function of the catalyst; however a more detailed study is needed.

With respect to the copolymer morphology, studied by wide angle X-ray scattering, there is a consensus that increasing NB content gives rise to a low angle peak[8, 10, 12] similar to bulk polynorbornene (PNB), suggesting that an increase in NB content results in an increasing backbone rigidity giving rise to the higher T_g. Haselwander et al.[22] found two wide-angle peaks, located at 2θ (2θ is the scattering angle) ~ 10° and 19°, in PNB homopolymer. The first peak was attributed to norbornene blocks and this was confirmed with the work of Rische et al.,[8] where they observed that the intensity of the peak at 10° increases with an increasing NB content. They also reported the existence of a peak of higher intensity at 17° instead of the one at 19°. The position of this peak was invariant with the NB content and thus was attributed to the component common to all the COCs used, i.e., the alternating sequences. Scrivani et al.[10] studied the ethylene/norbornene copolymers, together with PNB, and reported about two amorphous halos in their WAXS diffractograms. The peak at lower angle became prominent and closer to the PNB pattern for copolymers containing a norbornene content of more than 50 mol %. Only one peak at 17° and the absence of the low angle peak at 10° was observed by Ekizoglou et al.[13] The lack of this peak was attributed to the absence of norbornene blocks in the samples studied. For force-field calculations[22] for PNB homopolymer the following force-field equation was employed

$$E = \frac{1}{2}k_e(R - R_e)^2 + \frac{1}{2}C_{ijk}\left[\cos\Theta_{ijk} - \cos\Theta_j^0\right]^2 + \frac{1}{2}V_{ij}\left\{1 - \cos\left[n_{jk}\left(\varsigma - \varsigma_{jk}^0\right)\right]\right\}$$
$$+ \frac{1}{2}C_1\left(\cos\psi - \cos\psi_1^0\right)^2 + D_0\left[\rho^{-12} - 2\rho^{-6}\right] + \left[\left(322.0637\frac{Q_iQ_j}{\varepsilon R_{ij}}\right)\right] \qquad (1.1)$$

where the first term refers to harmonic oscillator (k_e is the spring constant, R_e is the equilibrium position), the second term describes the energy for two bonds ij and jk sharing a common atom, Θ is the angle between these bonds, Θ_j^0 the equilibrium angle, and C_{ijk} is related to the force constant. The third term reflects the torsion interaction; ς is the dihedral angle, n_{jk} is the periodicity, V_{ij} is the barrier to rotation, and ς_{jk}^0 is the equilibrium angle. Ψ is the angle between ijk and jkl planes of non-planar geometries, Θ_j^0 is the equilibrium angle. The fifth term is the distance-dependent

potential with D_0 constant. The last term describes the electrostatic interaction between two charges Q_i and Q_j in a distance R_{ij}, ε is the dielectric constant.
The simulations were used in obtaining the radial distribution function (see Fig. 1.3 below) (defined as the distribution of internuclear distances) that, in agreement with the X-ray studies, produced two maxima of intra-chain origin with corresponding distances

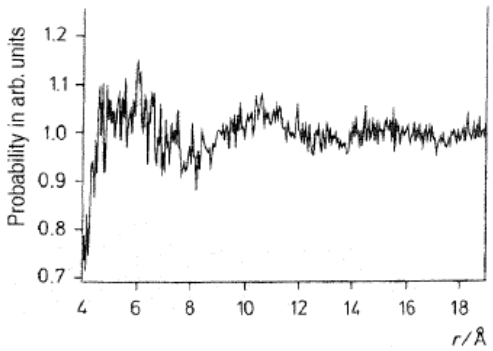

Fig. 1.3 Radial distribution curve of polynorbornene as obtained from force-field calculations (eq. 1.1) (after T. F. A. Haselwander, Macromol. Chem. Phys. ***1996,*** *197, (10), 3435-3453).*

produced two maxima of intra-chain origin with corresponding distances of 0.6 and 1 nm. The rotational potential for the rotation about the single bond connecting two adjacent norbornene monomers revealed three minima occurring at torsional angles of: 60°, 170° and 310°, a large maximum at 240°, and that two of the minima possess an energy of 16 kJ/mol relative to the one of the global minimum (see Fig. 1.4). The zero-angle scattering intensity from small-angle X-ray scattering and differential scanning calorimetry were employed[22] in estimating the T_g of bulk PNB, which is of importance in discussing the complete $T_g(w)$ (w is the weight fraction) dependence in the copolymers. From these measurements it was suggested that the T_g of PNB is roughly 493 K (we will explore this point in Section 4.2). In addition, molecular dynamics

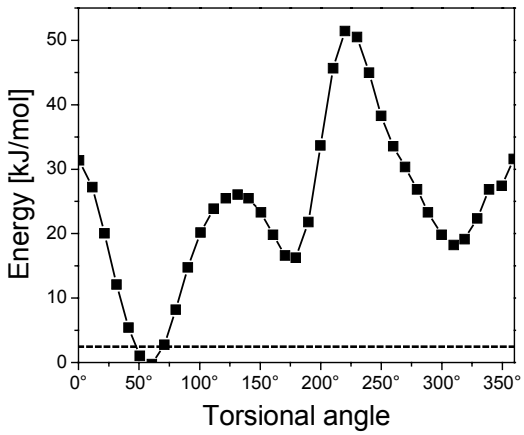

Fig. 1.4 Rotational potential around a single bond between two norbornene monomers. The dashed line is the energy at room temperature (2.479 kJ/mol) (after T. F. A. Haselwander, Macromol. Chem. Phys. ***1996,*** *197, (10), 3435-3453).*

simulations were performed[22] and the characteristic ratio $C_\infty = \langle r^2 \rangle / (nl^2)$, where $\langle r^2 \rangle$ is the mean square end-to-end distance, n is the number of segments and l is the segment length, was calculated as $C_\infty \sim 12$, that is typical for semiflexible chains. The dynamic behaviour of a polynorbornene single chain was simulated[22] allowing observation of the chain trajectories as a function of time (Fig. 1.5).

Fig. 1.5 Snapshots from the trajectory of a single chain of polynorbornene as obtained from molecular dynamics simulations in a 40 ps sequence at 293 K (after T. F. A. Haselwander, Macromol. Chem. Phys. ***1996,*** *197, (10), 3435-3453).*

The stress-strain behavior, microhardness and some fragmentary dynamic mechanical properties were also reported for the COCs.[10, 11, 13] Scrivani et al.[10] observed that the inclusion of norbornene units in the copolymer chain, accompanied by increase in T_g, led to considerably higher Young moduli and microhardness values in the COCs studied (31 to 62 mol % NB), as displayed in Figure 1.6. Similar was the result for the yield stress where this parameter showed an increase by a factor of two. Dynamic mechanical analysis performed under "isochronal" conditions by the same group revealed two relaxation processes, the high temperature α – process, and the γ – subglass process. The results showed that the latter had a similar origin to that of PE and therefore its intensity was diminishing with the decrease in ethylene monomers in the copolymers. On the other hand, the α – relaxation was attributed to the glass transition. Forsyth et al.[11] noticed that the α – process had an asymmetric shape, reaching a low temperature shoulder for the copolymers containing the lowest NB content. They concluded that this could suggest the overlapping with a β relaxation produced by the interfacial content present in the copolymers. In addition, it was observed[11] that the position of the γ – process was shifted to lower temperatures as the NB content increased, which is also the case in copolymers of ethylene and α – olefins.[23] The studies above provided only with some fragmentary mechanical properties. A full investigation of the rheological properties including thermorheological simplicity vs. complexity is needed.

The oxygen diffusion properties of the cycloolefin copolymers were discussed as well as the size and concentration of free volume holes in relation to the gas barrier properties.[24] Poulsen et al.[24] measured the oxygen diffusion coefficients (D), and

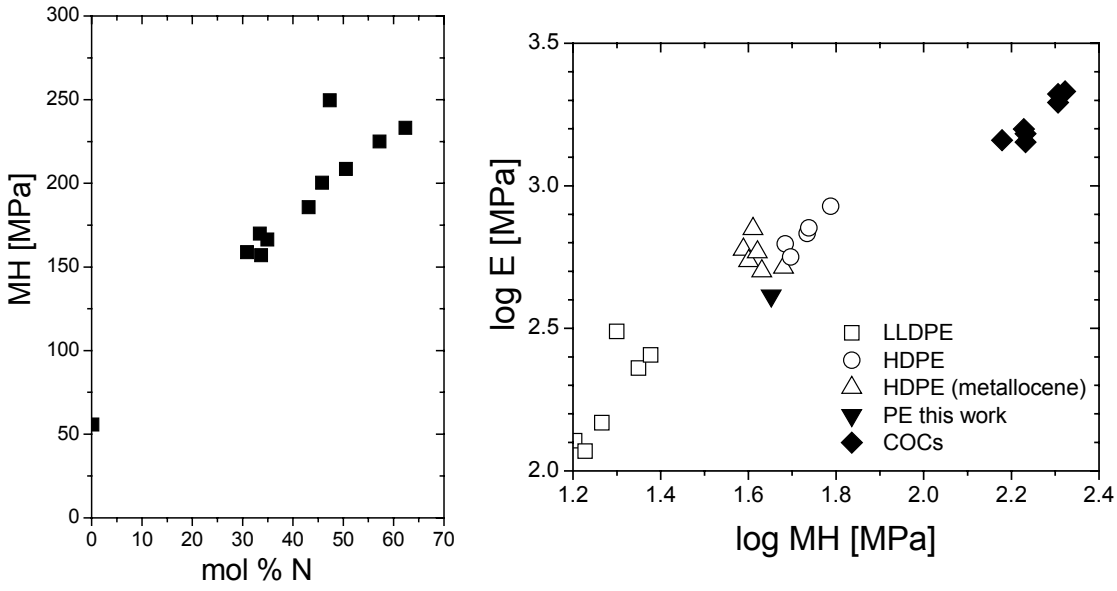

Fig. 1.6 (left): microhardness as a function of norbornene content, (right): Young moduli vs. microhardness for cycloolefin copolymers (COCs) and other polymers (after T. Scrivani, Macromol. Chem. Phys. 2001, 202, 2547-2553).

apparent diffusion activation barriers (E_{act}) for the NB content in the range from 35 to 62 % mol. Only slight changes were observed in both D at 25°C (2-6 x 10^{-8} cm^2 s^{-1}) and E_{act} (35-40 kJ mol^{-1}) within this composition range; the values of D at 25°C correlated reasonably well with calculated values of the copolymer free volume and with the average free volume cavity size determined by positron annihilation lifetime spectroscopy (PALS). The PALS study, carried out on COCs by Djourelov et al.[25], revealed an increasing cavity size with increasing NB content in the backbone. Zamfirova et al.[26] showed that the microhardness and consequently plastic and elastic properties of COCs, synthesized using different metalocene catalysts, do not depend linearly on NB content. This is due to the different microstructures resulting from various catalytic systems. Moreover, Vickers microhardness turned out not to be sensitive either to dimensions and quantity of the pores or to the free volume (examined by PALS). However, long ethylene sequences were related to total microhardness, i.e., during penetration they contributed to the elastic deformation.

Motivation

Despite these early mechanical and thermodynamic investigations of COC, the thermorheological properties of the copolymers are largely unexplored. In addition, the dynamics at the segmental and chain length scales are totally unexplored and this is despite the great industrial/technological interest. Issues that are studied here for the first time include:

- the thermorheological simplicity/complexity of the copolymers:

for this purpose a total of 17 copolymers are used with compositions in the range from 36 to 68 mol % (5 copolymers are commercially available and 12 are made for the purpose of this study) and investigated the thermal and rheological properties of both the segmental and chain (terminal) processes. The thermorheological simplicity is tested by making use of the time-Temperature superposition (tTs) principle. To quantify the efficacy of tTs the temperature dependence of the minimum of loss tangent ($d\tan\delta_{min}/dT$) is employed. A weak T-dependence was found in all copolymers investigated suggesting that tTs is valid and that the systems are thermorheologically simple. Furthermore, both segmental and therminal dynamics in the copolymers can be well described by the Vogel-Fulcher-Tammann or the Williams-Landel-Ferry equations.

- the critical molecular weight for entanglements (M_c):
  by studying the chain relaxation times as a function of copolymer molecular weight the critical molecular weight for entanglements was estimated.

- the origin of the liquid-to-glass transition in the copolymers:
  despite the importance of the composition dependence of the glass temperatures $T_g(w)$ – frequently used to estimate the norbornene content – the origin of the freezing of the segmental dynamics at T_g remains unknown. For this purpose we employ thermodynamic measurements (i.e., Pressure-Volume-Temperature) providing the equation of state in order to obtain the ratio of the activation energy E_V^* to the enthalpy of activation H^*, E_V^*/H^*. This ratio is used to quantify the relative contribution of density and temperature on the segmental dynamics. From the value of this dynamic quantity as a function of NB content we find that free-volume becomes increasingly important with increasing NB content. In contrast to this, in copolymers with low NB content the segmental dynamics are largely determined by the thermal energy required to explore the energy landscape. As a side product of this investigation we discuss the pressure dependence of T_g and find a distinct $T_g(P)$ dependence on NB content. In addition, the dynamic fragility *m* is evaluated and found to exhibit a certain relation to the NB content of the copolymers.

- relation between structural and dynamic heterogeneity:
  several structural probes (NMR, X-rays) provided evidence for increased structural heterogeneity with increasing NB content. Herein we are investigating a possible connection between the structural and dynamic heterogeneity as revealed by the values of the activation ratio E_V^*/H^*, the pressure coefficient of T_g and the dynamic fragility *m*.

- relation of glassy dynamics to free volume:
  the copolymers were investigated by positron annihilation lifetime spectroscopy (PALS) aiming at obtaining the size and numbers of cavities within the glassy state. PALS revealed that the size of cavities increases with increasing NB content in the copolymers. Furthermore, the existence of subglass relaxation processes observed by dynamic mechanical measurements was found to affect the PALS signal. Ethylene groups seem to be involved in generating the free volume holes. On the other hand, increasing NB content causes worse packing and reduces the density of free volume holes.

- miscibility of COC blends:
  the second part of this study deals with the miscibility of COC blends. Mixing COC copolymers is an easy way of producing new copolymers with desired compositions, provided that the blends are miscible. An earlier theoretical study on the mutual miscibility of COC blends revealed large departures from the Flory-Huggins theory; a recent lattice cluster theory (LCT) demonstrated a dependence of miscibility on the actual copolymer chemical compositions x and y on top to the $|x - y|$ dependence. Within the LCT (applied for symmetric blends), three different theoretical models were applied to assess the relevance of chain stiffness within the norbornene monomers as well as of the steric interactions between successive NB monomers on the mutual miscibility.

  It was found[27] that the miscibility of COCs blends is mostly determined by the entopic portion χ_S of the interaction parameter, and the presence of stiffness either in the NB side group or in the chain backbone enhanced the miscibility of COCs.

  In the present work, three different blends of various compositions were examined by rheology and differential scanning calorimetry. The aim of the thermal investigation was to provide the T_g as well as the width, ΔT_g, as a function of blend composition; these results were compared with the pure components of the blends. Rheology on the other hand, provides a more stringent test of miscibility and was employed in order to test the range of validity of the time-temperature superposition principle, i.e. the thermorheological simplicity. The present investigation delineates the composition range of the COC blends that are thermorheologically simple/complex. The experimental results were compared to the above theoretical models and the reason for the miscibility/immiscibility is discussed. Furthermore, we provide experimental miscibility diagrams for asymmetric blend compositions that have not been investigated either theoretically or experimentally so far.

2. Experimental Methods and Data Analysis

2.1 Dynamic Mechanical Experiment

Dynamic mechanical spectroscopy (DMS) is a method that allows characterization of the material by analyzing its deformation and flow behavior. Advantage is taken of the material reaction to periodic variation (oscillations) of the applied external mechanical field. The response to such a field (stress or strain) is either dissipating of the input energy in a viscous flow (non-reversible response), or storing the energy elastically (reversible response), or combination of both of these two extreme (ideal) cases. By means of DMS it is possible to detect variation of both contributions as a function of temperature or deformation rate (i.e., the frequency of the oscillatory deformation) and determine relaxation processes, which govern the viscoelastic behavior of a given material. As a result, DMS is a well-established technique in studying the viscoelasticity of homopolymers and polymer blends.[28]

2.1.1 Definitions

- **Hooke's and Newton's law**

Polymers are viscoelastic and exhibit some of the properties of both viscous liquids and elastic solids. In order to discuss the mechanical behavior in a quantitative way, it is necessary to derive expressions that relate stress and strain. An ideal elastic solid obeys Hooke's law that states

$$\sigma = E\varepsilon \tag{2.1}$$

where the linear strain ε is the change in length divided by the original length when a tensile stress σ, the force per unit cross-sectional area, is applied. E is Young's modulus of the material. The force applied to an elastic solid (an ideal spring) is proportional to the displacement x of the spring from equilibrium

$$F = -kx \tag{2.2}$$

where k is the spring constant (material-specific).
In case of shearing, a shear stress σ is related to the corresponding shear strain γ by the analogous to (2.1) relationship

$$\sigma = G\gamma \tag{2.3}$$

where G is the *shear* modulus.

Similar to the ideal elastic solid, an ideal viscous liquid can be defined. Such a liquid obeys the Newton's law of viscosity

$$\tau = \eta \frac{\partial V}{\partial y} \tag{2.4}$$

where V is the velocity and y is the direction of the velocity gradient in the liquid. For a velocity gradient in the xy plane we obtain

$$\sigma = \eta \frac{\partial \gamma}{\partial t} \tag{2.5}$$

where the *shear* stress σ is directly proportional to the rate of change of *shear* strain γ in time ($\dot{\gamma}$); η is the viscosity of the liquid.

Combining the equations 2.3 and 2.5, a linear viscoelastic behavior can be formulated, under the assumption that the shear stresses related to strain and strain rate are additive

$$\sigma = G\gamma + \eta \frac{\partial \gamma}{\partial t} \tag{2.6}$$

This equation represents one of the simple models for linear viscoelastic behavior, the Voigt model, which is discussed in detail in Section 2.1.3.

- **Stress and strain in dynamic mechanical spectroscopy**

By means of DMS the relationship between deformation (strain) and the resulting stress is examined. If a sample under investigation is confined between two parallel plates (Fig. 2.1), from which the upper one moves at a constant velocity while the lower plate is at rest, the force F needed to move the upper plate of contact area A is

$$F = \sigma A \tag{2.7}$$

where σ is the shear stress (the shear stress is constant through the gap).
The shear deformation (shear strain) is defined as the ratio of the horizontal displacement of the moving palate and the distance between both plates

$$\gamma = \frac{\Delta x}{H} \tag{2.8}$$

The applied strain in a *dynamic mechanical* experiment is a time- and frequency-dependent sinusoidal shear strain of a given amplitude γ_0

$$\gamma(t) = \gamma_0 \sin(\omega t) \tag{2.9}$$

Provided that the behavior of the material is linear, the response (shear stress) to such a deformation remains sinusoidal and can differ only by amplitude and phase shift

$$\sigma(t) = \sigma_0 \sin(\omega t + \delta) \tag{2.10}$$

The principle of the dynamic mechanical measurement is as follows: a sinusoidal strain is applied, and the resulting response (i.e. the stress), is simultaneously measured. The latter depends on the type of the material; in case of ideal elastic system, the stress signal is in phase with the applied strain, whereas for ideal viscous system, the stress is

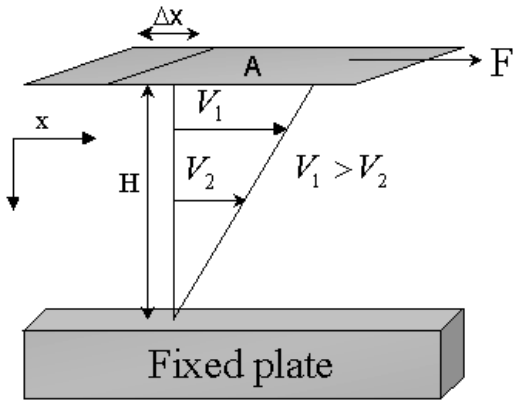

Fig. 2.1 Shear strain and stress. The sample is placed between two plates, a fixed one (lower) and a moving one (upper) with a constant velocity; the contact area is denoted by A and the force by F.

90° out of phase with the strain (or is in phase with the strain rate). Real polymers exhibit viscoelastic behavior and the input and output signals are shifted at phase angle $0° < \delta < 90°$. Linear viscoelastic are materials that follow the Boltzmann superposition principle, stating that the response of the material to a given load is independent of the response to any load, which is already on the material. Suppose that the incremental strains $\Delta\gamma_1, \Delta\gamma_2, \Delta\gamma_3$, etc. are applied to the material at times τ_1, τ_2, τ_3, respectively. Then the total stress at time t is then given by

$$\sigma(t) = \Delta\gamma_1 G(t-\tau_1) + \Delta\gamma_2 G(t-\tau_2) + \Delta\gamma_3 G(t-\tau_3) + \ldots \tag{2.11}$$

where $G(t-\tau_1)$ is a decreasing function of time, the stress relaxation modulus. The summation of (2.11) can be generalized in integral form as

$$\sigma(t) = \int_{-\infty}^{t} G(t-\tau)\, d\gamma(\tau) \tag{2.12}$$

- **Types of test geometries in oscillatory experiment**

In oscillatory shear experiments four different sample geometries, depending on the material state, are used as illustrated in Figure 2.2. Plate-plate and cone-plate are typically used for melts, rectangular bars for solids, and couette for polymer solutions or liquids.

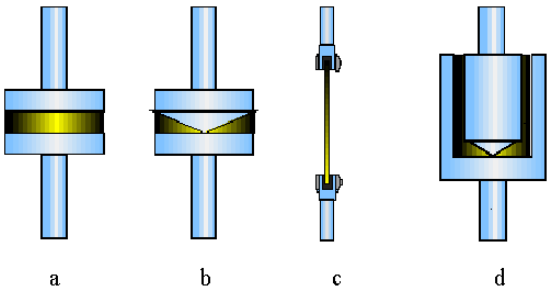

Fig. 2.2 Various test geometries used for different states of materials; (a) plate-plate and (b) cone-plate for the melt, (c) rectangular bars for solids and (d) couette for polymer solutions or liquids. In the present investigation geometries a (at $T>T_g$) and c (at $T<T_g$) were used.

➢ Storage G' and loss G'' shear moduli

The properties of linear viscoelastic materials can be described by the so-called storage G' and loss G'' moduli, corresponding to the elastic and viscous components, respectively (the units of both these moduli are Pa).

In dynamic mechanical experiment of isotropic materials a sinusoidal shear strain $\gamma(t)$ (dimensionless quantity) of amplitude γ_0 and angular frequency ω (2.9) is applied and the resulting stress $\sigma(t)$ (in Pa) of amplitude σ_0 and phase lag δ is simultaneously measured (Fig. 2.3).

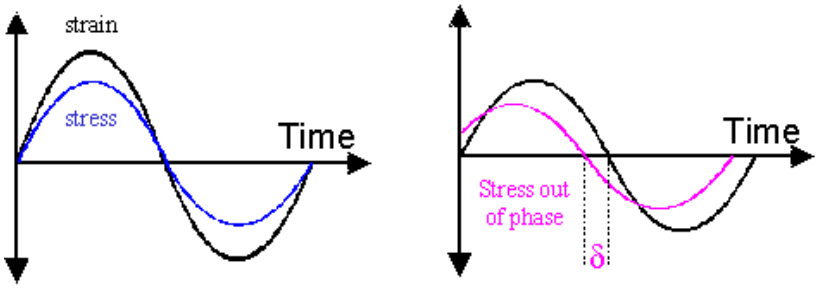

Fig. 2.3 Time profile of a simple shear experiment (see Fig. 2.1) with sinusoidally varying shear.

By expanding equation (2.10)

$$\sigma(t) = (\sigma_0 \cos\delta)\sin(\omega t) + (\sigma_0 \sin\delta)\cos(\omega t) \qquad (2.13)$$

it becomes evident that the stress can be considered to consist of two components: one of magnitude $(\sigma_0 \cos\delta)$ in phase with the strain; and another one of magnitude $(\sigma_0 \sin\delta)$ being 90° out of phase with the strain.

The stress-strain relationship can therefore be defined by a quantity G' in phase with the strain and by a quantity G'' 90° out of phase with the strain, i.e.

$$\sigma = \gamma_0 \left[\mathrm{G'}(\omega) \sin(\omega \mathrm{t}) + \mathrm{G''}(\omega) \cos(\omega \mathrm{t}) \right] \tag{2.14}$$

where

$$\mathrm{G'}(\omega) = \frac{\sigma_0}{\gamma_0} \cos\delta \qquad \text{and} \qquad \mathrm{G''}(\omega) = \frac{\sigma_0}{\gamma_0} \sin\delta \tag{2.15}$$

- **Complex notation of shear modulus and compliance**

Due to the phase lag δ it is convenient to deal with the shear stress and shear strain by using complex notation:

$$\gamma^* = \gamma_0 (\cos\omega \mathrm{t} + \mathrm{i} \sin\omega \mathrm{t}) = \gamma_0 \exp(\mathrm{i}\omega \mathrm{t}) = \gamma' + \mathrm{i}\gamma'' \tag{2.16}$$

$$\sigma^* = \sigma_0 [\cos(\omega \mathrm{t} + \delta) + \mathrm{i} \sin(\omega \mathrm{t} + \delta)] = \sigma_0 \exp\left[\mathrm{i}(\omega \mathrm{t} + \delta)\right] \tag{2.17}$$

Hence, the complex shear modulus (Fig. 2.4) is defined as:

$$\mathrm{G}^* = \frac{\sigma^*}{\gamma^*} = \frac{\sigma_0}{\gamma_0} \exp(\mathrm{i}\delta) = \frac{\sigma_0}{\gamma_0} \cos\delta + \mathrm{i} \frac{\sigma_0}{\gamma_0} \sin\delta = \mathrm{G'} + \mathrm{iG''} \tag{2.18}$$

$$\text{and} \qquad \left|\mathrm{G}^*\right| = \frac{\sigma_0}{\gamma_0} = \sqrt{\mathrm{G'}^2 + \mathrm{G''}^2} \tag{2.19}$$

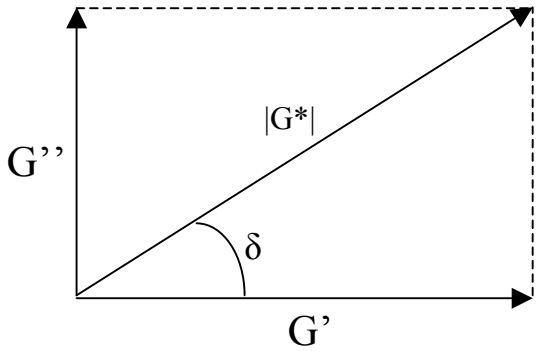

Fig. 2.4 Phasor diagram of complex modulus $\mathrm{G}^* = \mathrm{G'} + \mathrm{iG''}$. *G' corresponds to the storage modulus (elastically stored energy) and G'' to the loss modulus (dissipated energy in the system).*

Sometimes instead of the shear modulus G^*, the *compliance* J^* is used defined by

$$J^* = J' - iJ'' \tag{2.20}$$

Hence we obtain that

$$J' = \frac{G'}{G'^2 + G''^2} \quad \text{and} \quad J'' = \frac{G''}{G'^2 + G''^2} \tag{2.21}$$

A useful parameter, which is a measure of the ratio of energy lost (as heat) to energy stored in a material in one cyclic deformation, is the *loss tangent*

$$\tan\delta = \frac{G''}{G'} \tag{2.22}$$

The tan δ is sometimes referred to as damping and its particular temperature dependence will be employed as test of thermorheological simplicity.

2.1.2 The oscillatory response of real systems – frequency dependence

The general $G'(\omega)$ and $G''(\omega)$ behavior of amorphous, uncrosslinked polymers is illustrated in Figure 2.5, where the frequency dependence for an amorphous, ethylene-norbornene copolymer is shown. Notice that the G' and G" posses values in the range from 1 to 10^9 Pa . Contrast this with the situation in crystalline solids where a constant, i.e., frequency independent modulus of about 10^{11} Pa is obtained. The large variation of the modulus with temperature/frequency is the characteristic of soft viscoelastic materials, including polymers.

A number of specific *regions* of the "master curve" can often be differentiated (the construction of the master curve is discussed later with respect to Fig. 2.9):

a) an elastic response at the higher frequencies, where storage modulus G' predominates and reaches the value of about 10^9 Pa, known as the glassy state. In this region the polymer maintains the disordered nature of the melt but lacks molecular mobility since motions longer than a segment are practically frozen. Nevertheless, some localized motions are still possible giving rise to weak sub-glass relaxations. Such relaxations are characteristic of all amorphous polymers and glass-forming liquids in general.[29]
segmental region that indicates a "*transition"* from the glassy to the rubbery (viscoelastic) state. However, the transition is not a real thermodynamic transition (there is no heat of fusion associated with it but only a change in the specific heat). In this region the loss modulus (G'') predominates and decreases slower than G'; this is due to the energy dissipation (as heat) caused by friction of the main chain segments (segments consist of a few monomers), which become mobile and as a

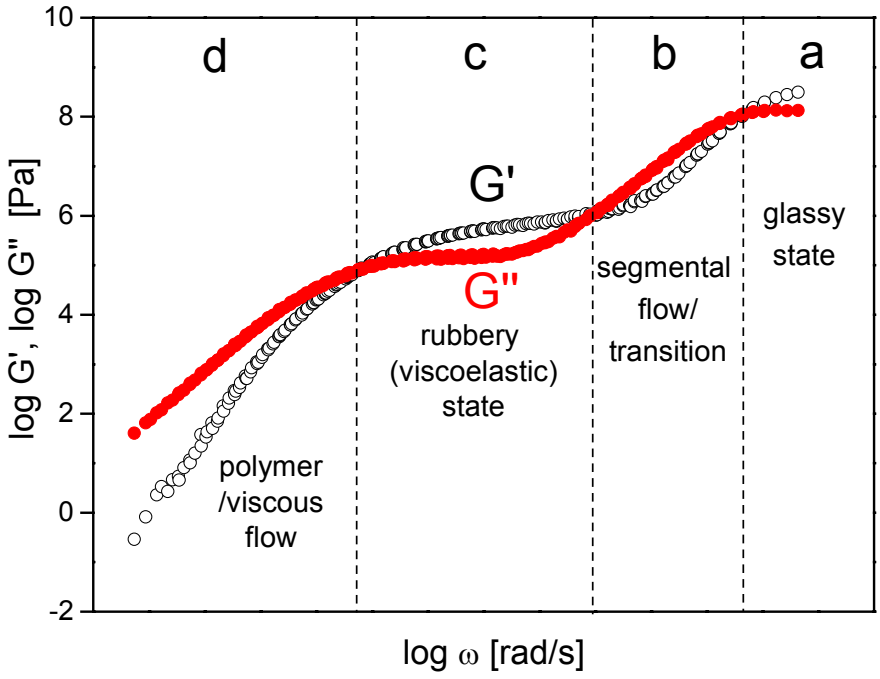

Fig. 2.5 The various regions (a, b, c and d – see text) in the viscoelastic spectrum of an amorphous polymer.

result can move on the segmental level. As the temperature continues to increase, a growing fraction of chain segments acquire enough energy to overcome the intra- and inter-molecular barriers.

b) the rubbery (viscoelastic) state, where elastic behavior dominates (G'>G'') and the shear modulus decreases around three decades (to circa 10^6 Pa) compared to the glassy state. The plateau is never ideal flat; there is always a slight increase of G' with frequency, but it can be as small as few percent increase in modulus per decade increase in frequency. Within this region, when the slope of G' is small, G'' decreases with increase in frequency, toward a minimum before rising again. The lower the slope of G' curve, the deeper the minimum of G''. This effect is due to the increasing separation of the segmental and chain modes. The plateau exists (is built) only if the molecular weight of the polymer is greater than the so-called entanglement molecular weight M_e, which corresponds to the molecular weight contained between two physically entangled points (two entanglements). The onset of entanglement is believed to occur at a critical molecular weight $M_c \approx 2.4M_e$.[30-32] The extension of the plateau is proportional to the polymer molecular weight and the height of the plateau is inversely proportional to M_e. The M_e determination will be shown below.

c) polymer flow in a viscous region, where G'' predominates and dissipation of energy prevails. At such a low frequency (long times), motions of whole chains take place. At low enough frequencies, G'' increases linearly with frequency and G' is proportional to quadratic frequency. This behavior can be derived from simple

models of viscoelastic systems such as the Maxwell model (this model as well as the Voigt model are discussed below).

- **Definition of relaxation times**

1) At the border of glassy state and segmental region, the G' and G'' cross (see Figure 2.5). This crossover point is used to determine the segmental relaxation time τ_s, which is given by the inverse of the frequency at that point ($\omega\tau_s = 1$). For narrow dispersions the crossing frequency is identical to the frequency where G'' develops a maximum.
2) The chain (terminal) relaxation time is determined (using $\omega\tau_c = 1$) from the crossover point of G' and G'', which precedes the viscous region.

The correspondence of these two crossover points to relaxation times in the polymer systems is only approximate. Another measure of the characteristic relaxation times is the maximum in G'', which is located in the vicinity of the crossing (for narrow molecular weight distributions). For broad distributions the crossing of the moduli and the maximum in G'' are shifted away from each other.

The relaxation times (both segmental and chain) as a function of temperature can be determined from the following equation

$$\log\tau(T) = \log\tau(T_{ref}) + \log(a_T) \tag{2.23}$$

where T_{ref} is the so-called reference temperature and a_T is the shift factor. Eq. (2.23) is applicable only for systems that are thermorheologically simple (see below).

- **Entanglement molecular weight**

Chain entanglement is a kind of intermolecular interaction, which does not involve an energetic change and is purely an entropic, topological phenomenon. Chain entanglement mainly affects polymer chain motions. The molecular weight between two adjacent temporary entanglement points (defined as the entanglement molecular weight M_e) can be calculated from the plateau modulus G_N as

$$M_e = \frac{\rho_N RT_N}{G_N} \tag{2.24}$$

where ρ_N is the density of the polymer at temperature T_N, at which the plateau modulus G_N was measured and R is the gas constant (R=8.314 $Jmol^{-1}K^{-1}$). The value of the plateau modulus, G_N, can be obtained from the frequency where the minimum of the loss tangent $\tan\delta$ is located, i.e., from

$$G_N = G'(\omega)_{\tan\delta_{min}} \tag{2.25}$$

The M_e values for the different copolymers investigated herein will be discussed later in section 4.5

2.1.3 Mechanical models of linear viscoelasticity

The linear viscoelastic behavior of materials may be represented by simple models consisting of massless Hookean springs that obey Hooke's law and Newtonian dashpots, obeying Newton's law (see section 2.1.1), the latter being considered as oil-filled cylinders in which a loosely fitting piston moves at a rate proportional to the viscosity of the oil and to the applied stress. In the simplest case consisting of a spring and a dashpot two models can be constructed; these elements are either coupled in series (the Maxwell model), or in parallel (the Voigt model) as illustrated in Figure 2.6.

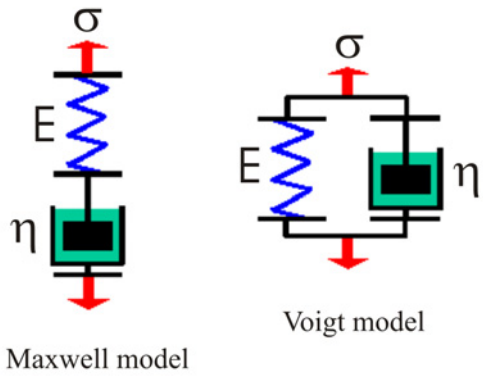

Fig. 2.6 Mechanical models for viscoelastic behavior.

Each model is described in detail below; the viscoelastic functions exhibited in each one are summarized in Table 2.1.

Table 2.1 Viscoelastic functions of the Maxwell and the Voigt model.

The Maxwell model	The Voigt model
$J(t) = J_0 + t/\eta$	$J(t) = J_0(1 - e^{-t/\tau})$
$E(t) = E_0 e^{-t/\tau}$	$E(t) = E_0$
$E'(\omega) = E_0\omega^2\tau^2(1+\omega^2\tau^2)$	$E'(\omega) = E_0$
$E''(\omega) = E_0\omega\tau(1+\omega^2\tau^2)$	$E''(\omega) = E_0\omega\tau = \omega\eta$
$\eta'(\omega) = \eta/(1+\omega^2\tau^2)$	$\eta'(\omega) = \eta$
$J'(\omega) = J_0$	$J'(\omega) = J_0/(1+\omega^2\tau^2)$
$J''(\omega) = J_0/\omega\tau = 1/\omega\eta$	$J''(\omega) = J_0\omega\tau/(1+\omega^2\tau^2)$
$\tan\delta = 1/\omega\tau$	$\tan\delta = \omega\tau$

- **The Maxwell model**

The stress-strain relation for the spring (see eq. 2.1) can be written as

$$\sigma = E\varepsilon_1 \tag{2.26}$$

and for the dashpot

$$\sigma = \eta \frac{d\varepsilon_2}{dt} \tag{2.27}$$

The stress is exactly the same for both the spring and the dashpot, and the total strain is the sum of the strain in the spring and the dashpot ($\varepsilon = \varepsilon_1 + \varepsilon_2$).
Thus, the equation of motion in this model is

$$\frac{d\varepsilon}{dt} = \frac{d\varepsilon_1}{dt} + \frac{d\varepsilon_2}{dt} = \frac{1}{E}\frac{d\sigma}{dt} + \frac{\sigma}{\eta} \tag{2.28}$$

We can now discuss two cases:

a) stress relaxation for a constant (in time) strain ($d\varepsilon/dt = 0$)

$$\frac{1}{E}\frac{d\sigma}{dt} + \frac{\sigma}{\eta} = 0 \tag{2.29}$$

with solution

$$\frac{d\sigma}{\sigma} = -\frac{E}{\eta}dt \tag{2.30}$$

Integration leads to

$$\sigma = \sigma_0 \exp\left(-\frac{Et}{\eta}\right) = \sigma_0 \exp\left(-\frac{t}{\tau}\right) \tag{2.31}$$

where σ_0 is the initial stress at time $t = 0$, and $\tau = \eta/E$ is the *relaxation time* in this model. From equation (2.31) follows that in the Maxwell model the stress decays exponentially with the time t. In real polymers the stress relaxation behavior cannot usually be represented by a single exponential decay term, nor does it necessarily decay to zero at infinite time.[33]

b) constant (in time) stress ($d\sigma/dt = 0$). Then, from equation (2.28) we obtain that $d\varepsilon/dt = \sigma/\eta$, which is a constant value. This result implies that the Maxwell model cannot describe creep.

Insertion of the time dependence of stress (compare eq. (2.18))

$$\sigma = \sigma_0 \exp(i\omega t) \tag{2.32}$$

into equation (2.28) for the Maxwell model yields the frequency dependence of storage and loss moduli (Fig. 2.7)

$$E' = \frac{E_0 \omega^2 \tau^2}{1 + \omega^2 \tau^2} \qquad \text{and} \qquad E'' = \frac{E_0 \omega\, \tau}{1 + \omega^2 \tau^2} \tag{2.33}$$

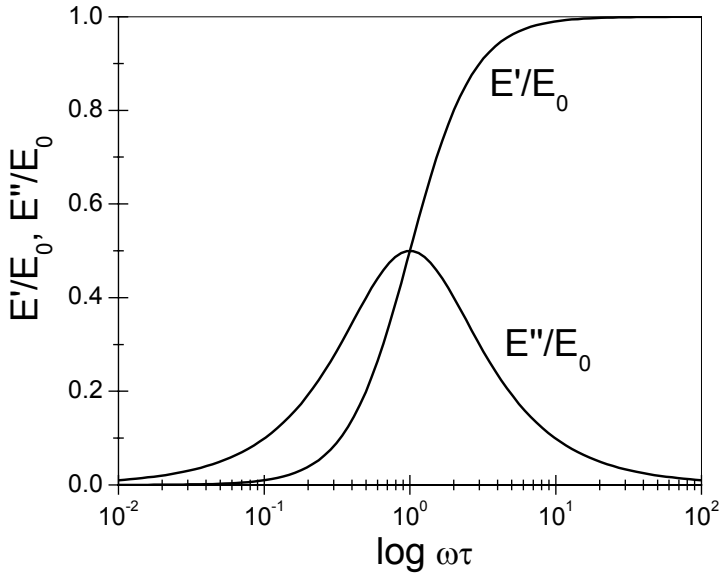

Fig. 2.7 Frequency dependence of E' and E'' according to the Maxwell model.

In the high frequency range the plateau of E' prevails over E'', which is characteristic for the elastic behavior. The elastic modulus of a material in this frequency range is given by

$$E_0 = \lim_{\omega \to \infty} E'(\omega) \tag{2.34}$$

In the low frequency region $E'' >> E'$, which is typical for the Newtonian flow. In this range E' and E'' are proportional to ω^2 and ω (on a logarithmic scale E' and E'' have the slopes of 2 and 1, respectively; see Fig. 2.5). The zero shear viscosity can be obtained in this range according to

$$\eta_0 = \lim_{\omega \to 0} \frac{E''(\omega)}{\omega} \tag{2.35}$$

- **The Voigt model**

The Voigt model, as mentioned above, consists of a spring and dashpot *in parallel.* In this system the displacements (the strains) of the spring and the dashpot are equal, whereas the total stress σ comes from both of these elements

$$\varepsilon = \varepsilon_1 = \varepsilon_2 \qquad \text{and} \qquad \sigma = \sigma_1 + \sigma_2 \tag{2.36}$$

Thus from equations (2.26 and 2.27) follows the equation of motion

$$\sigma = E\varepsilon + \eta\frac{d\varepsilon}{dt} \tag{2.37}$$

Integration of (2.37) leads to

$$\varepsilon = \frac{\sigma_0}{E}\left[1 - \exp\left(-\frac{E}{\eta}t\right)\right] \tag{2.38}$$

where σ_0 is the constant stress; the strain ε rises exponentially to the value of σ_0/E with *retardation time* $\tau' = \eta/E$. Equation (2.38) and hence the Voigt model can describe time dependence of creep, however, this model cannot predict the stress relaxation.

The Maxwell and the Voigt models are simplifications and cannot properly describe the viscoelastic behavior in a wide frequency range and fail totally, as already mentioned, at creep and stress relaxation prediction, respectively. In order to describe more precisely the real behavior of polymer systems, one can, for instance, couple several Maxwell units in parallel or combine the Voigt and Maxwell units in series (Burger's model, see Fig. 2.8), etc.

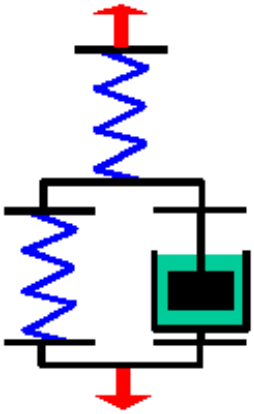

Fig. 2.8 Three-element model (Burger's model) of viscoelasticity.

2.1.4 Thermorheological simplicity and the principle of time-Temperature superposition (tTs)

The typical frequency range accessible for dynamic mechanical spectrometers lies between 10^{-3} and 500 rad/s[28]. From Figure 2.5 can be seen that the frequency range of the "master curve" covers many decades, which are not possible to be measured directly. In order to overcome the limits of the apparatus, master curves are constructed which combine results of measurements performed at various temperatures within the same frequency window, typically 10^{-1} to 10^{2} rad/s as illustrated in Figure 2.9. One of

these dependences (located above the glass transition) is taken as a reference (is not shifted) and all other curves are shifted along the frequency scale to overlap with dependences measured at adjacent temperatures. G' and G'' responses obtained at higher and lower temperatures, than the reference temperature, are shifted to lower and higher frequencies, respectively. The final result is a *continuous* master curve corresponding to the chosen reference temperature T_{ref}.

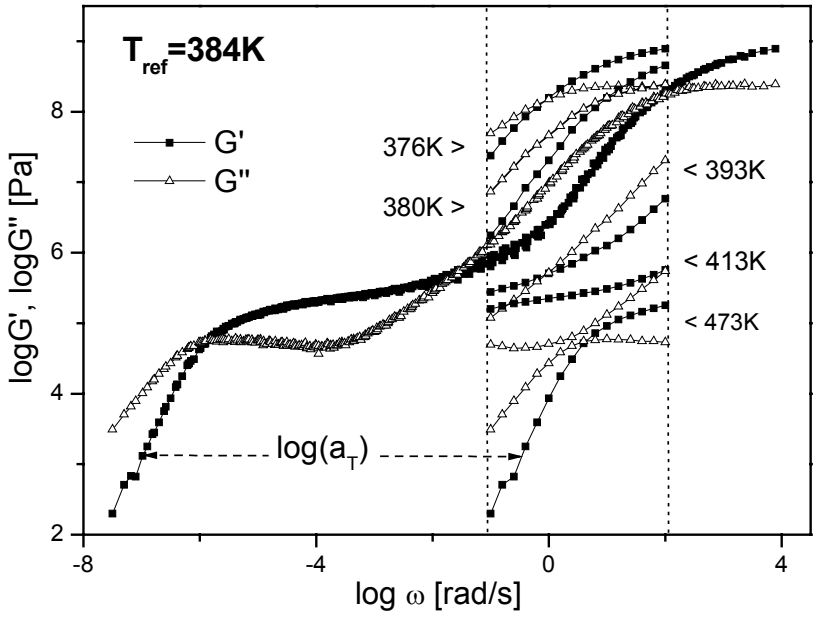

Fig. 2.9 Construction of a master curve for a polystyrene test sample (M_w=200 kg/mol). Frequency dependences of G' and G'' are measured at various temperatures with a fixed frequency window (dotted lines). One of these dependencies is taken as a reference and is not shifted. All the others are shifted horizontally only by $\log a_T$ *to overlap with dependencies measured at adjacent temperatures; as indicated, dependencies measured at high and low temperatures are moved to lower and higher frequencies, respectively.*

The justification of the determination procedure of the storage and loss moduli over a very broad frequency range is based on the so-called time-temperature or frequency-temperature equivalence (or correspondence) principle. It implies that the viscoelastic behavior at one temperature can be related to that at another temperature by a change in the time-scale only[33]. In other words, the temperature change is equivalent to the change of the deformation frequency of a given material.

The correspondence principle is valid only for *thermorheologically simple* materials, that is, materials where the distribution of relaxation times does not change with temperature; obviously it does not work in the temperature/frequency range where relaxation processes with different temperature dependencies of relaxation times overlap[34]. The principle holds only for amorphous homopolymers, and does not hold for semicrystalline polymers, for polymer blends or block copolymers. In the case of semicrystalline polymers and block copolymers the reason for the pronounced failure of tTs is the existence of molecular and supramolecular organization that change as a

function of temperature. In the case of *immiscible* polymer blends tTs fails again as a result of the different shift factors for the different components in the blend. Interestingly, in the case of *miscible* polymers tTs fails again provided that the difference in the glass temperatures (T_g) of the two components is above 40 K.

- **The Williams-Landel-Ferry (WLF) equation**

The horizontal shift of the G', G'' dependencies obtained at various temperatures provides directly the temperature dependence of shift factor, $\log a_T(T, T_{ref})$, as illustrated in Figure 2.10. This shift factor-temperature relation, known as the WLF equation, was postulated by Williams, Landel and Ferry[35], who found that

$$\log a_T = \frac{C_1^{T_{ref}}(T - T_{ref})}{C_2^{T_{ref}} + T - T_{ref}} \tag{2.39}$$

where $C_1^{T_{ref}}$ and $C_2^{T_{ref}}$ are material dependent constants that depend on the reference temperature T_{ref}. It can by of interest, for comparison purposes for example, to express these constants in correspondence to another reference temperature, particularly the glass transition temperature T_g. The new constants then, C_1^{Tg} and C_2^{Tg} with T_g as a reference temperature, can be determined using the following conversion relations

$$C_1^{Tg} = \frac{C_1^{T_{ref}} C_2^{T_{ref}}}{C_2^{T_{ref}} + T_g - T_{ref}} \tag{2.40}$$

$$C_2^{Tg} = C_2^{T_{ref}} + T_g - T_{ref} \tag{2.41}$$

An analysis of limited data led to the postulation that C_1^{Tg} and C_2^{Tg} were universal constants, however, this assumption was not supported when the results obtained for a wide variety of viscoelastic materials were considered.[29] From (2.40) and (2.41) follows that

$$C_1^{Tg} C_2^{Tg} = C_1^{T_{ref}} C_2^{T_{ref}} \tag{2.42}$$

$$T_g - C_2^{Tg} = T_{ref} - C_2^{T_{ref}} \equiv T_\infty \tag{2.43}$$

where T_∞ is a fixed temperature (known as the Vogel temperature or the "ideal" glass temperature) at which, regardless of the arbitrary choice of T_{ref}, $\log a_T$ becomes infinite in accordance with equation (2.39).

The WLF equation holds above the glass temperature, i.e., until T_g + 100 K.[31] The equation was originally based purely on empirical observations, it can, however, be derived directly from free volume theories.[33]

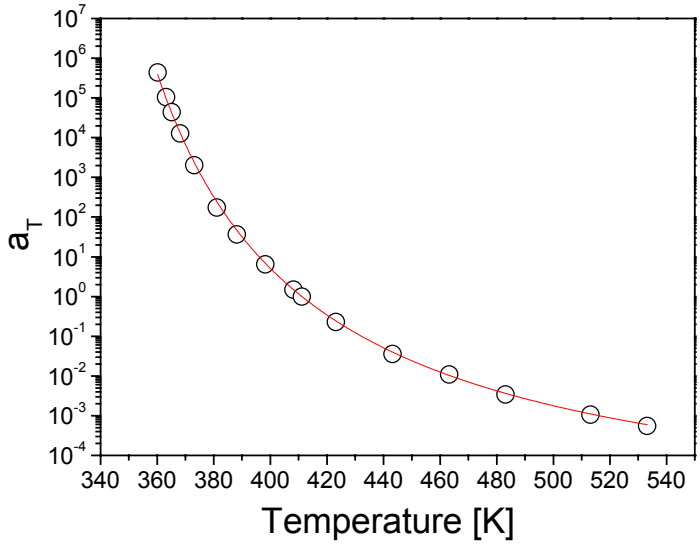

Fig. 2.10 Temperature dependence of a shift factor a_T *for cycloolefin copolymers taken as an example;* $C_1^{T_{ref}}$ *=6.16,* $C_2^{T_{ref}}$ *=381.7 K,* T_{ref}*=411 K. The line is a fit to the WLF equation (2.39) (Topas 8007).*

2.1.5 Origin of the liquid-to-glass "transition"

A complete theoretical understanding of the liquid-to-glass "transition" is not yet available. The origin of the dramatic "slowing-down" of the relaxation times (τ) of a system (liquid or polymer) as it approaches its "glass temperature" (T_g) is still an unresolved issue. The origin of this process is one of the most fundamental problems in polymer physics of liquids, in general, with several technologically important aspects such as physical aging, refractive index stabilization, etc.[36-38] Identifying the main control thermodynamic parameter that dominates the slow dynamics in glass-forming liquids that give rise to the dynamic arrest at T_g is a point of debate. Theoretical predictions consider two extreme cases:

$\Rightarrow$ Thermally activated processes on a constant density "energy landscape"[36, 37]

$\Rightarrow$ Free-volume theories[31, 39, 40]

In the former picture the controlling parameter is temperature (T), the landscape is considered as fixed and the super-Arrhenius dependence of relaxation times on T ($\tau(T)$) is attributed to changes in the barriers and the minima encountered in the exploration of the landscape. In the latter picture, the controlling parameter is volume (V) or better density (ρ) and the slowing-down results from the decrease of the available (or free) volume. Clearly these pictures should be considered as extreme cases since, molecular transport in general, is driven by thermal activation processes with

potential energy barriers hat depend on local density.[41] Both approaches are described below.

A. Free volume theories of the glass "transition"

Free volume theories assume that, if conformational changes of the polymer chains are to take place, there must be space available for molecular segments to move into. The total amount of free space per unit volume of the polymer is called the fractional free volume V_f. As the temperature of the polymer system decreases towards the glass temperature the macromolecules rearrange to reduce the free volume until, eventually, the polymer chains become so slow that they cannot rearrange within the time-scale of the experiment and the volume of the material contracts like that of a solid. If V_g is the fractional free volume at T_g, then ideally, above T_g, the fractional free volume can be expressed as

$$V_f = V_g + \alpha_f (T - T_g) \tag{2.44}$$

where α_f is the expansion coefficient of free volume.
Based on experimental data for monomeric liquids, Doolittle's equation[42] relates the viscosity to the free volume through

$$\eta = A \exp\left(\frac{B}{V_f}\right) \tag{2.45}$$

where A and B are constants. Taking into account the relation between zero shear viscosity and the shift factor

$$\frac{\eta_0(T)}{\eta_0(T_{ref})} = a_T \tag{2.46}$$

we obtain that

$$a_T = \frac{\exp\left(\frac{B}{V_f}\right)}{\exp\left(\frac{B}{V_f^r}\right)} = \exp\left(B\left(\frac{1}{V_f} - \frac{1}{V_f^r}\right)\right) \tag{2.47}$$

where V_f is the fractional free volume at T and V_f^r is the fractional free volume at the reference temperature. If the reference temperature is set as the glass transition temperature and if fractional free volume at this temperature is V_f^g, the following equation results

$$a_T = \exp\left(B\left(\frac{1}{V_f} - \frac{1}{V_f^g} \right) \right) \tag{2.48}$$

Insertion of equation (2.44) into equation (2.48) gives

$$a_T = \exp\left(\frac{\left(-\frac{B}{V_f^g} \right)\left(T - T_g \right)}{\left(\frac{V_f^g}{\alpha_f} \right) + T - T_g} \right) \tag{2.49}$$

Taking the logarithm of equation (2.49) results in

$$\log a_T = -\frac{\left(\frac{B}{2.303 V_f^g} \right)\left(T - T_g \right)}{\left(\frac{V_f^g}{\alpha_f} \right) + T - T_g} \tag{2.50}$$

which is the WLF equation (2.39) with $C_1 = B/2.303\,V_f^g$ and $C_2 = V_f^g/\alpha_f$. It will be shown below that the WLF equation is equivalent to the Vogel Fulcher Tammann (VFT) equation, and hence the latter can also be derived from the free volume theory.

- Vogel-Fulcher-Tammann (VFT) relation

An empirical equation that successfully relates viscosity to temperature was introduced by Fulcher[43, 44] and Tammann and Hesse[45]

$$\eta_0(T) = A \exp\left(\frac{B}{T - T_\infty} \right) \tag{2.51}$$

$$\log \eta_0(T) = \log A + \left(\frac{B^*}{T - T_\infty} \right) \tag{2.52}$$

where η_0 is the zero shear viscosity, $A = \eta_0(T_{ref})$, B is the "activation parameter", $B^* = B \log e$ and T_∞ is a temperature at which the viscosity becomes infinite. Taking into account the relation between zero shear viscosity and relaxation time

$$\frac{\eta_0(T)}{\eta_0(T_{ref})} = \frac{\tau(T)}{\tau(T_{ref})} = a_T \tag{2.53}$$

we obtain that

$$\tau(T) = A \exp\left(\frac{B}{T - T_\infty} \right) \tag{2.54}$$

$$\log \tau(T) = \log A + \left(\frac{B^*}{T - T_\infty} \right) \tag{2.55}$$

Equations (2.51, 2.52) or, equivalently equations (2.54, 2.55), are known as the Vogel-Fulcher-Tammann (VLF) equation.

- Equivalence of VFT and WLF equations

Having an equation for the temperature dependence of the viscosity (2.52), we may also formulate the shift factor $\log a_T$. Equations (2.53) and (2.52) yield

$$\log a_T = \log \frac{\eta_0(T)}{\eta_0(T_{ref})} = \log \eta_0(T) - \log \eta_0(T_{ref})$$

$$= \log A + \frac{B^*}{T - T_\infty} - \left(\log A + \frac{B^*}{T_{ref} - T_\infty} \right)$$

$$= B^* \left(\frac{T_{ref} - T}{(T - T_\infty)(T_{ref} - T_\infty)} \right)$$

$$= \frac{B^*}{T_{ref} - T_\infty} \cdot \frac{T - T_{ref}}{T - T_{ref} + (T_{ref} - T_\infty)} \tag{2.56}$$

The last part of this equation can be expressed as

$$\log a_T = \frac{C_1 (T - T_{ref})}{C_2 + T - T_{ref}} \tag{2.57}$$

where

$$C_1 = \frac{B^*}{T_{ref} - T_\infty} \text{ and } C_2 = T_{ref} - T_\infty \tag{2.58}$$

This indicates that WLF and VFT equations are in fact equivalent.

A comprehensive conversion list of VFT into WLF parameters and vice versa is the following

$$\begin{array}{l|l} A = \log \tau(T_{ref}) - C_1 & \log \tau(T_{ref}) = A + \dfrac{B^*}{T_{ref} - T_\infty} \\ B^* = C_1 C_2 & C_1 = \dfrac{B^*}{T_{ref} - T_\infty} \\ T_\infty = T_{ref} - C_2 & C_2 = T_{ref} - T_\infty \end{array} \tag{2.59}$$

B. Thermally activated processes

The second approach to the liquid-to-glass "transition" is associated with the thermally activated processes on a constant "energy landscape" that is considered as fixed (does not change while cooling) for the whole system (all conformations of the particles). A schematic representation of such an energy landscape is illustrated in Figure 2.11. The potential energy depends on the spatial location of all the particles

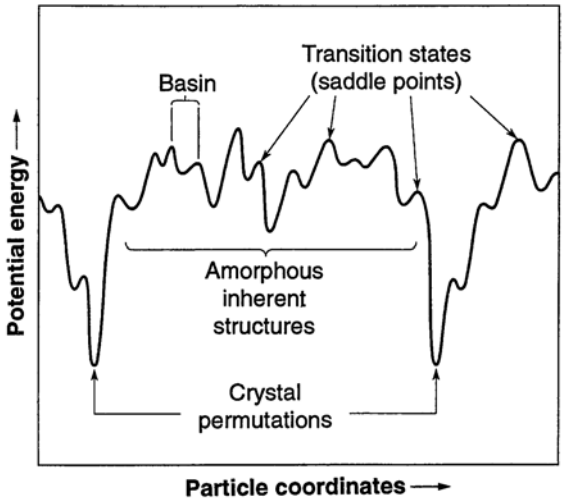

Fig. 2.11 A schematic diagram of the potential energy ("energy landscape") in the multidimensional configuration space for a many-particle system (after F.H. Stillinger, Science 1995).

constituting the system, and includes contributions from electrostatic multipoles and polarization effects, covalency, hydrogen bonding, electron-cloud-overlap repulsions and intermolecular force fields among other things.[37] The minima in Fig. 2.11 correspond to mechanically stable arrangements of all particles; any small displacement from such an arrangement gives rise to restoring forces to the undisplaced arrangement. Equivalent minima can be achieved by permutations of identical particles. The lowest lying minima are occupied by the system provided that is cooled to absolute zero slowly enough to maintain thermal equilibrium; pure substances become then virtually perfect crystals.[37] Higher lying minima correspond to less ordered systems with some or completely amorphous regions.

C. Quantitative measure of the relative contribution of density and temperature on the segmental dynamics

As already indicated, liquid-to-glass "transition" is a contentious issue and, hence, the domination of one of the two parameters (density or temperature) controlling the slowing-down process is still an open question. It is possible, however, to determine, which one of the two parameters plays the most important role with respect to the dynamics. This can be made by calculation the ratio of the activation energy at constant volume to enthalpy of activation, E_V^*/H^*. This dynamic quantity provides a quantitative

measure of the relative importance of density and temperature on the dynamics[46] of the α-process. Defining the enthalpy of activation as

$$H^* = R\left(\frac{\partial \ln \tau}{\partial(1/T)}\right)_P \tag{2.60}$$

and the activation energy at constant volume as

$$E_V^* = R\left(\frac{\partial \ln \tau}{\partial(1/T)}\right)_V, \tag{2.61}$$

it can be shown that the ratio E_V^*/H^* can be expressed as[46-48]:

$$\frac{E_V^*}{H^*} = 1 - \left(\frac{\partial P}{\partial T}\right)_V \left(\frac{\partial T}{\partial P}\right)_\tau \tag{2.62}$$

$$\frac{E_V^*}{H^*} = 1 - \frac{\left(\frac{\partial \rho}{\partial T}\right)_P \left(\frac{\partial \ln \tau}{\partial P}\right)_T}{\left(\frac{\partial \rho}{\partial P}\right)_T \left(\frac{\partial \ln \tau}{\partial T}\right)_P} \tag{2.63}$$

$$\frac{E_V^*}{H^*} = 1 - \frac{\left(\frac{\partial \ln \tau}{\partial \rho}\right)_T}{\left(\frac{\partial \ln \tau}{\partial \rho}\right)_P} \tag{2.64}$$

Since changing temperature (T), affects both the thermal energy (k_BT) and the density (ρ), it is impossible to separate the two effects by T alone. In order to disentangle the effects of T and ρ on the dynamics, pressure-dependent measurements have been of paramount importance[49-52] since pressure (P) can be applied isothermally (affecting only ρ), and have been employed to provide a quantitative assessment of their relative importance. Pressure-dependent experiments provide not only the $T_g(P)$ dependence but also the origin of the freezing of the segmental relaxation times (τ_S) at the liquid-to-glass transition. For example, measuring the relaxation times as a function of the thermodynamic variables T, P coupled to the equation of state, allow quantifying the role of temperature and density on the segmental dynamics.[46, 49, 53, 54] The ratio E_V^*/H^* can vary from 0 (corresponding to volume dominated dynamics) to 1 (thermal energy dominates) with the monomeric volume to play a key role in controlling the actual value.[55] This ratio can in principle be calculated for any substance provided that it is possible to measure the $\tau_S(T)$ and $\tau_S(P)$ dependencies, normally through dielectric spectroscopy measurements and the equation of state from PVT measurements.

However, the low dielectric activity in the ethylene/norbornene copolymers precludes such an investigation.
Ferrer et al.[50], however, have shown that the same ratio of activation energies can be obtained from the ratio of the isobaric $\alpha_P = (\partial \ln V/\partial T)_P$ to the isochronic $\alpha_\tau = (\partial \ln V/\partial T)_\tau$ thermal expansion coefficients as

$$\frac{E_V^*}{H^*} = \frac{1}{1-\frac{\alpha_P}{\alpha_\tau}} \tag{2.65}$$

The origin of the liquid-to-glass transition in the cycloolefin copolymers will be discussed in the results and discussion (Section 4.4).

- **Thermodynamic scaling of the glass transition dynamics**

Various approaches have been proposed to account for the scaling of the relaxation time and the very different E_V^*/H^* values for different polymers and glass-forming liquids. A few scaling variables were proposed so far:

- $\log\tau \propto T^{-1}V^{-\gamma}$,[47, 52, 56] where γ is a material constant that provides a measure of the relative importance of ρ as opposed to T. The $\gamma = 4$ is of particular interest since it can be linked[52, 56] with the soft-sphere repulsive forces ($\sim r^{-3\gamma}$) that constitute the first (repulsive) part of the more general distance-dependent potential: $U(r) \propto 4\varepsilon\left[(\sigma/r^{-12}) - (\sigma/r)^{-6}\right]$, where ε and σ have the units of energy and length, respectively. However, very low x values found for some glass-forming systems (with γ as low as 0.13[56]), leading to excessively long-ranged repulsive interactions.
- $\ln\tau \propto (\rho - \rho^*)T^{-1}$, where ρ^* is an adjustable parameter. This thermodynamic scaling gives in many cases equally good results[57-60] except perhaps under very large T and ρ ranges.[59]
- monomer volume V_m and its correlation to the dynamic quantity E_V^*/H^*. It has been shown that $E_V^*/H^* \sim$ 0.72-0.77 V_m for a series of glass-forming liquids suggesting that the reason for the low E_V^*/H^* values in a number of glass-forming liquids and polymers is their large monomer size. This last approach suggests that monomer volume and local packing play a decisive role in controlling the dynamics.

D. Other possibilities beyond free volume and thermal activation

In general, molecular transport is driven by thermal activation processes with potential energy barriers E that depend on local density.[41] Then, the probabilities for local rearrangements can by given by

$$P(V,T) = \exp\left(-\frac{E(V)}{kT}\right) \tag{2.66}$$

Based on eq. 2.66, it becomes apparent that the Arrhenius and the free volume models are two extreme cases of the E vs. V (V is the local volume) dependence (Figs. 2.12a and 2.12b). In the case of the Arrhenius model, a volume independent activation energy is assumed, whereas, in the case of the free volume model, the assumptions made can be interpreted as a discontinuous change of the activation energy at certain V_c, from an infinite value below V_c to 0 above V_c.[41] Figure 2.13 shows the temperature dependencies of relaxation times for the considered models for E(v) in the form of the so called Angel plot. This indicates that a variation of behavior of the model system can

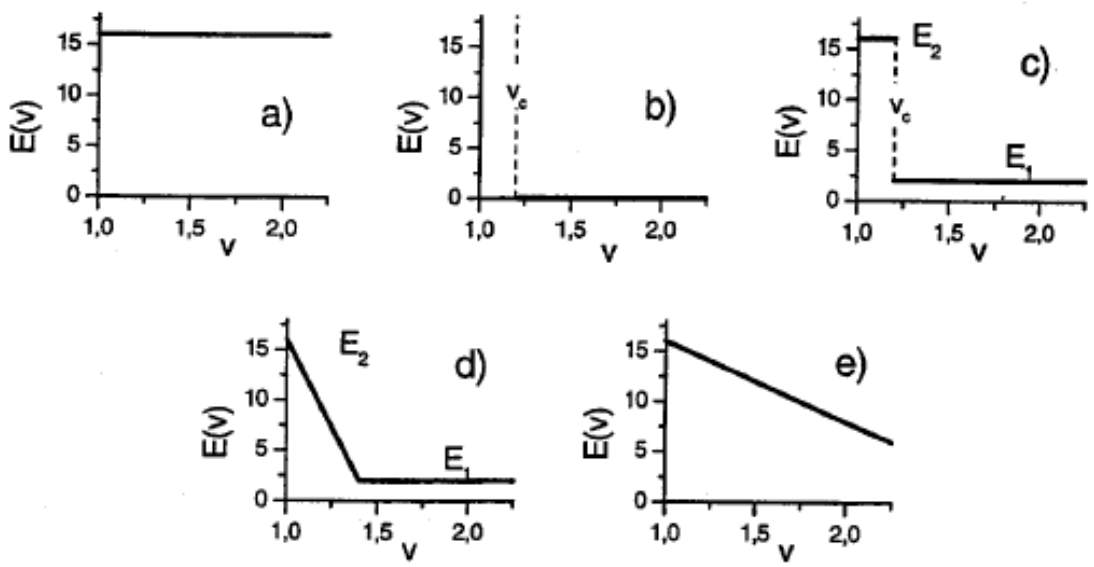

Fig. 2.12 Various dependences of the activation energy for local molecular rearrangements vs. local volume: (a) corresponding to the Arrhenius model, (b) corresponding to the free volume model and (c-e) some other possible dependencies (after T. Pakula, J. Mol. Liq. 86, 2000, 109-121).

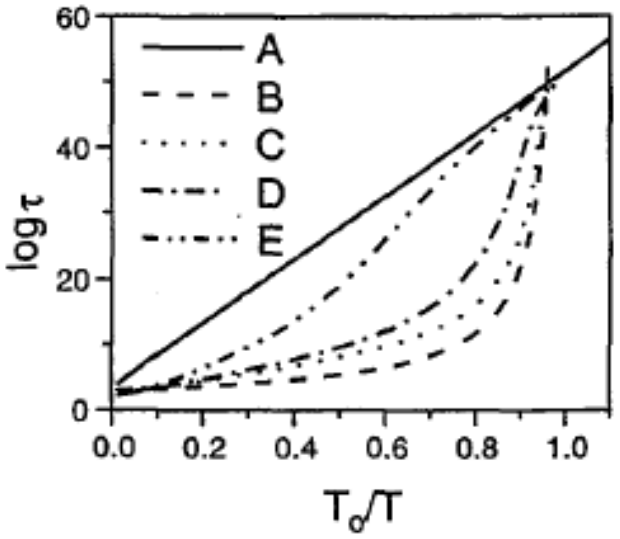

Fig. 2.13 Temperature dependencies of relaxation times calculated using E(v) dependencies shown in Fig. 2.12 (lines A-E correspond to cases (a)-(e) of Fig. 2.12, respectively) (after T. Pakula, J. Mol. Liq. 86, 2000, 109-121).

be obtained which approximately corresponds to the variation of properties observed for real systems. The different activation energies and relaxation time dependencies should be regarded only as examples illustrating the possibilities to describe a class of behaviors ranging between the Arrhenius case, on one side, and the typical non-Arrhenius case described by the traditional free volume model, on the other side.

2.1.6 Proposed fit function for the master curve

In order to fully describe the frequency dependence of storage and loss moduli, all the master curves were successfully fitted to the following function

$$y = \log\left(\frac{A_1}{10^{-b_1(x-lt_1)}+10^{-b_2(x-lt_1)}}+\frac{A_2}{10^{-b_3(x-lt_2)}+10^{-b_4(x-lt_2)}}\right)$$
$$z = \log\left(\frac{A_1}{10^{-c_1(x-lt_1)}+10^{-c_2(x-lt_1)}}+\frac{A_2}{10^{-c_3(x-lt_2)}+10^{-c_4(x-lt_2)}}\right) \quad (2.67)$$

where A_1, A_2 are related to the height of the plateaus of the real part of the modulus (storage modulus) above the frequency corresponding to the reciprocal relaxation time; $lt_1 = -\log\tau_s$, $lt_2 = \log\tau_c$ (τ_s and τ_c are the segmental and chain relaxation times, respectively); $b_1,\ldots, b_4$, $c_1,\ldots,c_4$ are parameters that describe the slopes on both sides of the characteristic frequency related to the reciprocal relaxation. All the fit parameters are illustrated in Figure 2.14.

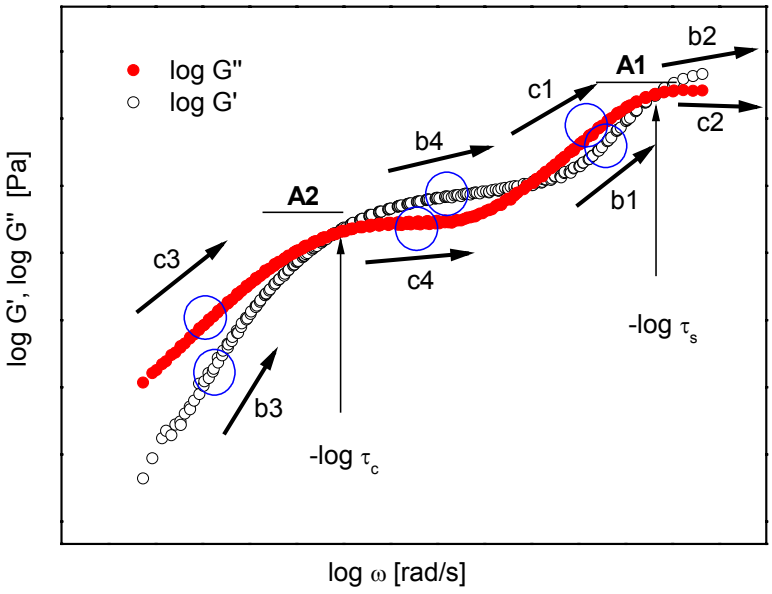

Fig. 2.14 Fit parameters of the empirical function (eqs. 2.67).

2.2 Pressure-volume-temperature dilatometry

Pressure-volume-temperature (PVT) measurements are concerned with the dimensional changes of matter that occur in response to temperature and pressure variations. PVT is a direct thermodynamic method that provides all the required thermodynamic parameters of the system. We will employ this method in studying the dependence of the glass temperature on pressure but in principle it can be applied for studying any phase transitions (crystallization/melting etc.).

If the volume of the material is a function only of the current values of external variables, such as temperature and pressure, and does not depend on the past history of these variables, the material is said to be in an equilibrium state. In this state the volume can be expressed by an equation of state, which describes the dependence of volume on the state variables (T, P).[61] Several empirical and theoretical equations of state are available to describe polymer melts, crystals and glasses. Most useful and used in this work is the empirical Tait equation that describes melts as well as the glassy state[62, 63]

$$V(P,T) = V(0,T)\left(1 - C \cdot \ln\left(1 + \frac{P}{B(T)}\right)\right) \tag{2.68}$$

where $V(0,T) = A_0 + A_1 T + A_2 T^2$, B(T) is a temperature dependent constant with the same dimension as pressure (MPa), V is the specific volume given in cm^3/g, T in °C and P in MPa; C is a constant (best average value: C=0.0894). The temperature dependent factor B(T) can be expressed by

$$B(T) = B_0 e^{-B_1 T} \tag{2.69}$$

where B_0 (in MPa) and B_1 (in $°C^{-1}$) are empirical constants. These parameters for the different copolymers will be given in Chapter 4.

➢ Pressure dependence of glass temperature $T_g(P)$

Increase in pressure results in the increase of the glass transition temperature; this relation can be described using the empirical equation[64, 65]

$$T_g(P) = T_g(0)\left(1 + \frac{\nu}{\mu} \cdot P\right)^{\frac{1}{\nu}} \tag{2.70}$$

where $T_g(0)$ is the glass transition temperature at pressure P=0; ν (dimensionless), μ (MPa) are constant parameters, (P in MPa).

From the PVT data (temperature and pressure dependencies of volume), some useful parameters of the material can be determined. For example, the volume thermal expansion coefficient α_P can be calculated as

$$\alpha_P(P,T) = \frac{1}{V(P,T)}\left(\frac{\partial V(P,T)}{\partial T}\right)_P \tag{2.71}$$

and the isothermal compressibility coefficient κ_T is defined as

$$\kappa_T(P,T) = -\frac{1}{V(P,T)}\left(\frac{\partial V(P,T)}{\partial P}\right)_T \tag{2.72}$$

Knowledge of the Tait equation of state allows extracting all required thermodynamic parameters.

2.3 Positron Annihilation Lifetime Spectroscopy

Positron annihilation spectroscopy (PAS) is a common name for a set of techniques based on measurements and analysis of the annihilation characteristics of a positron e^+ (antiparticle of electron) and its bound form with an electron e^-, so-called positronium (Ps)[66].

Positron annihilation lifetime spectroscopy (PALS) measures positron and positronium lifetimes and their relative intensities, giving information about the physical microstructure of polymers such as the mean free volume hole size, the free volume hole size distribution, the anisotropy of free volume holes and the free volume hole fraction[66]. PALS probes the inter- and intra-chain space on the molecular level, which is related to the chain packing and chain dynamics.[67]

The principle of the technique is as follows: positrons are generated by the radioactive decay of certain unstable isotopes, usually $^{22}_{11}\mathrm{Na}$ in the form of $^{22}\mathrm{NaCl}$. Injection of the positrons into a material causes the loss of their kinetic energy by a sequence of inelastic collisions with the particles of the material. Finally, the positrons annihilate due to interaction with electrons of the substance. Prior to the annihilation, a positron can exist in polymers in a free nonbounded state or as a bound metastable form of positron and electron (positronium - Ps).
There are two ground states of positronium:

1. singlet para-positronium (*p*-Ps) with antiparallel spins with the total spin of the system S=0
2. triplet ortho-positronium (*o*-Ps) with parallel spins with the total spin S=1

Both the positron and positronium annihilation is accompanied by emission of γ rays; two and three γ photons from *p*-Ps and *o*-Ps annihilations, respectively.

The various states of positrons in the condensed phase differ in their lifetime: a short lifetime of *p*-Ps with $\tau_1 \cong 0.1-0.2$ ns, a middle lifetime of free positron annihilation with $\tau_2 \cong 0.3-0.4$ ns, and a long lifetime of *o*-Ps with $\tau_3 \cong 0.5-5$ ns. Of particular interest is the *o*-Ps (τ_3) lifetime, which is sensitive to the free-volume hole size in polymers.

The positron lifetime τ is a function of the electron density at the annihilation site. The annihilation rate λ, which is the reciprocal of the positron lifetime τ, is given be the overlap of the positron density $\rho_+(\vec{\mathrm{r}}) = \left|\psi^+(\vec{\mathrm{r}})\right|^2$ and the electron density $\rho_-(\vec{\mathrm{r}})$

$$\lambda = \frac{1}{\tau} = \pi \mathrm{r}_0^2 \mathrm{c} \int \left|\psi^+(\vec{\mathrm{r}})\right|^2 \rho_-(\vec{\mathrm{r}})\,\mathrm{d}^3\mathrm{r} \tag{2.73}$$

where r_0 is the classical electron radius, c the speed of light, and $\vec{\mathrm{r}}$ the position vector.

Since τ_3 is inversely proportional to the square of the overlap of the positron component of the Ps wave function with the lattice or cavity wall electron wave function, it is therefore related to the size of low electron density free-volume sites.[68]

Assuming spherical free-volume sites of radius R_h, obtained by using a spherical potential of radius R_0 with an electron layer of thickness $\Delta R = R_0 - R_h$, a semiempirical equation between τ_3 in ns, R_h and R_0 in Å was established and optimized (by fitting the observed lifetimes in molecular compounds, such as zeolites and molecular crystals, with the known hole and cavity sizes) with $\Delta R = 1.656$ Å for molecular solids[69-71]

$$\tau_3 = \frac{1}{2}\left[1 - \frac{R_h}{R_0} + \frac{1}{2\pi}\sin\left(\frac{2\pi R_h}{R_0}\right)\right]^{-1} \tag{2.74}$$

Equation (2.74) can be used for the determination of hypothetical radii and volumes of free-volume holes.

The *o*-Ps formation probability is called *o*-Ps intensity, I_3, and is proportional to the number of holes (free volume hole density) in polymers.[72] The free volume fraction is then given by the semiempirical equation

$$f_h = CV_h(T)I_3(T) \tag{2.75}$$

where C is the proportionality coefficient and V_h is the mean hole volume.

- **Positron annihilation lifetime spectroscopy measurements**

All PALS measurements reported herein were made in the Institute of Physics of SAS by Dr. Josef Bartoš. PALS spectra were obtained by the conventional fast–fast coincidence method using plastic scintilators coupled to Philips XP 2020 photomultiplier tubes. The time resolution for the prompt spectra was about 320 ps. All samples were measured for longer than two hours with ^{22}Na positron source of 4 MBq activity. Measurements were performed in the temperature range from 15 – 300 K under vacuum. A standard PATFIT – 88 software package[73] was used to perform a common three component analysis in terms of two short-term components: para – positronium (*p*-Ps), τ_1, and "free" positron, τ_2, as well as a long-term one, related to free volume microstructure: ortho - positronium (*o*-Ps), τ_3.

Samples were prepared by heating around 100°C above T_g and then press moulded under low pressure (<10 MPa) to the thickness of 2 mm. Then they were cut with a diamond saw (to avoid cracks formation) in pieces of 10x10 mm.

2.4 Wide angle X-ray scattering

Wide angle X-ray scattering (WAXS) is a technique used for investigating polymer structure within the size range of around 0.2 to 5 nm. Typically, it is used to provide information about the degree of crystallinity, orientation and the size of any repeat distance in the polymer system. The unit cell, space group and full structure of a crystalline or semicrystalline polymer may be determined as well.[74] In case of amorphous systems inter- and intrachain distances can be obtained, as discussed below.

The scattering of X-rays occurs as a result of interaction with electrons in the material. The X-rays scattered from different electrons interfere with each other and produce a diffractive pattern that varies (if the polymer is not amorphous) with scattering angle. The variation of the scattered intensity with angle provides information on the electron density distribution, and hence the atomic positions in the material.

The sample is irradiated with a collimated beam of X-rays and the scattered intensity as a function of the scattering angle 2θ (the angle between the scattered and incident beam) is measured (Fig. 2.15).

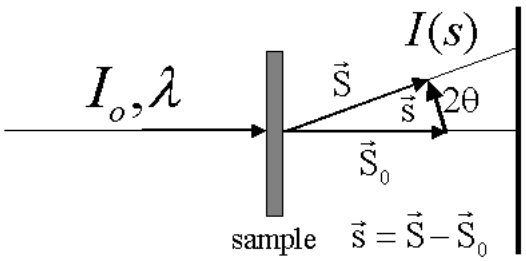

Fig. 2.15 Scattering of X-rays of the intensity I_0 *and the wavelength* λ*. Definition of the scattering vector* $\vec{s}$*.*

The incident and the scattered beams are described by the unit vectors $\vec{S}_0$ and $\vec{S}$, respectively. The scattering vector $\vec{s}$ is defined as

$$\vec{s} = \frac{\vec{S} - \vec{S}_0}{\lambda}, \tag{2.76}$$

where λ is the wavelength of the X-rays. The length of the scattering vector $\vec{s}$ is then

$$s = \frac{2\sin\theta}{\lambda} \tag{2.77}$$

In the literature the scattering vector $\vec{q}$ is often used, which is defined as the difference between the scattering wave vector $\vec{k}_s$ and the incident wave vector $\vec{k}_i$

$$\vec{q} = \vec{k}_s - \vec{k}_i \tag{2.78}$$

Therefore the length of the $\vec{q}$ vector is equal to

$$\vec{q} = \frac{4\pi}{\lambda} sin^2\left(\frac{\theta}{2}\right) \tag{2.79}$$

From equation (2.77) and (2.79) the relation between the two scattering vectors is

$$\vec{q} = 2\pi\vec{s} \tag{2.80}$$

The X-ray waves scattered coherently from individual electrons interfere with each other. The total amplitude of the X-ray beam scattered from a group of n atoms in the direction $\vec{s}$ gives the *structure factor* $F(\vec{s})$

$$F(\vec{s}) = \sum_{n=1}^{N} f_n(\theta) \exp(2\pi i \vec{s} \cdot \vec{r}_n) \tag{2.81}$$

where $f_n(\theta)$ is the atomic structure factor (or scattering factor) for the *n*th atom located at the position $\vec{r}_n$. When the discrete points in positions $\vec{r}_n$ can be replaced by a continuous function, that is, the electron density distribution $\rho(\vec{r})$, equation (2.81) becomes

$$F(\vec{s}) = \int \rho(\vec{r}) \exp(2\pi i \vec{s} \cdot \vec{r}) dv_{\vec{r}} \tag{2.82}$$

where v is the volume sampled.

The scattered intensity $I(\vec{s})$ is proportional to the scattering factor squared

$$I(\vec{s}) \propto F(\vec{s})F^*(\vec{s}) \propto \left|F(\vec{s})\right|^2 \tag{2.83}$$

where $F^*(\vec{s})$ is the complex conjugate of $F(\vec{s})$.

The WAXS spectra of semicrystalline polymers show sharp diffraction peaks whose intensities and widths reflect the frequencies and periodicities, respectively, of some characteristic distances, which can be determined by Bragg's law $2d\sin\theta = \lambda$. The scattering patterns of amorphous polymers lack the sharp diffraction peaks, and hence, they consist of one or more diffusive peaks, called also amorphous halos. Thus, the assignment of a Bragg spacing from the maximum of these halos is only a crude approximation. Hence, in amorphous systems we can only speak about the *equivalent* Bragg spacings.[75] The peak at low and high scattering vector $\vec{q}$ (or $\vec{s}$) is usually referred to as the low van der Waals (LVDW) and van der Waals (VDW) peak, respectively. In amorphous polymers the relative contribution of inter- and intra-molecular correlation to the WAXS curves is still an open issue.

3. Samples and sample characterization

3.1 Samples

Polymers investigated in this work are statistical amorphous cycloolefin copolymers (COC) consisting of ethylene (E) and norbornene (NB) comonomers provided by Dr. M. Bruch, Ticona, Germany. The samples were prepared according to the methods described in ref [9, 76]. The monomers are copolymerized using metallocene catalysts in a solution process. The amount of ethylene can be varied easily by changing the ethylene pressure applied during the polymerization. The glass temperature T_g of the copolymers can be adjusted within a broad range by variation of the concentration of norbornene and the pressure of ethylene. The molecular weight can be adjusted by addition of hydrogen to the reactor vessel. The commercially available copolymers differ in composition from around 36 to 62 molar % of NB, have similar molecular weights (about 10^5 g/mol), and polydispersities in the range from 1.8 to 2.0. The sample characteristics, i.e. number and weight average molecular weights and composition are given in Table 3.1. For comparison purposes a polynorbornene (PNB) sample was examined as well.

Table 3.1 Sample characteristics and thermal properties obtained from DSC (rate 10 K/min).

Sample	M_w x 10^3 [g/mol]	M_n x 10^3 [g/mol]	NB content [mol %]	T_g [K]	Δc_p [J/g/K]
COC1	2.8	1.2	40	326	-
COC2	4.0	1.7	39	320	-
COC3	4.1	2.0	68	423	-
COC4	4.9	1.5	68	420	-
COC5	14.6	5.5	41	327	-
COC6	21	8.1	54	372	-
COC7	26	9.9	66	416	-
COC8	35	14.2	63	403	-
COC9	51	20	67	417	-
COC10	67	16.5	52	415	-
COC11	73	24	65	470	-
COC12	102	52	53	420	-
5013[a]	92	45	50	408	0.37
6013[a]	101	56	52	415	0.31
8007[a]	104	59	36	352	0.39
6017[a]	106	51	62	454	0.30
6015[a]	109	53	56	434	0.35
PNB	-*	-*	100	647	0.30

[a] commercially available copolymers

*: The PNB molecular weights could not be determined because of solubility reasons

3.2 Copolymer microstructure (NMR)

Nuclear Magnetic Resonance (NMR) was employed to identify the microstructure of the copolymers investigated. NMR spectra were obtained using a Bruker DMX500 spectrometer operating at 125.76 MHz for 13C with a 10 mm diameter sample at 363 K. Samples were dissolved in C2D2Cl4, which was used as a reference (chemical shift of 74.00 ppm). The current and earlier NMR[8, 77] and X-ray studies[8, 10, 11, 13, 22] (see also Section 3.3) of the microstructure and local packing provided sufficient evidence for morphological heterogeneity driven by the copolymer microstructure. ^{13}C NMR spectra from all the commercial copolymers (see Table 3.1) are shown in Figure 3.1. Different resonances are shown that are assigned to the different carbons as indicated. The resonance at 47.65 ppm has been assigned to C2/C3 methine carbons in alternating units of the polymer chain. The resonance at 47.0 ppm has been assigned to C2/C3 methine carbons bonded to at least two ethylene units. The broad resonance group between 48 and 52 ppm with a peak at 48.9 ppm has been assigned to C2/C3 methine carbons in blocks of two or more norbornene units. With increasing NB content the relative intensity of the signals at 47.65 and 47.0 ppm decreases suggesting the decrease of the fraction of C2/C3 methine carbons bonded in alternating units and bonded to ethylene sequences of at least two units, respectively. In contrast to this, the relative intensity of the signal at 48.9 ppm increases with increasing NB content. Therefore, in the copolymers with norbornene content above 50 mol%, the structure consists of blocks of norbornene of varying length, linked in both stereogenic positions, together with some alternating norbornene/ethylene units. With decreasing NB content to below 50 mol%, the NMR spectra change; now the intense resonances at 47.65 and 47.0 ppm suggest an increasing fraction of C2/C3 methine carbons bonded in alternating units and to at least two ethylene units, whereas the signal at 48.9 ppm arising from blocks of norbornene is diminished (below 15% in the 8007 copolymer with 36 mol% in NB). Therefore in the copolymers with low norbornene content (below 50 mol%) the structure consists mainly of alternating norbornene/ethylene sequences and some ethylene sequences of two or more units. Overall the NMR data on the current copolymers are in agreement with the ones from ref [8] suggesting the same microstructure in both systems.

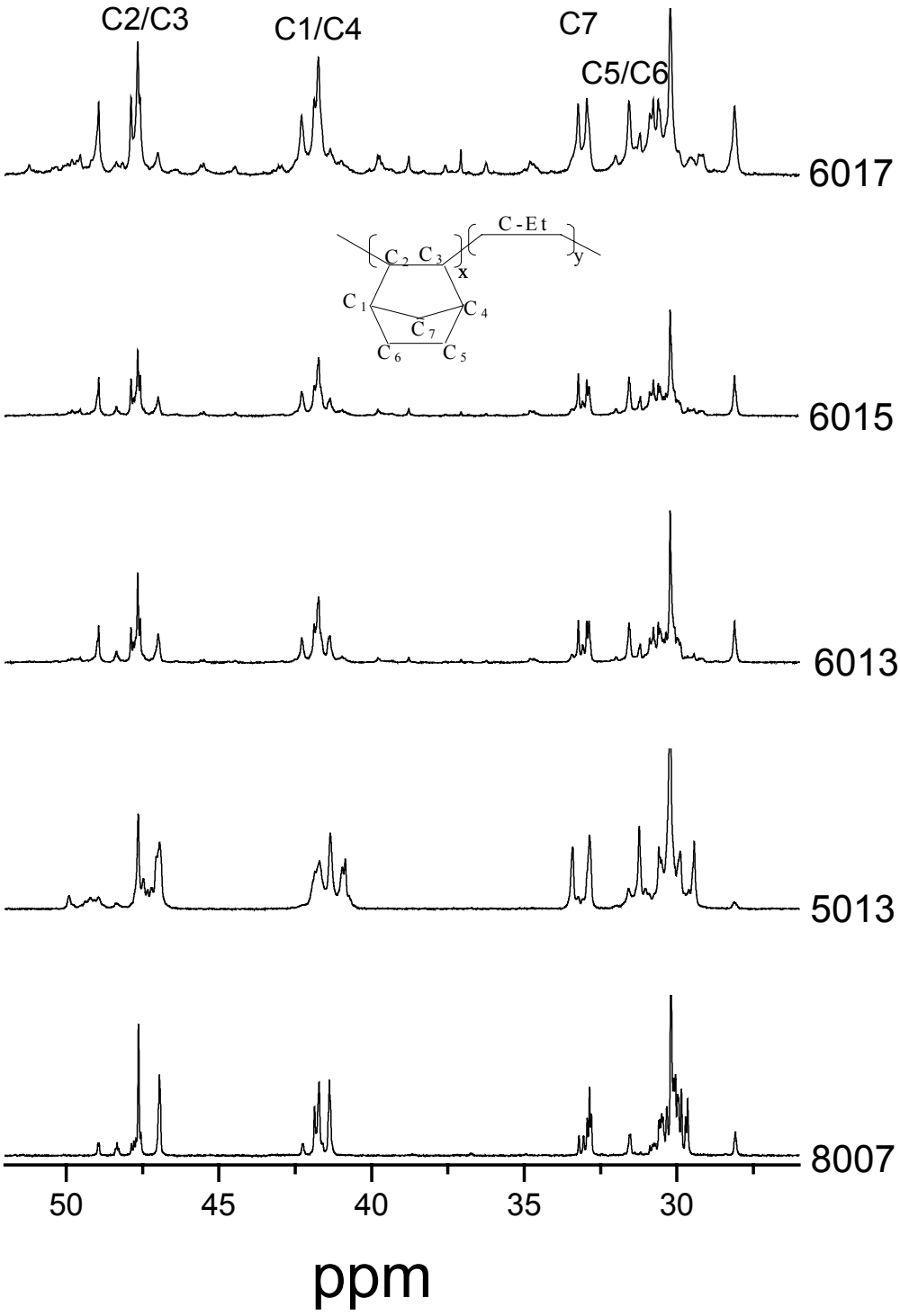

Fig. 3.1 ^{13}C NMR spectra of all the commercial copolymers investigated. The resonances at 47.65 and 47 ppm are related to C2/C3 methine groups in alternating units and C2/C3 methine carbons bonded to at least two ethylene units, respectively. The broad resonance group between 48 and 52 ppm with a peak at 48.9 ppm has been assigned to C2/C3 methine carbons in blocks of two or more norbornene units.

3.3 Structure analysis (WAXS)

WAXS 2D patterns were recorded at room temperature using the X-ray beam with a pinhole collimation and a two-dimensional detector (Siemens Serial A102647) of 1024x1024 pixel resolution. A double graphite monochromator for the CuK_α radiation (λ=0.154 nm) was used. The beam diameter was about 0.5 mm and the sample to detector distance was 83.5 mm. The recorded scattered intensity distributions were integrated over the azimuthal angle and are presented as functions of the scattering vector $\vec{s}$ (see Eq. 2.77).

As already indicated in section 3.2, the NMR studies provided clear evidence for morphological heterogeneity driven by the microstructure. This microstructural heterogeneity reflects also on the local packing as revealed by the wide angle X-ray (WAXS) diffraction patterns of the copolymers and the bulk PNB (Fig. 3.2). The copolymers with less than 50 mol% in NB that, according to the NMR study, have alternating ethylene/norbornene sequences together with ethylene sequences, display a single broad peak in the wide-angle region characteristic of all amorphous polymers (the VDW peak).[75] The peak reflects the closest approach of atoms and for "isotropic", i.e., spherically symmetric molecules, the relation between the diffraction angle maximum

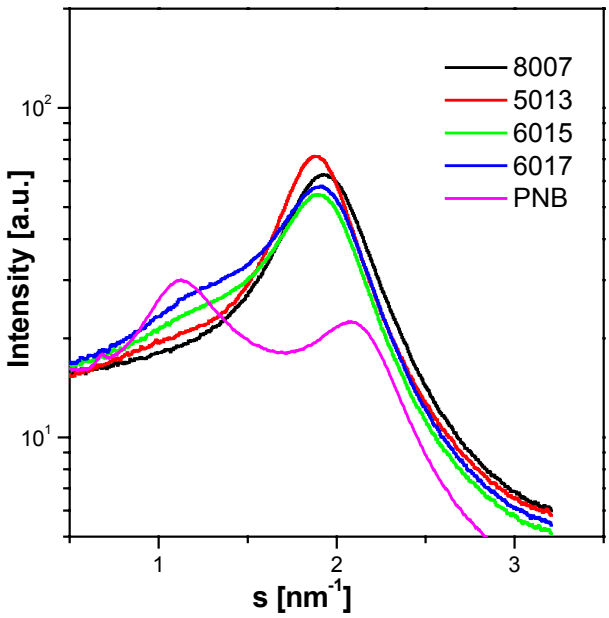

Fig. 3.2 Wide angle X-ray diffractograms of cycloolefin copolymers and the bulk polynorbornene.

(θ_m) and the distance of closest approach (d_m) is $2d_m \sin\theta_m = K\lambda$, where λ is the wavelength and K=1.23 assuming nearest neighbor correlations only.[75] The obtained VDW distance amounts to 0.6 nm for all copolymers. In contrast, the copolymers with higher NB content (above 50 mol%) display increasing intensity at a position characteristic of the bulk PNB scattering with a characteristic distance of 1 nm. This peak (the low van der Waals (LVDW))[65], reflects mainly intramolecular correlation of

the PNB backbone. The existence of the LVDW peak in the NB-rich copolymers is a manifestation of sequence of norbornene units along the chains. This is in accord with the NMR results (see Section 3.2) that have shown the existence of blocks of NB comonomers, together with some alternating norbornene/ethylene units. In the next Chapter (4) we will explore the dynamic consequences of this "static" morphological/structural heterogeneity.

3.4 Differential Scanning Calorimetry (DSC)

A Mettler 30 DSC was used to determine the glass temperatures and the associated step in specific heat. Experiments were conducted with cooling and heating rates of 10 K/min. The glass temperatures (T_g) were determined from the second heating run at the inflection point. The T_g's and associated specific heat steps Δc_p can be found in Table 3.1.

3.5 Pressure-Volume-Temperature (PVT)

For the PVT measurements a GNOMIX high-pressure dilatometer was used, based on the confining fluid principle. In this technique the sample is at all times immersed in a confining fluid (mercury in this case) and the combined volume changes of sample and confining fluid are measured. PVT data consists of records of the specific volume of a material as a function of pressure and temperature. The volume changes in the sample can be calculated by subtracting the known volume change of mercury. A detailed description of the apparatus can be found in the book of Zoller[78]. Prior to the first run (in isothermal mode) every sample was heated to remove the internal stresses caused by press moulding of the specimens. The samples in the shape of a cylinder were made from around 1g of the material.

Measurements of volume changes were first carried out in the isothermal mode. At a fixed temperature, starting at low temperature (heating mode), the pressure was increased from 10 to 200 MPa. On completion of measurements along one isotherm, the temperature was decreased, then the pressure changed and a new measurement begun. These isothermal measurements were followed by the measurements in the isobaric mode in the range of 10 to 200 MPa and for temperatures in the range from 293 to 590 K. Starting from low pressures, the volume change was measured in the heating mode. Absolute density measurements of the copolymers, at ambient temperature, were made using a helium pycnometer (Quantachrome micropycnometer model MPY-2). The temperature dependencies of specific volume for various pressures obtained in the isobaric mode were fitted *simultaneously* to the Tait equation (2.68); the regions below and above the glass transition were fitted separately.

3.6 Dynamic mechanical spectroscopy (DMS)

Dynamic mechanical spectroscopy measurements on the copolymers were made with a Rheometrics Mechanical Spectrometer RMS 800, which is schematically illustrated in Figure 3.3. For the measurements above the glass temperature, samples (pellets of 6 mm diameter and around 1 mm thickness) were placed between two parallel plates. The specimens were first heated above T_g to become soft, and therefore a good contact to the plates could be established. The measurements started from high temperatures and proceeded to lower temperatures. The examination at low temperatures (below the glass temperature) was performed using a rectangular bar geometry (Figure 2.2 c) and nitrogen as a cooling medium. In this latter experiment the sample dimensions were 60 x 10 x 1 mm. Different shear experiments were made:

⇒ "isothermal" strain sweeps at different temperatures aiming at separating the linear from the non-linear viscoelastic regimes. The strain dependent torque was measured and compared with the strain dependence of storage (G') and loss (G'') moduli (Fig. 3.4).

⇒ "isothermal" frequency sweeps, aiming at obtaining the compete viscoelastic response. In the frequency range of 0.1-100 rad/s the storage (G') and loss (G'') moduli were determined at various temperatures (Fig. 3.5). The value of the torque (the deformation) was chosen to within the linear regime.

⇒ "isochronal" temperature scans at selected frequencies (1, 10 and 100 rad/s), aiming at obtaining the different dynamic processes, particularly at low temperatures (sub-glass processes). The G' and G'' moduli for these frequencies were obtained simultaneously using the so-called multiwave temperature ramp test in which the sample is subjected to deformation being a superposition of sinusoidal signals of these three frequencies (Fig. 3.6). The results from the isochronal sweeps all correspond to the linear regime.

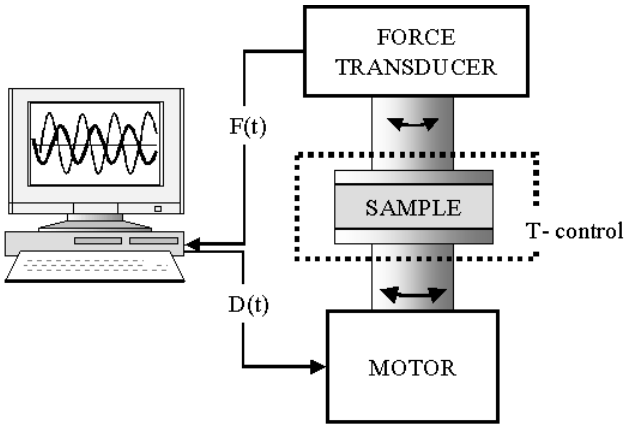

Fig. 3.3 A schematic illustration of the dynamic mechanical spectrometer system. The deformation (shear strain) input signal D(t) is applied by the motor and the resulting torque F(t) is measured by the force transducer. The sample is placed between two parallel plates with the possibility of temperature control measurements.

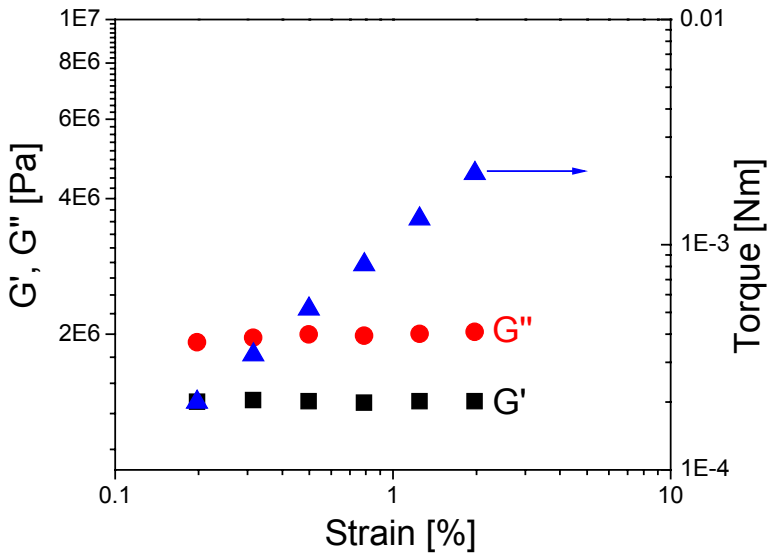

Fig. 3.4 Isothermal strain sweep for an ethylene-norbornene copolymer taken as an example. The sample is sheared between two plates (see Figure 2.2) and the resulting torque is recorded. Notice the insensitivity of the shear moduli to the applied strain (linear viscoelastic regime).

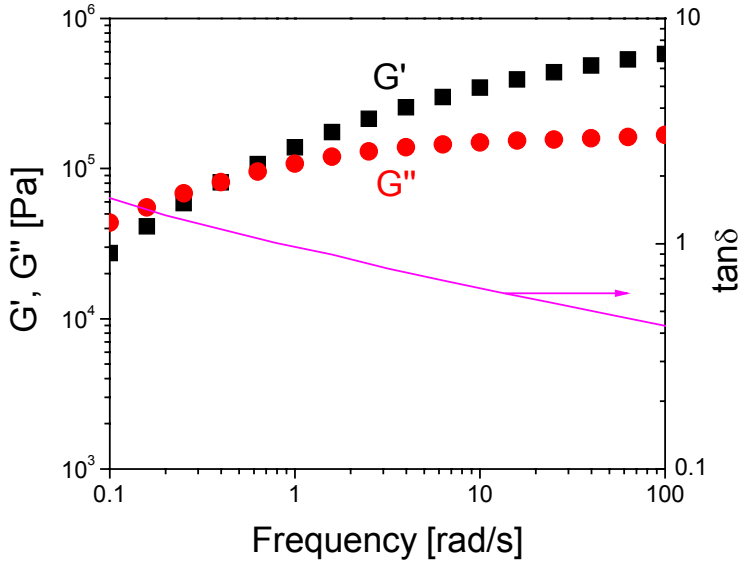

Fig. 3.5 Exemplary isothermal (T=135°C) frequency sweep (0.1-100 rad/s) from an ethylene-norbornene copolymer sample. The storage (G'), loss (G'') modulus and tanδ were determined from equations (2.15).

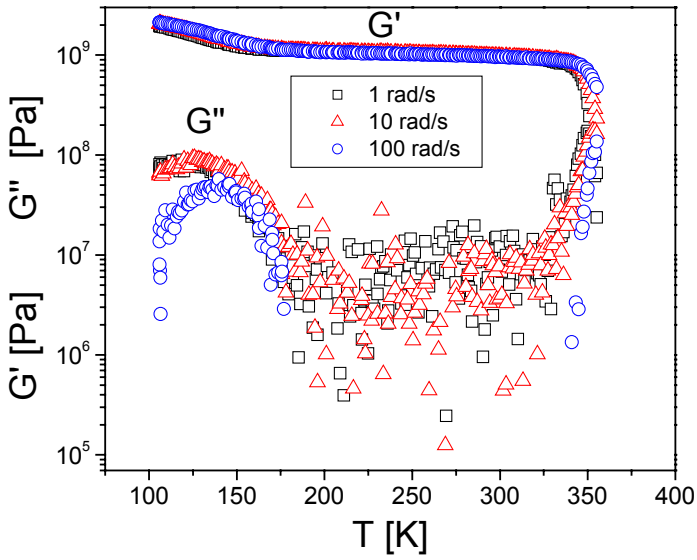

Fig. 3.6 Temperature dependence of storage G' and loss G'' moduli obtained with the rectangular bar geometry (see Fig. 2.2, geometry c). All the frequencies (1, 10, 100 rad/s) were measured simultaneously. The different dynamic processes in the glassy state will be explained later in Chapter 4.

4. Results and discussion

4.1 Free volume in cycloolefin copolymers (PALS)

Positron annihilation lifetime spectroscopy (PALS) is a technique that allows obtaining information about the free volume in the polymer system (see Section 2.3 for details). PALS was applied in an effort to understand how the free volume affects the molecular mobility below the glass temperature. To study the dynamic processes in the glassy state we employ rheology and perform isochronal heating experiments on three copolymers (8007, 6013 and 6017). The results of these experiments are depicted in Figure 4.1. Notice that within the temperature range shown the storage moduli of these copolymers display values typical of glassy polymers (G'~10^9 Pa). Three different molecular processes were found: the segmental α-process, and the low temperature β - and γ - processes.

The high temperature segmental process is related to the unfreezing of the backbone dynamics. The position of this process displays a strong dependence on NB content and shows the influence of the more rigid NB units on slowing-down the copolymer backbone dynamics. The effect of NB content on the temperature dependence of dynamics of both segmental and terminal relaxation times is described in Section 4.5. The origin of the α-process will be discussed in Section 4.4 with respect to the thermal (see Section 4.2) and thermodynamic (Section 4.3) results.

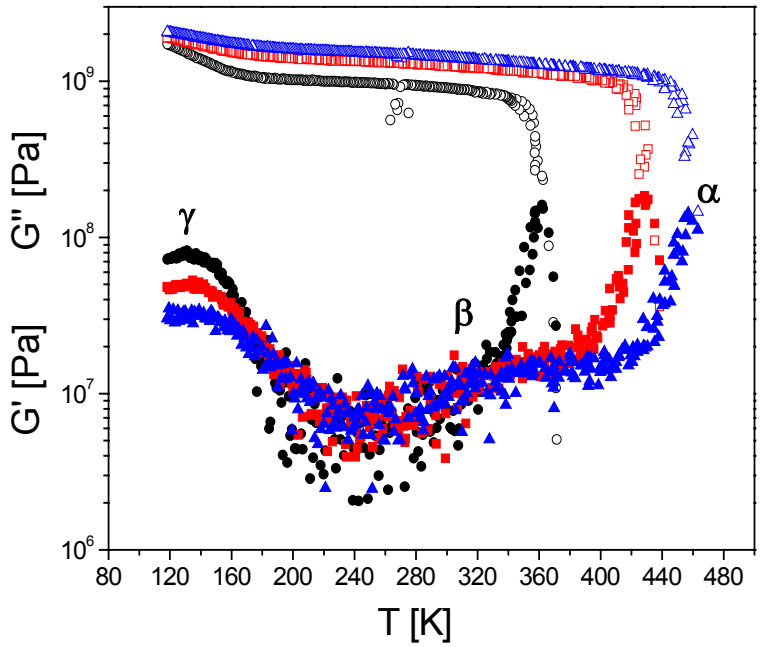

Fig. 4.1 Isochronal (ω=10 rad/s) heating runs of the storage (G': open symbols) and loss (G'': filled symbols) shear moduli for three copolymers: (circles): 36% in NB, (squares): 52%, (triangles): 62 %. Three main processes are seen denoted as γ, β and α.

At T~120 K the stepwise decrease of the storage moduli and the concomitant maximum in the loss moduli signify the presence of a process (γ-process) well within the glassy state. The strength of this process is increasing with ethylene content and its location is suggestive of a local process of the ethylene units in the copolymers. In Figure 4.2, the relaxation times corresponding to the maximum loss are plotted in the usual Arrhenius representation. The temperature dependence of the characteristic frequency at the G'' can be parameterized according to the Arrhenius equation

$$\tau = \tau_0 \exp\left(\frac{E}{RT}\right) \tag{4.1}$$

where τ_0 is the attempt rate at high temperatures and E is the activation energy. The values of τ_0, and E are $6.8\text{x}10^{-14}$, $1.6\text{x}10^{-17}$, $4\text{x}10^{-22}$ s and 30, 39 and 52 kJ/mol for the copolymers with 36, 52 and 62 % of NB, respectively (the very fast time for the 62% results from the limited frequency range over which was determined). The increasing activation energy with increasing NB content suggests an increasing hindrance by the presence of NB. Therefore, although the γ-process originates solely from the ethylene units, the increasing NB content hinders its mobility at least in the copolymers with the higher NB content.

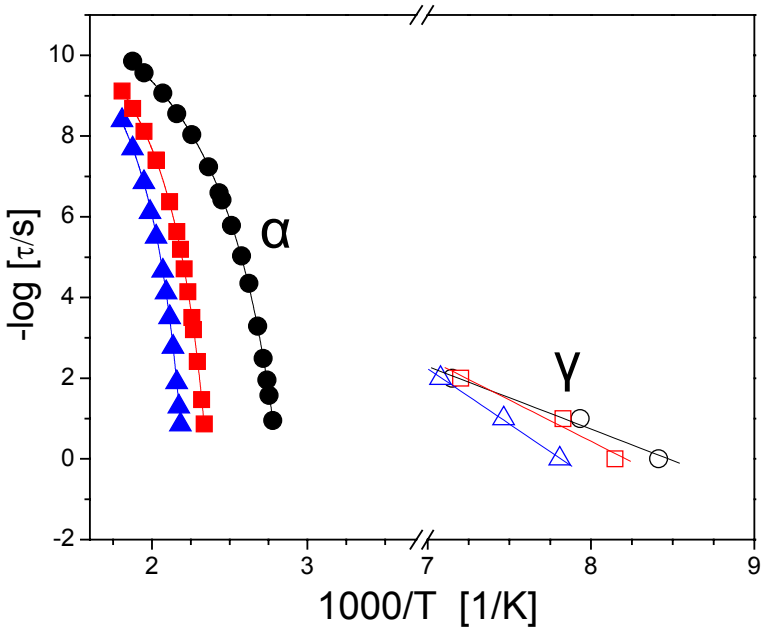

Fig. 4.2 Temperature dependence of the relaxation times in the usual Arrhenius representation. The relaxation times correspond to the segmental (α) process (filled symbols) and to the local (γ) process (open symbols). The lines are fits to the VFT ($T>T_g$) and Arrhenius ($T<T_g$) temperature dependencies (see text): (circles): 36%, (squares): 52%, (triangles): 62 %.

At even higher temperatures another broad process appears which is more clearly seen in the loss modulus (β-process). The origin of this very weak glassy process is

unclear at present but its small amplitude, the weak temperature dependence, the dependence on thermal history and its location, being in the vicinity of the primary segmental process, suggests inhomogeneous stress relaxation.

In order to understand how these molecular processes in the glassy state are affected by the free volume, *o*-Ps annihilation measurements were conducted on a series of copolymers (8007, 6013 and 6017), as well as on the bulk PNB, at room temperature (see Fig. 4.3). We can observe that the *o*-Ps lifetime, τ_3, increases gradually with increasing percentage of molar mass of norbornene comonomer. The minimal τ_3 value

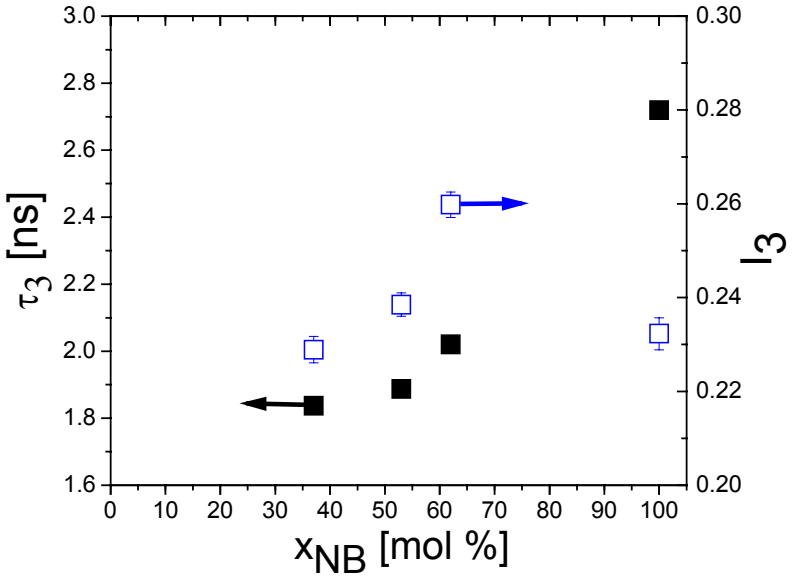

Fig. 4.3 Mean o-Ps lifetime, τ_3 (filled symbols), and relative intensity, I_3 (open symbols), on a series of copolymers (8007, 6013 and 6017) and the pure polynorbornene, at room temperature, plotted as a function of the composition.

is found for the copolymer with the highest content of ethylene comonomer, while the maximal τ_3 value is reached for the pure norbornene polymer. The other *o*-Ps annihilation quantity, *o*-Ps relative intensity I_3, exhibits a non-monotonous trend over the compositional range investigated. After an initial increase in I_3 with increasing molar % of NB from 36% up to 62%, the value for pure PNB falls on a level of the copolymer with the lowest content of NB.

The mean *o*-Ps lifetime, τ_3, as a measure of the spatial extent of local region of reduced electron density, can be converted into free volume hole radius, R_h, by means of the simple quantum - mechanical model following equation (2.74) (Section 2.3). Figure 4.4 shows the mean hole volume given by $V_h = (4\pi/3)R_h^3$, as a function of norbornene molar fraction (x_{NB}). As expected, V_h increases with increasing x_{NB}, and the highest volume corresponds to the pure PNB.

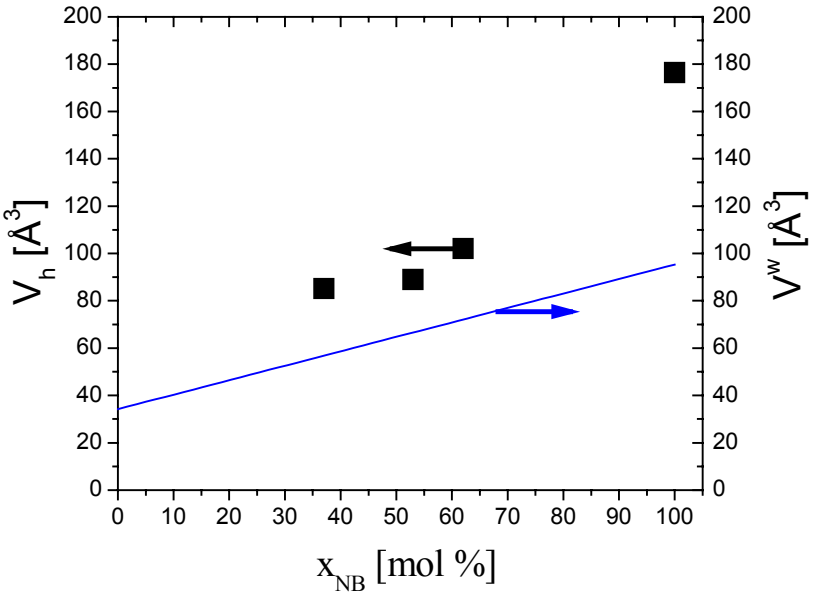

Fig. 4.4 Mean free volume hole size, V_h (symbols), and van der Waals volume of copolymer "unit", V^W (solid line), plotted as a function of norbornene content at ambient temperature.

To get some idea about the relative size of free volume hole regions, the V_h values can be compared to van der Waals volumes of both the respective monomer units as well as the compositionally averaged van der Waals volume of the copolymer "unit". The latter can be calculated from the following equation

$$V^W_{E-co-NB} = (1 - x_{NB})V^W_E + x_{NB}V^W_{NB} \qquad (4.2)$$

where V^W_E and V^W_{NB} are the van der Waals volumes of ethylene and norbornene monomer, being 34.2 Å ^{3} or 95.3 Å^3, respectively. From comparison of $V_h(x_{NB})$ with $V^W_{E-co-NB}(x_{NB})$ it follows that the mean free volume hole size is larger than the corresponding basic structural units of both monomer units as well as the compositionally averaged monomer "unit" of copolymers. At low contents of NB the mean free volume hole sizes reach about (1.4-1.5)x $V^W_{E-co-NB}(x_{NB})$. On the other hand, for the pure PNB the mean free volume hole size reaches to a value about twice the size of the NB monomer unit. These findings can be related to a difference in the chemical constitution of the respective monomers as well as their "statistical" (see Section 3.2 for details about the COC microstructure) distribution along the chains. Ethylene structural units are generally known to be flexible compared to norbornene ones as demonstrated, e.g., by a huge difference in the respective T_g values (see subsequent section). The rigidity of NB comonomers manifests profoundly also in the slowing-down process of the relaxation times as it approaches its glass temperature, and hence affects the origin of the liquid-to-glass transition (see Section 4.4). Thus, the similar values of V_h for the 8007 and 6013 copolymers suggest a localization of free volume holes in the vicinity of ethylene units linking larger NB units. On the other hand, the higher content of NB

comonomer implies larger mean hole volume size due to less effective packing of chain segments from relatively more rigid NB units. The observed large holes in bulk PNB and the finding of the minimal relative intensity, I_3, (being proportional to the free volume hole density[72]), suggests that a lower number of free volume holes but of a larger size are present in PNB.

It is of interest to make comparison between the mean free volume hole size and the actual comonomer volume. For this purpose PVT and the absolute density measurements (using a helium pycnometer) were made on the different copolymers with NB content: 36, 52 and 62 mol %. The results for the specific volume, at P = 0.1 MPa, are depicted in Figure 4.5; the complete thermodynamic equation of state will be discussed in more detail with respect to the origin of the glass transition (see Section 4.4). Notice the

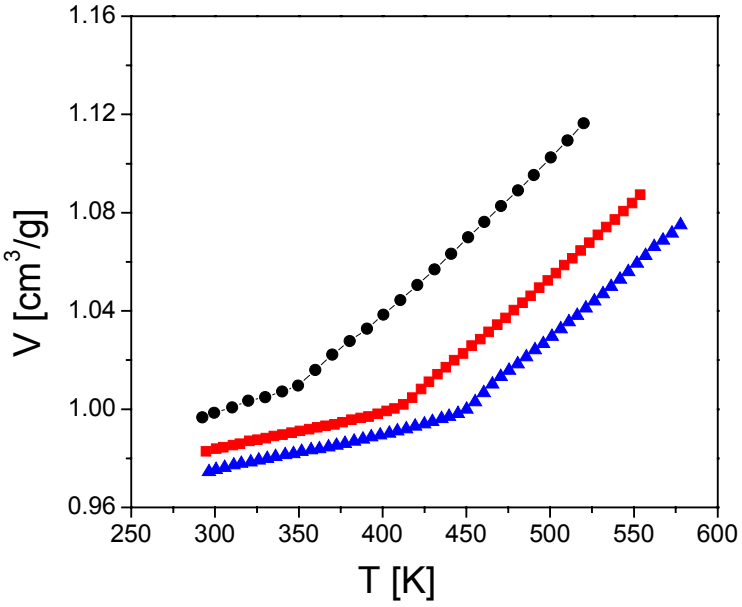

Fig. 4.5 Temperature dependence of the specific volume at P=0.1 MPa, for three copolymers; (circles): 36%, (squares): 52%, (triangles): 62 %. Notice the change in slope at the respective T_g.

change in slope at the respective T_g's that are in good agreement with the results from DSC and rheology (extrapolated α-relaxation times to a time of 100 s). From the slopes ($\beta = d(\ln V)/dT$) the thermal expansion coefficients were determined below and above T_g and are given in Table 4.1. The values of these coefficients decrease with NB content, which is observed both, below and above the glass transition temperature. The macroscopic volume of NB and E comonomers (V_{E+NB}) as a function of weight fraction can be determined from

$$V_{E+NB} = \frac{(1 - x_{NB}) \cdot M_E + x_{NB} \cdot M_{NB}}{\rho \cdot N_A} \qquad (4.3)$$

Table 4.1 Characteristics of the copolymers samples.

Norbornene content [x_{NB} %mol]	M_w [g/mol]	T_g [K]	ρ [g/cm^3]	β*10^{-4} [1/K] T<Tg	β*10^{-4} [1/K] T>Tg
36	104000	352	1.0031	2.29	6.05
52	101000	415	1.0177	1.47	5.73
62	106000	454	1.0260	1.42	5.43

where M_E and M_{NB} are the molar weights of ethylene and norbornene molecules, being 28.054 and 94.156 g/mol, respectively. The density ρ increases with increasing norbornene comonomer content from 1.0031 to 1.0260 g/cm^3 for specimens of 36 and 62 mol % of NB, respectively (Table 4.1). In Figure 4.6 the result of the analysis of the

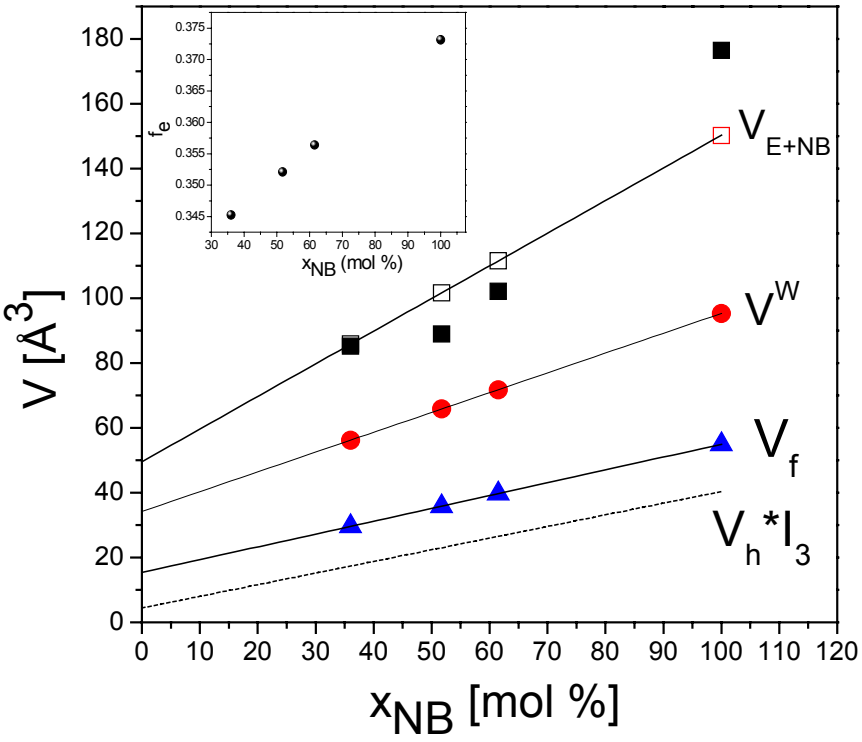

Fig. 4.6 Dependence of the free volume on norbornene content for the cycloolefin copolymers at room temperature. The filled squares give the average hole volume (PALS), the open squares the macroscopic volume of the ethylene-norbornene comonomer "unit" calculated from eg. (4.3), the filled circles give the van der Waals volume (V^W) calculated from eq. (4.2), the filled triangles give the empty free volume determined as V_{E+NB}-V^W. The dashed line shows the free volume as determined from PALS. Solid lines represent linear fits of the above-described quantities. In the inset the empty fractional free volume (f_e) is plotted as a function of composition for the same copolymers.

mean free volume hole size and its relation to the macroscopic volume of comonomer "unit" of COC is presented. It can be observed that the total macroscopic volume of E and NB molecules, V_{E+NB}, is comparable to the mean free volume hole size, V_h, determined by PALS, and that both quantities are increasing functions of the NB molar content. The macroscopic volume of copolymers, V_{E+NB}, increases faster than the van der Waals volume, the latter being determined by eq (4.2). The empty free volume in polymer matrices can be obtained by subtracting the van der Waals volume ($V^W_{E-co-NB}$) from the macroscopic volume (V_{E+NB}). The thus calculated empty free volume, V_f, is also plotted in Figure 4.6. Clearly, the empty free volume, connected with the structural unit, increases with NB content and is smaller than the corresponding mean free volume hole size. This points to a heterogeneous distribution of free volume accessible for *o*-Ps probe in the real systems. In addition to the free volume size, the fractional empty free volume, often used to characterized solid state chain packing, can be calculated as

$$f_e = \frac{V_{E+NB} - V^W_{E-co-NB}}{V_{E+NB}} \tag{4.4}$$

where V_{E+NB} is the specific volume of system from eq. 4.3, and $V^W_{E-co-NB}$ is the compositionally averaged van der Waals volume from eq. 4.2. This quantity is also plotted in Figure 4.6 as an inset and displays an increase with increasing NB content. The difference in the respective slopes for the fractional free volume, f_h, determined from PALS ($f_h \sim V_h \cdot I_3$) and f_e can be attributed to the fact that while the fractional empty free volume represents the entire free space in static structure for an infinitely small probe (such a probe has spatially unlimited access), the measurable free volume hole fraction from PALS, f_h, reflects its part accessible for the finite size of *o*-Ps probe in the real fluctuating structure.[79]

The results of the free volume analyses, namely the increase of (i) the mean free volume size, V_h, of (ii) the free volume hole fraction from PALS, $f_h \sim V_h \cdot I_3$, as well as of (iii) the empty free volume, f_e, from PVT with NB content is attributed to packing irregularities associated with the larger NB monomer as compared to ethylene.

4.2 Thermal properties

The DSC traces of the ethylene/norbornene copolymers and the bulk polynorbornene (PNB) are shown in Figure 4.7. The glass transition and the associated specific heat step, Δc_p, are included in Table 3.1. The thermograms reveal a single glass temperature that increases with the content of the NB comonomer in the backbone. The T_g of PNB (647 K) occurs prior to the degradation, which was determined by thermogravimetric analysis to appear at around 683 K (Fig. 4.7, right).

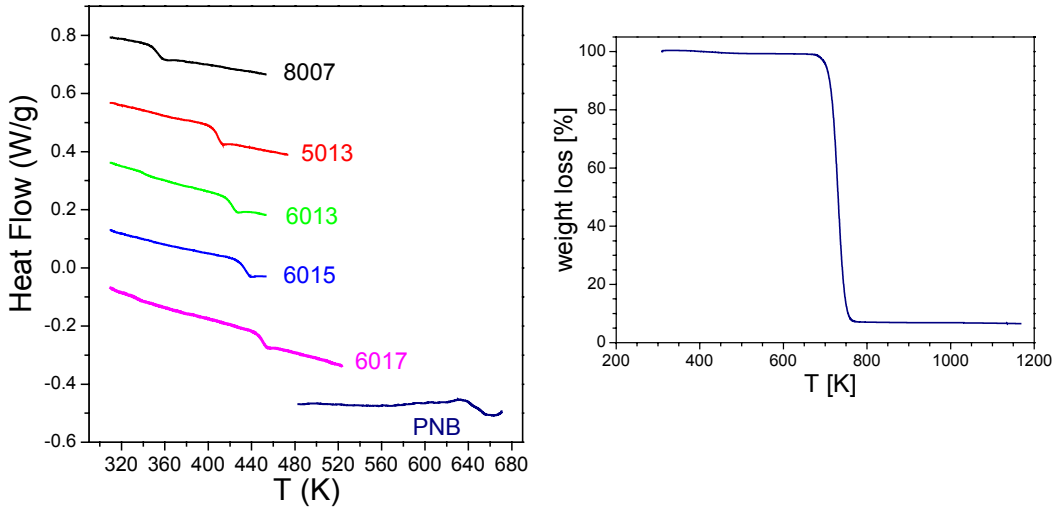

Fig. 4.7 (left): DSC traces obtained during the second heating run (rate 10 K/min) for the copolymers and the polynorbornene (PNB) homopolymer; the traces have been shifted vertically for clarity, (right): thermogravimetry of polynorbornene (rate 10 K/min)

Despite the large variation of ethylene comonomer in the copolymer, no crystallization could be observed. This means that the copolymers are fully amorphous within the investigated composition range. The single glass transition and the absence of any trace of ethylene crystallization suggest miscibility. However, as it was already shown in section 3.2 and 3.3 and will be shown in sections 4.3 and 4.4, the pressure dependence of T_g, the temperature dependence of the α-relaxation times and the ratio of activation energies E_V^*/H^* used to quantify the origin of the liquid-to-glass transition, provide evidence for local dynamic heterogeneity.

Several equations relating glass temperature of initial components to the glass temperature of the resulting blend, provided that the system is completely miscible. One of the most frequently used is the Fox equation

$$\frac{1}{T_g} = \frac{w_{PE}}{T_g^{PE}} + \frac{w_{PNB}}{T_g^{PNB}} \tag{4.5}$$

where w_i is the weight fraction of the components and T_g^i the corresponding glass temperature.

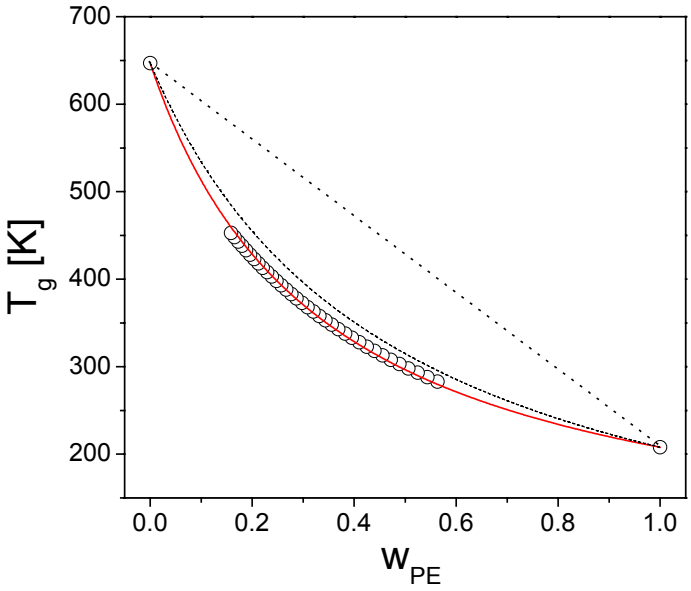

Fig. 4.8 Dependence of glass temperatures T_g on PE composition in the copolymers. The circles correspond to interpolations from various copolymer compositions. For the PNB and PE homopolymers the temperatures of 647 K and 208 K were used, respectively. The dashed line gives the prediction of the Fox equation (eq 4.5), whereas the solid (red) line is the prediction of the DiMarzio equation (4.6) with r=0.253. The dotted line is the linear rule.

For the homopolymer glass temperatures the measured T_g of PNB and the literature[80] value for PE (T_g^{PE} ~ 208K) were used. From Figure 4.8 can be seen that this equation (dashed line) does not adequately describe the compositional dependence of the glass transition temperature. Alternatively, the DiMarzio equation[81] (solid line), with one adjustable parameter (r = 0.253)

$$T_g = \frac{w_{PE} T_g^{PE} + r \cdot w_{PNB} T_g^{PNB}}{w_{PE} + r \cdot w_{PNB}} \qquad (4.6)$$

provides a better (albeit not perfect) description of the experimental data (Fig. 4.8). Nevertheless, both eqs. (4.5 and 4.6) have a shortcoming: both require knowledge of the pure component T_g's. Although the T_g of PNB is measured here, the T_g of PE is still an open issue (depends strongly on crystallinity, etc.)

4.3 Thermodynamic properties

The discussion on the origin of the liquid-to-glass transition requires knowledge of the system's thermodynamic state, i.e., of the PVT equation of state. The PVT measurements of the different copolymers are shown in Figures 4.9-4.12. The empirical Tait equation (2.68), was used to describe both the melt and the glassy state of the cycloolefin copolymers. The values of the fit parameters, A_0, A_1, A_2, and B_0, B_1, below and above T_g are summarized in Table 4.2.

Table 4.2 Parameters of the Tait equation used to describe the PVT data.

Sample	A_0 (cm^3/g)	A_1 ($cm^3/g/°C$)	A_2 ($cm^3/g/°C^2$)	B_0 (MPa)	B_1 ($°C^{-1}$)
8007					
$T<T_g$	0.995	$9x10^{-5}$	$8x10^{-7}$	282	$1.5x10^{-3}$
$T>T_g$	0.952	$6.5x10^{-4}$	$-5x10^{-9}$	272	$4.2x10^{-3}$
5013					
$T<T_g$	0.974	$1.3x10^{-4}$	$2x10^{-7}$	233	$5.7x10^{-4}$
$T>T_g$	0.919	$5.7x10^{-4}$	$1x10^{-7}$	236	$3.7x10^{-3}$
6013					
$T<T_g$	0.981	$1.1x10^{-4}$	$1x10^{-7}$	302	$1.2x10^{-3}$
$T>T_g$	0.927	$5.5x10^{-4}$	$-3x10^{-8}$	238	$3x10^{-3}$
6017					
$T<T_g$	0.974	$9x10^{-5}$	$2x10^{-7}$	265	$8.7x10^{-4}$
$T>T_g$	0.912	$5.6x10^{-4}$	$-2x10^{-7}$	188	$2.2x10^{-3}$

All the temperature and pressure dependencies of the V(T,P) data shown in Figures 4.9-4.12 were *simultaneously* fitted to this equation. However, the regions below and above the glass transition were fitted separately. From the crossing of the respective V(T) "isobars" below and above T_g, the $T_g(P)$ can be obtained and is plotted in Figure 4.13. A strong and non-linear pressure dependence, which agrees with the majority of polymers and glass-forming liquids, can be observed. The $T_g(P)$ dependence can be parameterized according to $T_g(P) = T_g(0)(1 + \nu/\mu \cdot P)^{1/\nu}$ (eq. 2.70). The ν and μ fit parameters in this equation are summarized in Table 4.3. The initial slope $(dT_g/dP)_{P\to 0}$ from the $T_g(P)$ dependence is also included in this Table. It can be seen that the slope exhibits composition dependence with significantly higher values for the copolymers with higher NB content; these values are among the highest reported for homopolymers.[53] This suggests an even stronger $T_g(P)$ dependence in bulk PNB, however, the high glass temperature of PNB precludes PVT measurements above T_g.

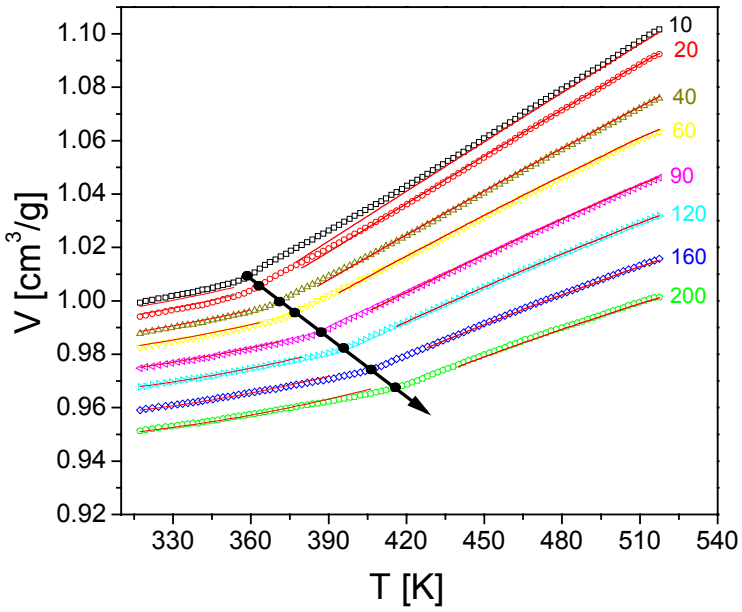

Fig. 4.9 PVT data for the 8007 copolymer obtained under "isobaric" conditions. Different isobars are shown within the pressure range 10-200 MPa. Notice the change of slope at the glass temperature. The lines are fits to the Tait equation (see text).

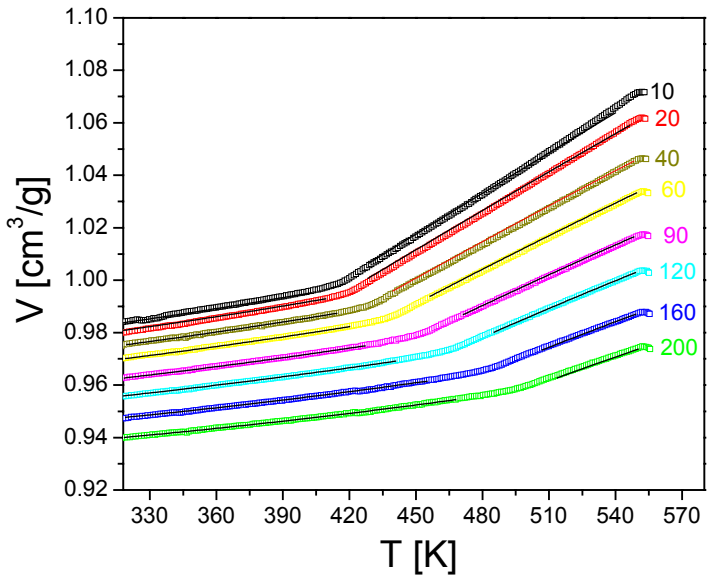

Fig. 4.10 PVT data for the 6013 copolymer obtained under "isobaric" conditions.

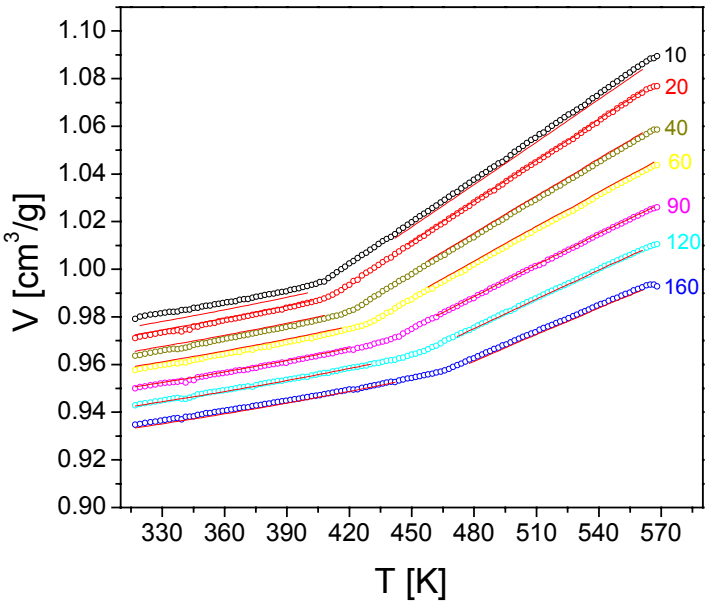

Fig. 4.11 PVT data for the 5013 copolymer obtained under "isobaric" conditions.

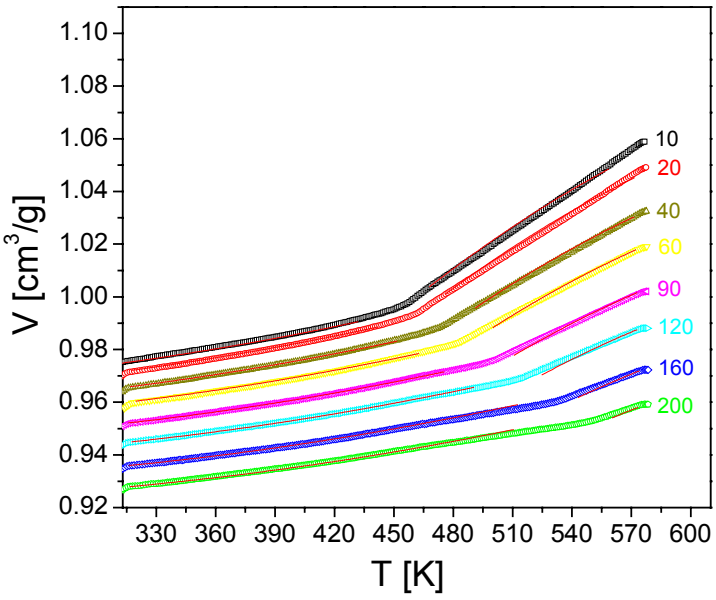

Fig. 4.12 PVT data for the 6017 copolymer obtained under "isobaric" conditions.

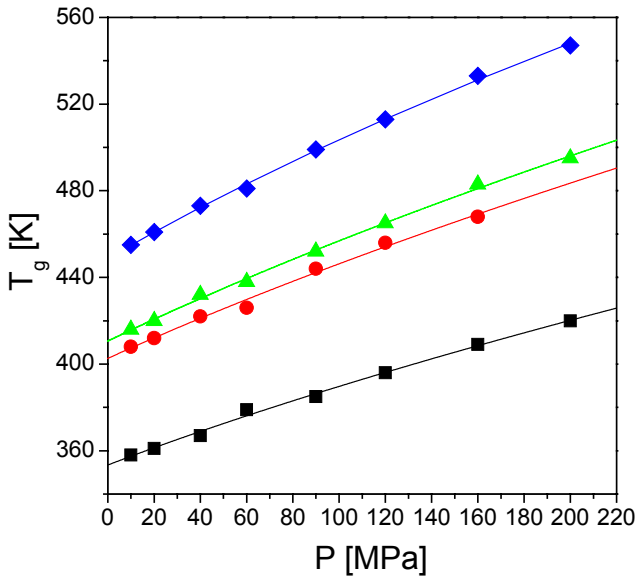

Fig. 4.13 Pressure dependence of the glass temperatures obtained from PVT; (squares): 8007, (circles): 5013, (up triangles): 6013 and (rhombus): 6017. The lines are fits to eq. (2.70).

Table 4.3 Parameters of the $T_g(P)$ dependence.

Sample	$T_g(0)$ [K]	ν	μ [MPa]	$\left.\frac{dTg}{dP}\right\|_{P\to 0}$ [K/MPa]
8007	352	3.87	792	0.44
5013	403	2.83	836	0.48
6013	411	2.77	807	0.51
6017	448	3.08	723	0.62

Nevertheless, these distinct dependencies call for some type of heterogeneity along the backbone that is exemplified in COC with higher NB content. As we will see below the pressure dependence can be used to quantify the origin of the liquid-to-glass “transition” in the copolymers.

4.4 Origin of the liquid-to-glass "transition" in the copolymers

The ratio of activation energies, E_V^*/H^*, can be obtained from the isobaric α_P and the isochronic α_τ thermal expansion coefficient as follows: $E_V^*/H^* = 1/(1-\alpha_p/\alpha_\tau)$ (see Section 2.1.5, eq. 2.65). The isobaric thermal expansion coefficient eq. (2.71) is determined from the Tait equation above T_g generated for 0.1 MPa; it is the slope of the linear region in the lnV vs. T plot (Fig. 4.14). The isochronic coefficient is calculated from $\alpha_\tau = d(\ln V(T_g))/dT_g(P)$, illustrated by the arrow in Figure 4.14, under the assumption that T_g occurs at isochronal conditions.

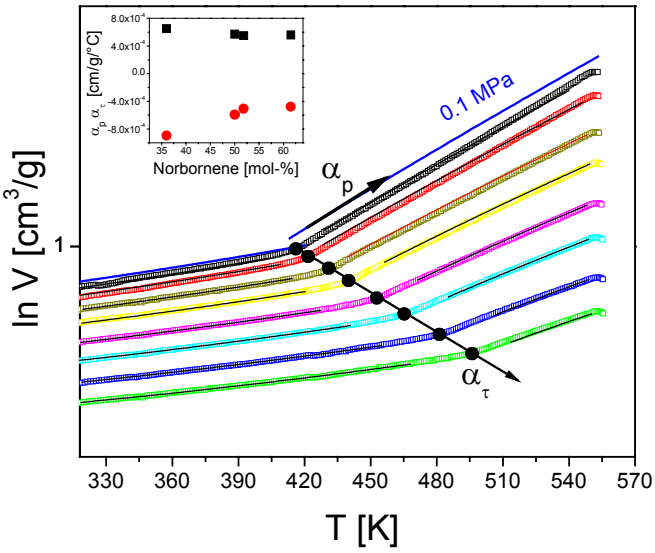

Fig. 4.14 PVT data for the 6013 copolymer. Determination of the isochronic α_τ and isobaric α_p thermal expansion coefficients. In the inset: (squares): isobaric coefficient, (circles): isochronic coefficient as a function of norbornene content.

The thus obtained E_V^*/H^* values are shown in Table 4.4. The ratio E_V^*/H^* can vary from 0 (corresponding to volume dominated dynamics) to 1 (thermal energy dominates). These results show increasing contribution from volume/density to the structural relaxation (segmental dynamics) with increasing NB content. The latter is anticipated by the higher monomeric volume of PNB as compared to PE[55] and suggests the existence of blocky structures. Thus the origin of the glass transition differs; in the copolymers with the lower NB content, glass formation is primarily due to the insufficient thermal energy required to explore the energy landscape, whereas in the copolymers with the higher NB content is primarily due to the insufficient free volume giving rise to a packing frustration at T_g. These results suggest increasing structural heterogeneity along the backbone.

Table 4.4 Activation energies ratio at the glass temperature.

Sample	E_V^*/H^* at T_g
8007	0.58±0.02
5013	0.51±0.01
6013	0.48±0.01
6017	0.46±0.01

The higher (lower) values of E_V^*/H^* for the copolymers with the higher (lower) ethylene content is in agreement with the recent experimental finding that the value of this dynamic quantity (E_V^*/H^*) is controlled by monomer size and packing properties.[55] The expectation is that bulk PE and bulk PNB would posses high and low E_V^*/H^* values, respectively. The extremely high T_g of PNB precludes, however, similar PVT analysis to obtain the dynamic ratio (due to the excessive temperature involved). Similarly, bulk PE is crystalline and this precludes measurements of E_V^*/H^*. Nevertheless, computer simulations[82] suggest values of E_V^*/H^* in the range 0.71-0.85. These high values for PE are in accord with the expectation born out by the monomer volume.

4.5 Viscoelastic properties

The dynamic mechanical investigation of COCs were carried out as described in the section *Dynamic mechanical spectroscopy (DMS)*. Every master curve was fitted with the function (2.67) to obtain the relevant parameters like e.g. relaxation times.

The aim of rheological investigation was

⇒ to test the validity of thermorheological simplicity in the copolymers
⇒ to extract the relevant time scales for the segmental and terminal relaxations

According to the principle of time-temperature superposition (tTs) (see Section 2.1.4), the frequency dependence of complex shear modulus G^* at any temperature can be obtained from a master curve at the reference temperature (T_{ref}) according to:

$$G^*(\omega;T) = b_T G^*(a_T\omega;T_{ref}) \tag{4.7}$$

When the tTs is valid, then at each temperature, a single frequency-scale shift factor a_T and a single modulus-scale shift factor b_T allow superposition of all viscoelastic data at temperature T with the results at the reference temperature T_{ref}. The superposition procedure involves independent estimation of the two shift factors by first shifting the loss tangent (tanδ=G''/G') data on the frequency scale, thus obtaining a_T, and subsequently determining b_T by an independent modulus-scale shift of G^*. Alternatively, if the sample geometry is controlled and remains the same for the different temperatures, then the G' and G'' need only to be shifted horizontally, i.e. b_T=1. Herein a controlled sample geometry have been used, hence only horizontal (i.e. frequency scale) shifts were performed. The result of the shifted storage (G'), loss (G'') modulus and tanδ are shown in Figure 4.15-4.19 for all copolymers investigated. In the G^* master curve, the two relaxation regimes of segmental (high frequencies) and terminal relaxation of chains (at low frequencies with G'~ω^2 and G''~ω) are well distinguishable. A quantitative method of checking the thermorheological simplicity of a given material can be made by using the temperature dependence of the local minimum in the loss tangent ($\tan\delta_{min}$). The $\tan\delta_{min}$ is located near the rubbery plateau and its T-dependence is a sensitive probe of the T-variation both of the high frequency modes associated with the segmental relaxation and the low frequency modes associated with the chain relaxation. These dependencies for the commercial copolymers are summarized in Figure 4.20; they indicate a very weak T-dependence with values given in Table 4.5 typical for thermorheologically simple polymers, i.e., polymers where tTs is valid. From this can be concluded that all ethylene/norbornene copolymers within the investigated composition range obey tTs except for a narrow T-range in the vicinity of the segmental process. The latter has been discussed in the literature[83-86] and its origin can be found in slightly different T-dependence of the terminal and segmental modes.[83-86] It is also known that rheology is not as sensitive as, for example, dielectric spectroscopy. In the latter technique the broader frequency range makes the identification of the different shift factors an easier task. However, the low dielectric activity of the ethylene/norbornene copolymers prevents such an investigation. The temperature dependence of the frequency-axis shift factors, $a_T(T)$, for the copolymers

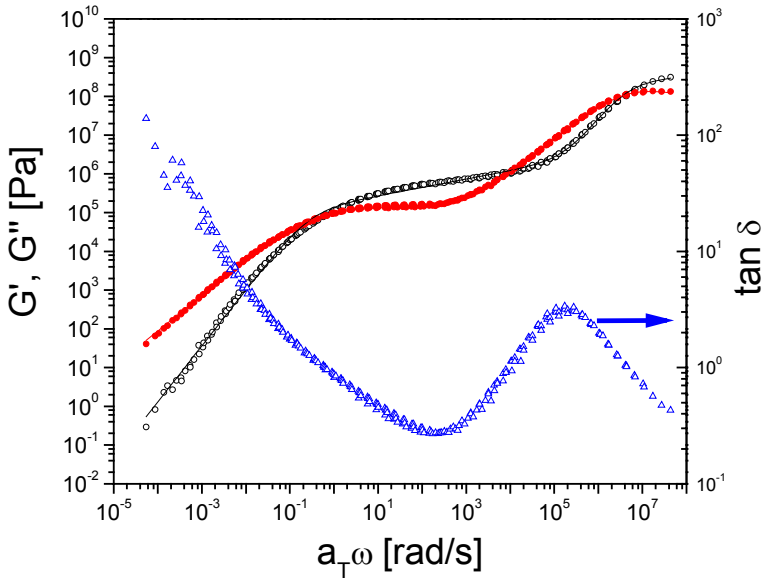

Fig. 4.15 Master curve for the storage modulus (G', open circles), the loss modulus (G", filled circles) and the loss tangent (tanδ, triangles) for Topas 8007 using data in the T-range 87 <T< 260°C. The reference temperature was at 138°C. The lines are fits to eq. (2.67).

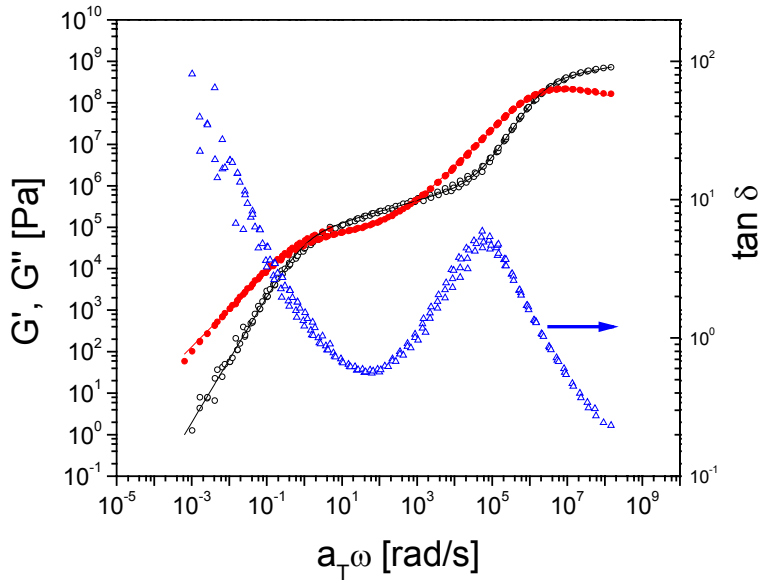

Fig. 4.16 The same as in Fig. 4.15 for Topas 5013. T-range 138 <T< 245°C. The reference temperature was at 185°C. Notice that tTs is valid except for a narrow T-range in the vicinity of T_g.

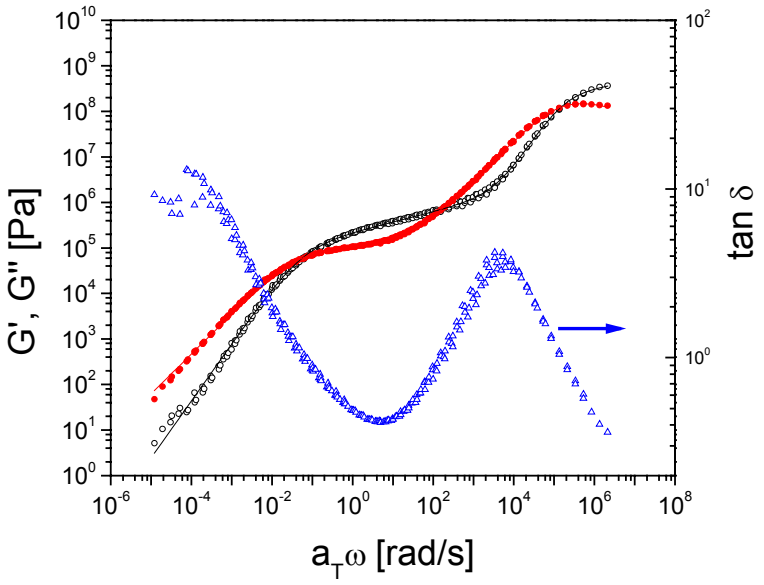

Fig. 4.17 The same as in Fig. 4.15 for Topas 6013. T-range 155 <T< 280°C. The reference temperature was at 185°C. Notice that tTs is valid except for a narrow T-range in the vicinity of T_g.

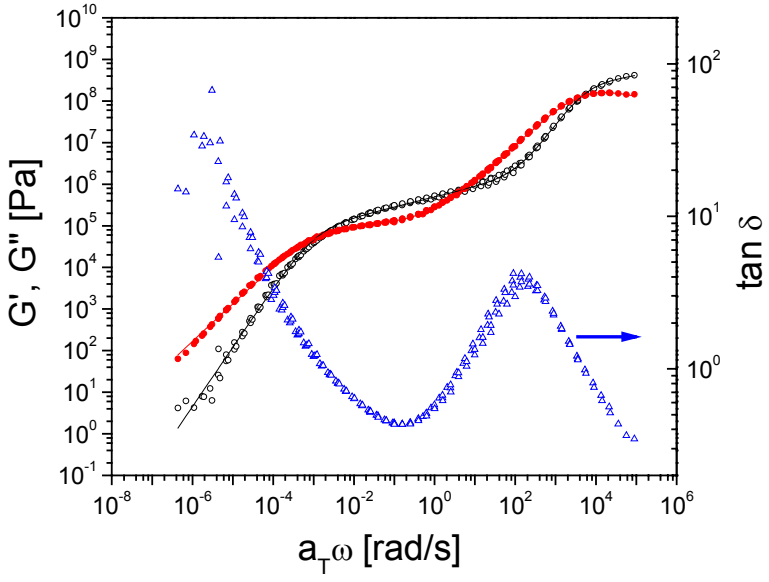

Fig. 4.18 The same as in Fig. 4.15 for Topas 6015. T-range 168 <T< 290°C. The reference temperature was at 185°C. Notice that tTs is valid except for a narrow T-range in the vicinity of T_g.

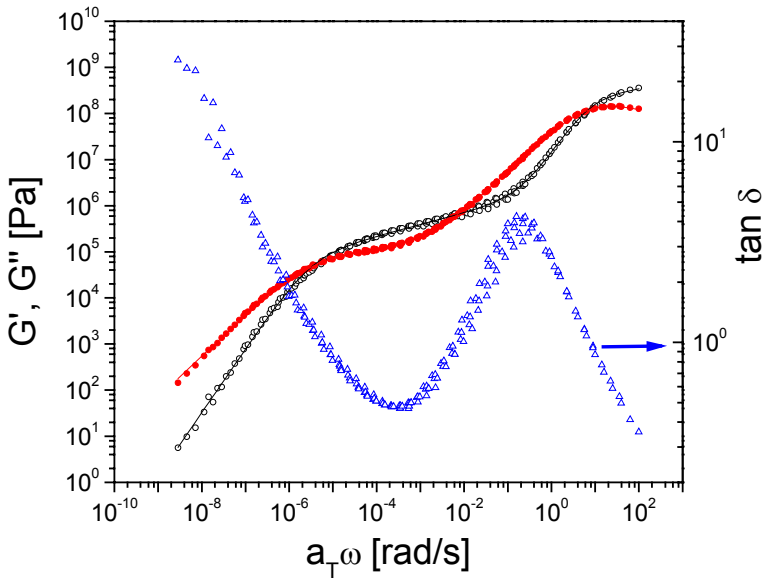

Fig. 4.19 The same as in Fig. 4.15 for Topas 6017. T-range 185 <T< 300°C. The reference temperature was at 185°C. Notice that tTs is valid except for a narrow T-range in the vicinity of T_g.

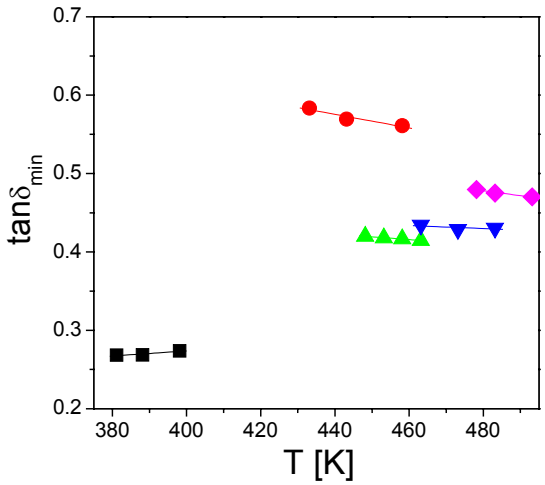

Fig. 4.20 Temperature dependence of the loss tangent minimum for the different copolymers; (squares): 8007, (circles): 5013, (up triangles): 6013, (down triangles): 6015 and (rhombus): 6017. The $d\tan\delta_{min}/dT$ values are summarized in Table 4.5.

Table 4.5 Values of the local minimum in the loss tangent used to quantify the efficacy of tTs.

Sample	NB content [mol %]	$\frac{d \tan \delta_{min}}{dT}$
8007	36	3.26E-4
5013	50	-8.68E-4
6013	52	-3.46E-4
6015	56	-1.95E-4
6017	62	-6.07E-4

Table 4.6 Williams-Landel-Ferry (WLF) and Vogel-Fulcher-Tammann (VFT) parameters.

Sample	NB content [mol %]	c_1^g	c_2^g [K]	A [s]	B [K]	T_0 [K]
8007	36	13.5	49.6	$3x10^{-13}$	1390	307.5
5013	50	13.0	32.9	$6x10^{-13}$	1290	365.1
6013	55	15.9	35.1	$4x10^{-13}$	1320	378.5
6015	56	13.7	43.1	$3x10^{-13}$	1360	390.9
6017	62	12.4	45.7	$4x10^{-13}$	1360	406.8

obeys the Williams-Landel-Ferry (WLF) equation (2.39).[31] The C_1 and C_2 parameters occurring in this relation can be re-calculated[31] at the respective glass temperature to obtain C_1^{Tg} and C_2^{Tg} (2.40, 2.41); the results for the different copolymers are summarized in Table 4.6. As already shown in Chapter 2.1.5 the WLF equation is an equivalent representation with the Vogel-Fulcher-Tammann (VFT) relation (2.54) giving the temperature dependence of the relaxation times as a function of three parameters A, B and T_∞ ($T_\infty = T_g - C_2^{Tg}$). Figure 4.21 gives the temperature dependence of the segmental (τ_S) and chain (τ_C) processes obtained by applying the a_T dependence (see eq. 2.23) to the crossings of G' and G'' at high and low frequencies, respectively. These dependencies can be well described by the VFT equation as indicated by the solid lines in this Figure; the VFT parameters are also summarized in Table 4.6.

In addition to the segmental and terminal dynamics, the shown master curves allow the estimation of the entanglement molecular weight (entanglement strand), M_e, from $M_e = \rho_N RT_N / G_N$ (eq. 2.24). The M_e values together with the densities and plateaus for all the copolymers are listed in Table 4.7. For the copolymers with higher NB content $M_e \sim 1.3x10^4$ g/mol.

The molecular weight dependence of the chain relaxation times can also be used in obtaining the critical molecular weights for entanglements. In Figure 4.22, the normalized chain relaxation times for a series of cycloolefin copolymers are plotted as a function of molecular weight. Actually it is the ratio of the chain to segmental times that is plotted, that reflects chain dynamics independent of other effects, such as temperature

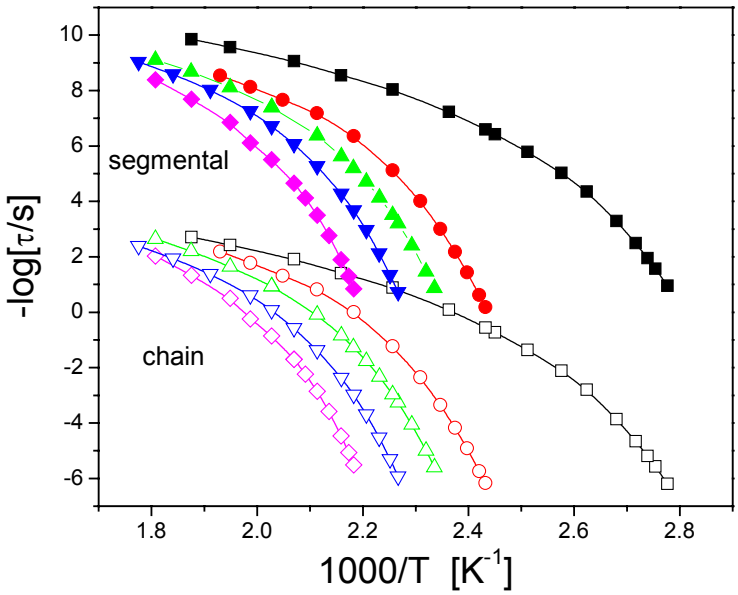

Fig. 4.21 Segmental (filled symbols) and chain (open symbols) relaxation times for the different commercial copolymers in the usual Arrhenius representation; (squares): 8007, (circles): 5013, (up triangles): 6013, (down triangles): 6015 and (rhombus): 6017. The lines are fits to the VFT equation.

Table 4.7 Plateau modulus and entanglement molecular weight.

Sample	Mw [g/mol]	Plateau from tan δ_{min} [Pa]	Density [g/cm^3]	M_e from tan δ_{min} [g/mol]
8007	10.4×10^4	5.7×10^5	1.0031	5.2×10^3
5013	9.2×10^4	2.1×10^5	1.0180	18.9×10^3
6013	10.1×10^4	3.0×10^5	1.0177	11.3×10^3
6015	10.9×10^4	3.4×10^5	1.021	12.3×10^3
6017	10.6×10^4	3.6×10^5	1.0260	13.3×10^3

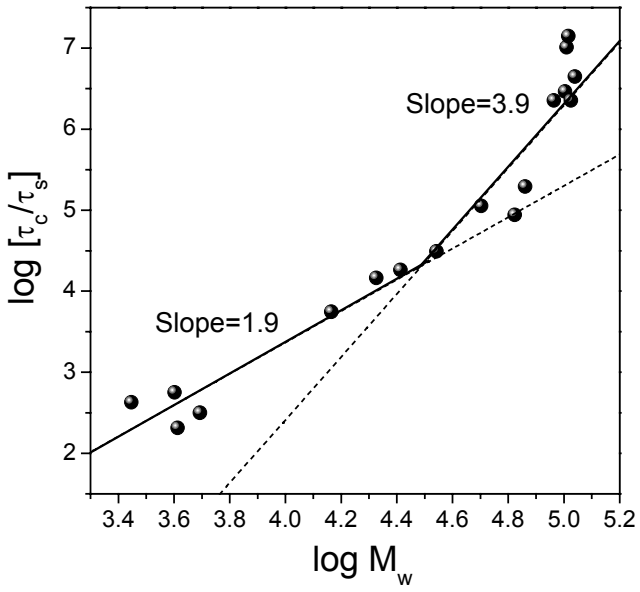

Fig. 4.22 Molecular weight dependence of the longest (chain) relaxation time normalized to the corresponding segmental time. The dashed and dotted lines with respective slopes of 1.9 and 3.9 are fits to the low - and high - molecular weight data. The approximate critical molecular weight (M_c), obtained from the crossing of the two curves, is at ~31000 g/mol.

and chain-end effects. Two regimes can be identified with respective molecular weight (M) dependencies as $\tau_c \sim M^{1.9}$ and $\tau_c \sim M^{3.9}$ at low and high molecular weights, that are close to the Rouse[85] ($\tau_c \sim M^{2.0}$) and terminal[31] ($\tau_c \sim M^{3.4}$) scaling regimes for unentangled and entangled chains, respectively. From the line intersection a critical molecular weight for entanglement $M_c \sim 31000$ g/mol, i.e., $M_c \sim 2.3 M_e$ can be determined.

For classification of relaxation processes in glass-forming systems the concept of "fragility" is used. It is often discussed in terms of the energy landscape model. According to this model a measure of the steepness of the excitation profile is given by the topology of the energy landscape, i.e., by the number of energy minima and the barrier heights in between. Fragile (strong) liquids are considered the ones that explore many (few) configuration states and this gives rise to substantial (smaller) changes in the relaxation times or the viscosity. Knowledge of the exact $\tau_s(T)$ dependencies for the different copolymers investigated allows their classification with respect to the "fragility" obtained directly from the steepness index as[87, 88]

$$m = \left. \frac{d(\log \tau_s)}{d(T_g/T)} \right|_{T=T_g} \tag{4.8}$$

Figure 4.23 shows the segmental relaxation times for the copolymers as a function of reduced temperature, where T_g is defined here as the temperature where the segmental relaxation time is at 1 s. It can be observed that the copolymers have distinctly different

τ_S(T) dependencies. In the inset, the fragility parameter m obtained from equation (4.8), is plotted as a function of norbornene content. There is a clear trend towards increasing fragility with increasing norbornene content suggesting a higher fragility for bulk PNB. This dynamic signature of heterogeneity reflects again the existence of norbornene blocks of varying lengths in the copolymers with the high norbornene content, as revealed by NMR studies.[8]

Based on ideas from the landscape model it has been proposed[89] that the dynamic fragility, m, can be obtained directly from thermodynamic quantities of glass-forming liquids as $m = \lambda T_g \Delta c_p / \Delta H_m$, where λ is an adjustable parameter (~56), and ΔH_m is the enthalpy of fusion. This dependence predicts a direct proportionality of m with the heat capacity step at T_g and has been verified for glass forming liquids.[89] Figure 4.24 provides a test of this proportionality for the ethylene/norbornene copolymers and displays the lack of such scaling as it was the case with some other homopolymers.[90] In energy landscape terms, the heights of the saddle points on the potential energy landscape do not scale with the depth of the connected minima.

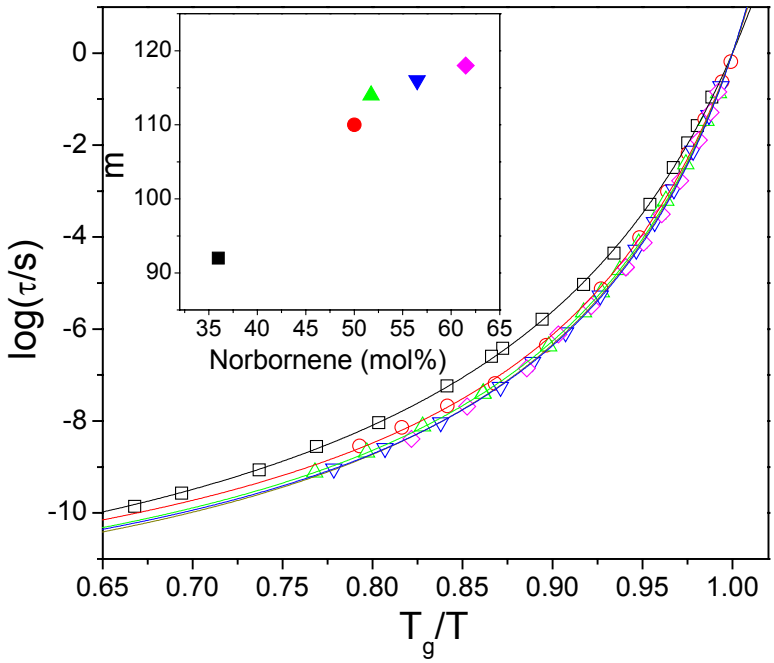

Fig. 4.23 Segmental relaxation times for the copolymers plotted as a function of reduced temperature; (squares): 8007, (circles): 5013, (up triangles): 6013, (down triangles): 6015 and (rhombus): 6017. The glass temperature (T_g) is defined here as the temperature where the segmental relaxation time is at 1 s. In the inset the fragility parameter m, extracted from these data, is plotted as a function of the norbornene content. Notice the trend towards increasing fragility with increasing norbornene content.

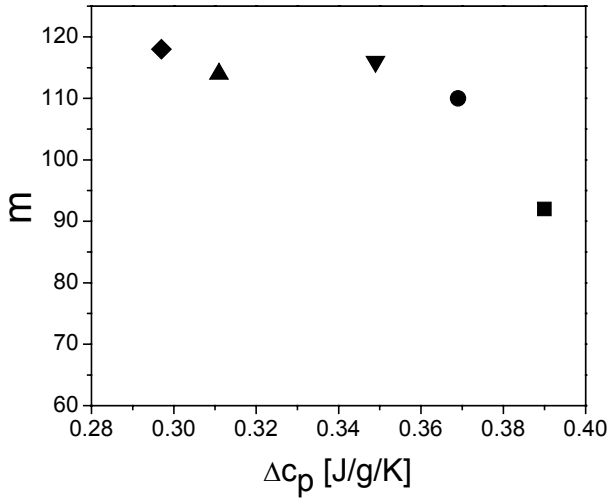

Fig. 4.24 Fragility versus heat capacity step at T_g for the different copolymers; (squares): 8007, (circles): 5013, (up triangles): 6013, (down triangles): 6015, and (rhombus): 6017.

4.6 Miscibility of cycloolefin copolymers

4.6.1 Experimental results

Blending existing copolymers can be an efficient way of producing new copolymers with desired compositions. However, this procedure requires knowledge of their miscibility phase diagram. For this purpose we are studying the miscibility of binary copolymer blends.

In the present work three ethylene/norbornene copolymer blends were investigated: 8007/6013 (36/52 mol % NB), 8007/6015 (36/56 mol % NB) and 8007/6017 (36/62 mol % NB). Each blend was prepared by a solution process in five different compositions with weight fractions: 0.1, 0.3, 0.5, 0.7 and 0.9. Pure Topas copolymers were dissolved in toluene, blended and precipitated in acetone. The obtained blends were dried in vacuum for several days. The thermal and rheological properties were studied aiming at obtaining the miscibility window. The results from rheology are compared to the theoretical predictions proposed by C. Delfolie et al.[27]

A. Thermal properties

Thermal analysis was performed by Differential Scanning Calorimetry (DSC) as described in Chapter 3.4. The DSC traces of the COC blends and the pure components are shown in Figures 4.25, 4.27 and 4.29. The curves indicate a single - albeit broad - transition except for three compositions: 50/50 in 36/56, 50/50 and 30/70 in 36/62 mol % NB blends. The width of the transitions is presented in Figure 4.31 as a function of the 8007 blend component (36 mol % NB); the values of the glass transition temperatures, determined from the inflection point of the heat flow curve, are also included in Table 4.8. In Figures 4.26, 4.28 and 4.30 the derivatives of the heat flow curves are shown for all blend compositions, together with the pure components. The blends exhibit a transition range, which is noticeably broader as compared to that for the pure copolymers; the width of these transitions, ΔT_g, are given in Table 4.8. Notice that ΔT_g increases and attains maximum values for the symmetric compositions. The broadening of the transition region is associated with the different molecular mobilities of the blend components resulting from the structural heterogeneity along the backbone (see Chapters 4.3-4.5). Based on the single T_g from the calorimetric study, for the majority of blends, one might draw the erroneous conclusion that the blends are thermorheologically simple. Despite this, rheology (see below) clearly shows the lack of thermorheological simplicity for the vast majority of blends.

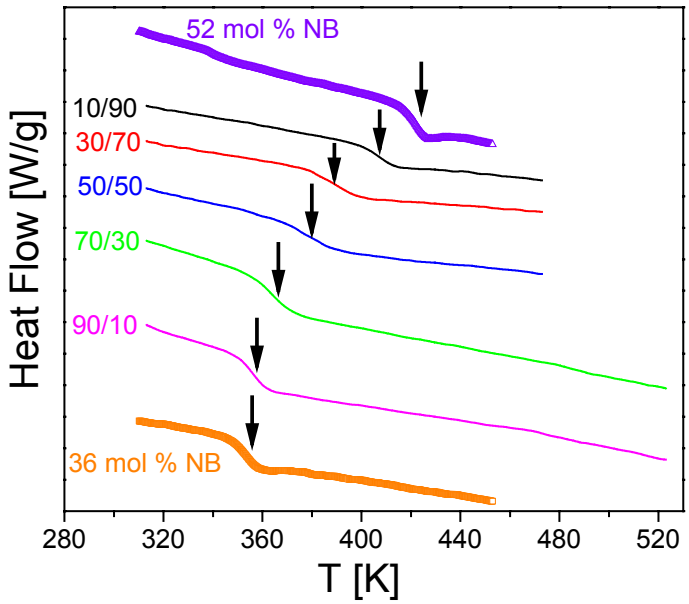

Fig. 4.25 DSC traces of the 36/52 mol % NB blends of various compositions (0.9/0.1, 0.7/0.3, 0.5/0.5,0.3/ 0.7, 0.1/0.9) and the pure components obtained during the second heating run (rate 10 K/min). Notice the single T_g in the blends. The traces have been shifted vertically for clarity.

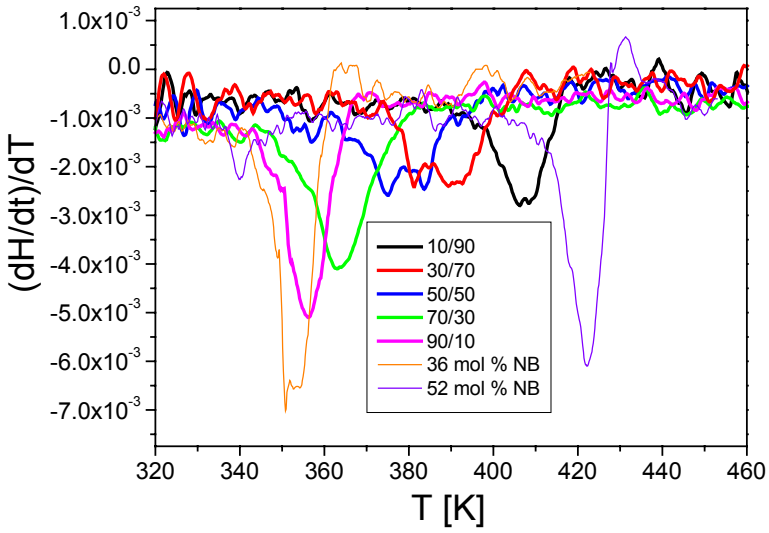

Fig. 4.26 Derivatives of the heat flow curves for the 36/52 mol % NB blends and the pure components. Notice the broadening of the transition at intermediate compositions.

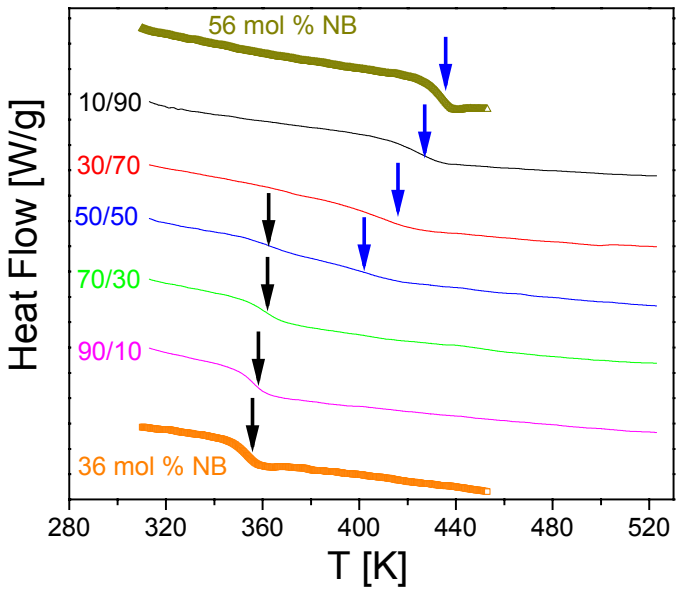

Fig. 4.27 The same as in Fig. 4.25 for the 36/56 mol % NB blends. Notice the bimodal T_g for the symmetric composition.

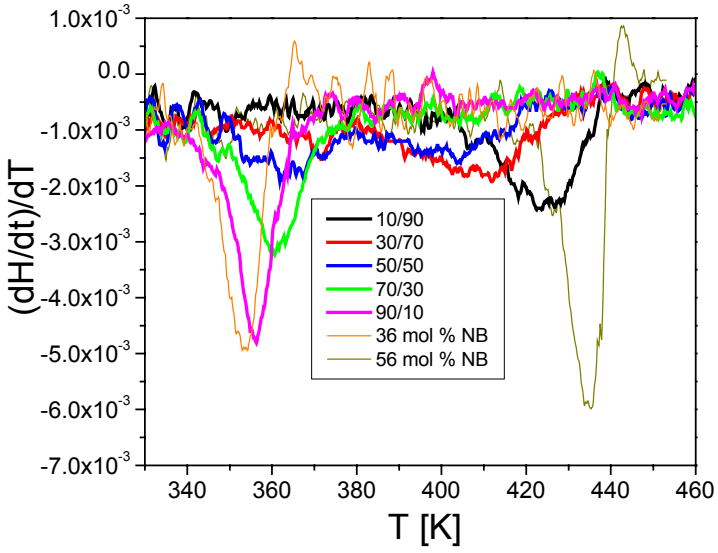

Fig. 4.28 Derivatives of the heat flow curves for the 36/56 mol % NB blends and the pure components. Notice the dual transition for symmetric composition.

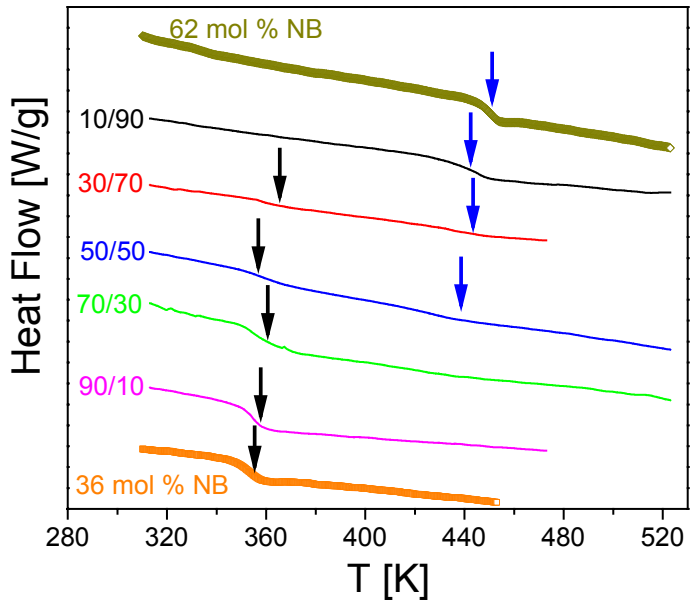

Fig. 4.29 The same as in Fig. 4.25 for the 36/62 mol % NB blends. Notice the dual transition for some compositions (50/50 and 30/70).

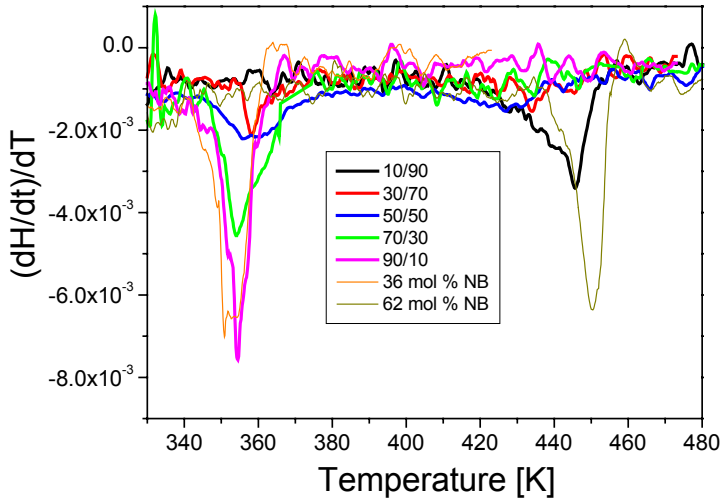

Fig. 4.30 Derivatives of the heat flow curves for the 36/62 mol % NB blends and the pure components.

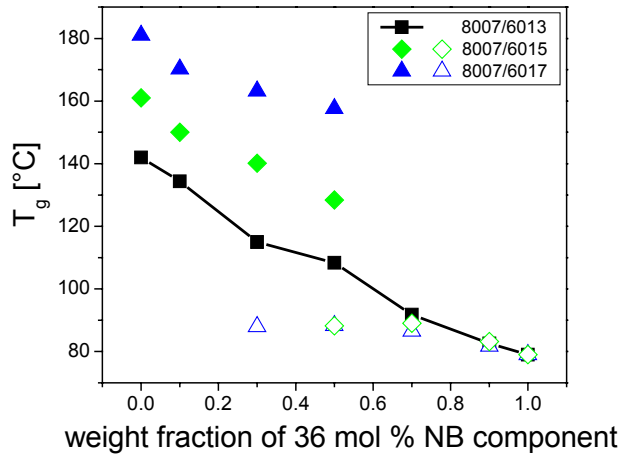

Fig. 4.31 Glass transition temperatures of the copolymers blends as a function of weight fraction of Topas 8007 obtained from DSC. Notice that a single T_g with a smooth $T_g(w)$ dependence exists only for the 36/52 mol % NB blend. For the other blends, with the higher disparity in NB content, the $T_g(w)$ dependence is not smooth and at some intermediate compositions two T_g's can be seen.

Table 4.8 Thermal properties of the ethylene/norbornene blends obtained from DSC.

Blend composition	NB content [mol%]	T_{g1} [°C]	ΔT_{g1} [°C]	T_{g2} [°C]	ΔT_{g2} [°C]
36/52 mol % NB					
52 mol % NB	52	142	20	-	-
10/90	50	134	28	-	-
30/70	47	115	38	-	-
50/50	44	108	47	-	-
70/30	41	92	35	-	-
90/10	38	83	26	-	-
36 mol % NB	36	79	28	-	-
36/56 mol % NB					
56 mol % NB	56	161	24	-	-
10/90	54	150	35	-	-
30/70	50	140	47	-	-
50/50	46	88	25	128	31
70/30	42	89	34	-	-
90/10	38	83	30	-	-
36/62 mol % NB					
62 mol % NB	62	181	20	-	-
10/90	59	170	35	-	-
30/70	54	163	93	88	10
50/50	49	158	32	88	29
70/30	44	86	26	-	-
90/10	39	82	28	-	-

B. Rheological properties

Blends of cycloolefin copolymers, in addition to the pure COCs (see Section 4.5), were examined by shear rheology to check the composition ranges that the different blends behave as thermorheologically simple, and thus could be effectively considered as one component systems (i.e. miscible). All three COC blends were investigated by dynamic mechanical spectroscopy (Section 3.6): 36/52, 36/56 and 36/62 mol % NB. An attempt to superimpose the moduli and the loss tangent ($\tan\delta = G''/G'$) for the symmetric blends is shown in Figures 4.32-4.34; master curves for the remaining compositions (90/10, 70/30, 30/70, 10/90) can be found in the Appendix.

We recall here that the pure components of the blends obey the time-temperature-superposition principle (tTs, see Chapter 2.1.4) indicating that thermorheological simplicity prevails (Figs. 4.15-4.19). To quantify the efficacy of tTs in the copolymer blends the same criterion as for the pure COCs is employed, namely the temperature dependence of the local minimum in the loss tangent, $d\tan\delta_{min}/dT$. The temperature dependence of $\tan\delta_{min}$ in the copolymers and the blends is plotted in Figures 4.35-4.37. It can be observed that while $\tan\delta_{min}$ shows very weak dependence in the pure components, it is temperature dependent for the majority of blend compositions. This dependence is the strongest for the symmetric blends and, additionally, increases with the difference in NB content between the blend compositions (later we will provide the details on the compositions for which the blends are immiscible). The values of the $d\tan\delta_{min}/dT$ for the different blends are given in Table 4.9. Notice that the magnitude for the majority of compositions is characteristic of blends that are acknowledged to violate tTs[91], i.e.,

$$\left|\frac{d\tan\delta_{min}}{dT}\right| \geq 5\times10^{-4}\,K^{-1}\ (^{\dagger}) \qquad (4.9)$$

The temperature dependence of the $\tan\delta_{min}$ is controlled by the difference in the temperature dependences of the terminal relaxations of the blend components. In the blends, the higher T_g component chains have a stronger temperature dependence of terminal relaxation times than the lower T_g component chains, yielding $d\tan\delta_{min}/dT < 0$.[92] In addition, the values of $d\tan\delta_{min}/dT$ increase with the increase in the widths of the glass transition of the blends (see Tab. 4.8).

The theoretical predictions of miscibility of ethylene/norbornene copolymers and the comparison against the rheology data is presented in Section 4.6.3.

[†] For COC copolymers the violation of tTs is assumed to occur for $d\tan\delta_{min}/dT > 6\times10^{-4}$

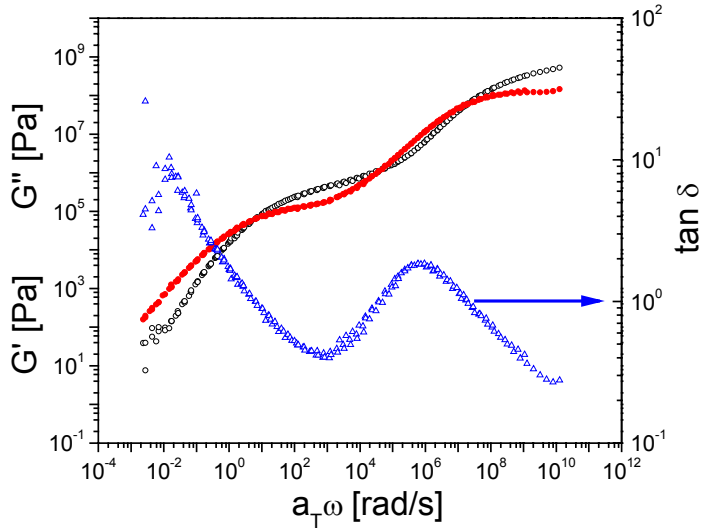

Fig. 4.32 Master curve for the storage modulus (G', open circles), the loss modulus (G", filled circles) and the loss tangent (tanδ, triangles) for the 50/50 composition of the 36/52 mol % blend using data in the T-range 105 <T< 230°C. The reference temperature was at 180°C.

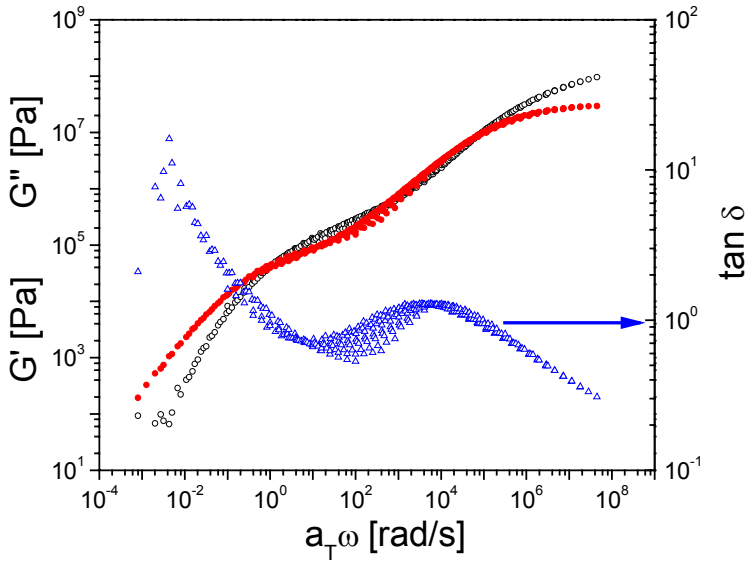

Fig. 4.33 The same as in Fig. 4.32 for the 50/50 composition of the 36/56 mol % blend using data in the T-range 129 <T< 240°C. The reference temperature was at 180°C.

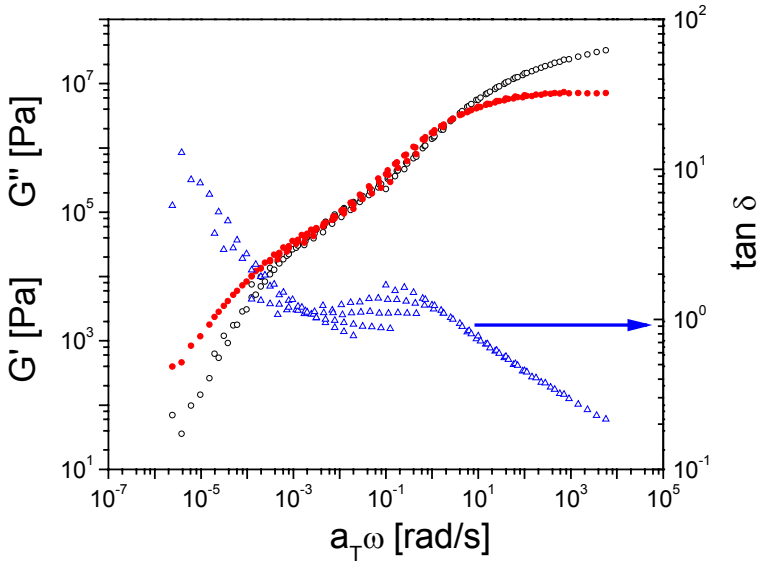

Fig. 4.34 The same as in Fig. 4.32 for the 50/50 composition of the 36/62 mol % blend using data in the T-range 150 <T< 240°C. The reference temperature was at 160°C.

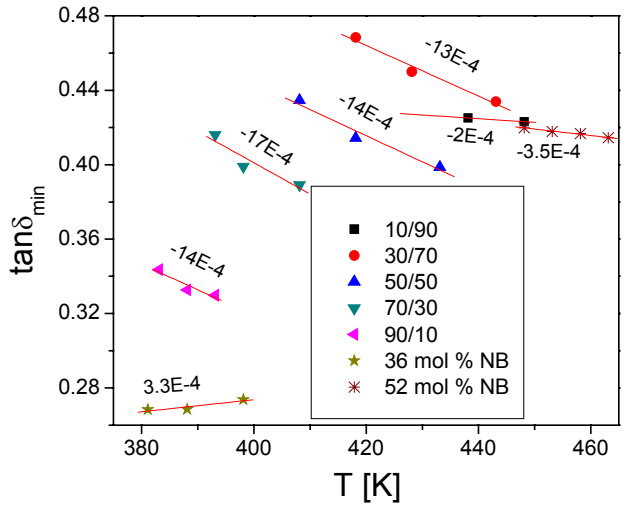

Fig. 4.35 Temperature dependence of the loss tangent minimum for the different compositions of the 36/52 mol % NB blend and the pure components. The lines represent linear fits.

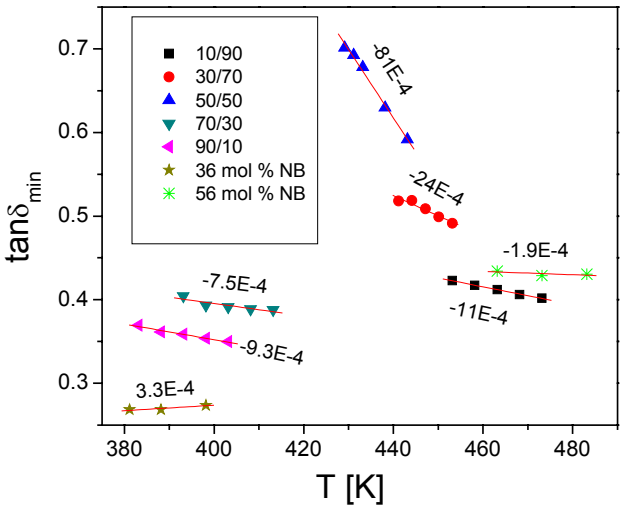

Fig. 4.36 The same as in Fig. 4.35 for the 36/56 mol % blend.

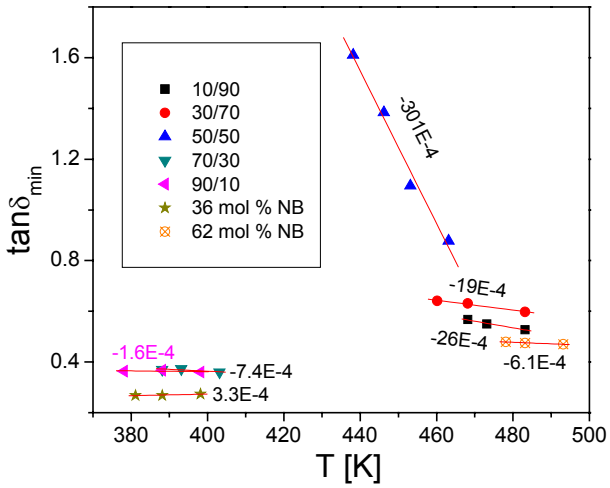

Fig. 4.37 The same as in Fig. 4.35 for the 36/62 mol % blend.

Table 4.9 Values of the local minimum in the loss tangent for the 8007/6013, 8007/6015, 8007/6017 blends and the pure components used to quantify the efficacy of the tTs. In red are indicated blend compositions that do not pass the stringent test of miscibility (i.e., eq. 4.9).

36/52 mol % NB	NB content [mol%]	$\frac{d \tan \delta_{min}}{dT}$ [K^{-1}]
0/100	52	-3.5E-4
10/90	50	-2E-4
30/70	47	-14E-4
50/50	44	-14E-4
70/30	41	-17E-4
90/10	38	-14E-4
100/0	36	3.3E-4

36/56 mol % NB	NB content [mol%]	$\frac{d \tan \delta_{min}}{dT}$ [K^{-1}]
0/100	56	-1.9E-4
10/90	54	-11E-4
30/70	50	-24E-4
50/50	46	-81E-4
70/30	42	-7.5E-4
90/10	38	-9.3E-4

36/62 mol % NB	NB content [mol%]	$\frac{d \tan \delta_{min}}{dT}$
0/100	62	-6E-4
10/90	59	-26E-4
30/70	54	-19E-4
50/50	49	-301E-4
70/30	44	-7.4E-4
90/10	39	-1.6E-4

4.6.2 Theoretical models of COC miscibility

A theoretical model for the analysis of the mutual miscibility of the cycloolefin copolymers was proposed by Delfolie et al.[27] It was designed to determine how the size and stiffness disparities of the ethylene and norbornene comonomers, and the microstructure (monomer sequence distribution) affect the miscibility patterns.

The simplest model for describing binary random copolymers is an extension[93, 94] of Flory-Huggins theory to random copolymers. For a blend of two copolymers of the same nature but different compositions (x, y), Flory-Huggins theory predicts that the miscibility region exists for

$$|x - y| < |x - y|_c$$

where subscript c denotes a critical value. Thus, the miscibility region is independent of the copolymer composition.[95]

To explain departures from random copolymer Flory-Huggins (FH) theory, a theory based on the so-called "united atom model" was applied to ethylene/norbornene copolymers. The theory is an extension of the lattice cluster theory (LCT)[96-98]; LCT includes contributions from local correlations and specifies structures for individual monomers. The limitations/assumptions of the theory include: (i) blend incompressibility, and (ii) the inability to describe monomers containing closed rings. Hence, the norbornene molecule is represented in an approximate way as shown in

Figure 4.38. Such a computation structure – which is different from the real NB

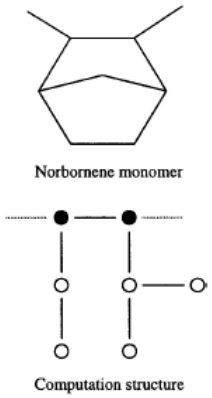

Fig. 4.38 United group model of norbornene. Each circle represents a single united atom CH_n (n=1, 2) group (Delfolie C. et al., Macromolecules 1999).

monomer – is designed to reflect the overall *size* and *shape* of the actual norbornene monomer, which is the important feature in computing the "entropic" portion of the interaction parameter χ.

On the other hand, the "enthalpic" part of χ is determined solely by one structural property of the monomers, namely, the numbers of united atom groups in the monomers of each species. Assuming a binary blend of N_xE_{1-x} and N_yE_{1-y} random copolymers, the enthalpic portion χ_h of the interaction parameter χ is obtained by extending the FH random mixing counting methods to random copolymers composed of monomers with united atoms groups as[27]

$$\chi_h = \left[\frac{s_N s_E (x-y)}{s_1 s_2}\right]^2 \frac{z\varepsilon}{2kT} \tag{4.10}$$

where s_N and s_E are the lattice sites of norbornene and ethylene, respectively. The norbornene monomer in Figure 4.38 contains seven united atoms groups and therefore occupies seven lattice sites, hence s_N=7, while the ethylene molecule is a two-bead dimer composed of two CH_2 that cover s_E=2 lattice sites; x and y are the amounts of norbornene in the components of the binary blend; s_1 and s_2 are defined as

$$s_1 = s_N x + s_E (1-x) \tag{4.11}$$

$$s_2 = s_N y + s_E (1-y) \tag{4.12}$$

and designate the average numbers of united atom groups in the monomers of component 1 and 2, respectively.[99] z is the lattice coordination number and is taken as z=6, k is Boltzmann's constant, T is the absolute temperature, and $\varepsilon = \varepsilon_{NN} + \varepsilon_{EE} - 2\varepsilon_{EN}$ is the exchange energy with ε_{NN}, ε_{EE} and ε_{EN} denoting the attractive van der Waals energies between united atom groups and the respective monomer pairs, assuming for

simplicity that all united atom groups of a given monomer interact with the same energy.

The "entropic" portion χ_s of the interaction parameter χ results from the high molecular weight athermal incompressible limit of the LCT as

$$\chi_s = \frac{1}{z^2}\left[\frac{N_2^{(1)}}{M_1} - \frac{N_2^{(2)}}{M_2}\right]^2 = \frac{1}{z^2}\left[\frac{s_N^{tri} s_E (x-y)}{s_1 s_2}\right]^2 \tag{4.13}$$

where $N_2^{(1)}$ and $N_2^{(2)}$ are the numbers of distinct pairs of consecutive bonds in single chains of copolymer species 1 and 2, respectively, and s_N^{tri} denotes trifunctional united atom groups in norbornene monomers. M_1 and M_2 are the site occupancy indices for the single $N_x E_{1-x}$ and $N_y E_{1-y}$ chains, respectively, and are defined as

$$M_1 = s_N n_1^{(N)} + s_E n_1^E \tag{4.14}$$

$$M_2 = s_N n_2^{(N)} + s_E n_2^E \tag{4.15}$$

where $n_i^{(N)}$ and $n_i^{(E)}$ are the average numbers of norbornene and ethylene monomers in copolymers of species i that satisfy:

$$\frac{n_1^{(N)}}{n_1^{(N)} + n_1^{(E)}} = x \text{ and } \frac{n_2^{(N)}}{n_2^{(N)} + n_2^{(E)}} = y \tag{4.16}$$

Three models are discussed: the first assumes fully flexible bonds. Combining entropic and enthalpic portions the interaction parameter for this model can be expressed as

$$\chi = \chi_s + \chi_h = \left[\frac{x-y}{s_1 s_2}\right]^2 \left[\frac{(s_E s_N^{tri})^2}{z^2} + (s_N s_E)^2 \frac{z\varepsilon}{2kT}\right] \tag{4.17}$$

The second model (rigid) introduces rigidity in the norbornene monomer by making the two (vertical) pairs of side group bonds (Fig. 4.38) completely stiff. By introducing the modification into χ_s leads to the following expression of the interaction parameter

$$\chi = \left[\frac{x-y}{s_1 s_2}\right]^2 \left[\frac{\left[s_E (s_N^{tri} - 2)\right]^2}{z^2} + (s_N s_E)^2 \frac{z\varepsilon}{2kT}\right] \tag{4.18}$$

The third model (semiflexible) is based on the assumption that adjacent norbornene monomers are connected by semiflexible bonds. The idea behind this model is based on the high disparity of chain stiffness between PE and PNB chains. The different bending energies for conformational transitions within the PNB chains (see Fig 1.4) may affect

the miscibility to some extent. In this case the enthalpic portion χ_h remains unchanged, while the entropic χ_s is modified to

$$\chi_s = \frac{1}{z^2}\left\{\frac{s_N^{tri}s_E(x-y)+2(g-1)(s_N-s_E)xy(x-y)+2(g-1)s_E(x^2-y^2)}{s_1s_2}\right\}^2 \quad (4.19)$$

where $g = z/[z-1+\exp(E_b/kT)]$ and E_b is the trans-gauche energy difference.[100] The latter can be taken for example from Figure 1.4.
The predictions for the χ parameters in the three models are summarized in the Table 4.10 below.

Table 4.10 The enthalpic (χ_h) and entropic (χ_s) blend interaction parameters for the various theoretical models.[27]

Model	χ_h	χ_s
fully flexible bonds (flexible)	$\left[\frac{s_N s_E(x-y)}{s_1 s_2}\right]^2 \frac{z\varepsilon}{2kT}$	$\frac{1}{z^2}\left[\frac{s_N^{tri}s_E(x-y)}{s_1s_2}\right]^2$
stiff NB side groups (rigid)	The same as for flexible	$\frac{1}{z^2}\left[\frac{(x-y)}{s_1s_2}\right]^2\left[s_E\left(s_N^{tri}-2\right)\right]^2$
semiflexible NB bonds (semiflexible)	The same as for flexible	$\frac{1}{z^2}\left\{\frac{s_N^{tri}s_E(x-y)+2(g-1)(s_N-s_E)xy(x-y)+2(g-1)s_E(x^2-y^2)}{s_1s_2}\right\}^2$

For each of the above models, the stability condition (i.e. spinodal line) for a mixture of two random copolymers is provided by

$$S \equiv \frac{1}{M_1\varphi_1}+\frac{1}{M_2\varphi_2}-2\chi = 0 \quad (4.20)$$

where φ_i are the volume fractions ($\varphi_1+\varphi_2=1$). Volume fractions are obtained from weight fractions (w) as

$$\varphi_1 = \frac{2+5x}{2+5x+\frac{(28+66x)(1-w_1)(2+5y)}{w_1(28+66y)}} \quad (4.21)$$

Below we have employed the stability condition to calculate the region of miscibility for our copolymer blends and for each of the models above.

4.6.3 Comparison between theory and experiment

As mentioned above, three different models for cycloolefin copolymers were proposed by Delfolie et al., ranging from a fully flexible chain model to models that include chain stiffness arising within each norbornene unit or from the steric interactions between neighboring norbornene monomers (semiflexible backbones). As

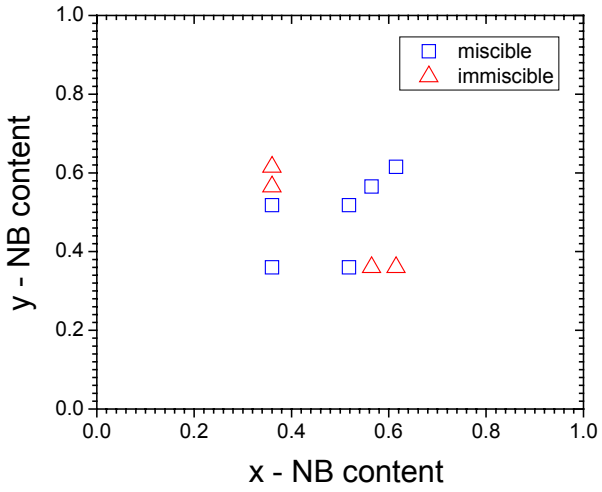

Fig. 4.39 Phase diagram of the different copolymers for equal weight fraction blends (symmetric) obtained from DSC. Squares and triangles denote the compositions (x,y) for which the system is miscible and immiscible, respectively.

already stated in Section 4.6.1, the calorimetric method is not sensitive enough to draw a conclusion about the thermorheological simplicity/complexity of the blends. Comparison of the phase diagrams obtained from DSC (Figs. 4.39 and 4.40 for the symmetric and asymmetric compositions, respectively) with these ones obtained from rheology (Figs. 4.41 and 4.42 for the symmetric and asymmetric compositions as well) show many discrepancies due to the above mentioned low sensitivity of the former technique. For that reason only the rheological data are compared with the theoretical models to test their validity for various COC compositions.

The miscibility diagrams in Figures 4.41 and 4.42 are constructed using the validity criterion of the time-Temperature-superposition (eq. 4.9). Except for two blends (10/90 in 36/52 and 90/10 in 36/62 mol % NB) all others are thermorheologically complex and thus immiscible. Notice, however, that the "degree" of immiscibility, given by the values of $d\tan\delta_{min}/dT$ (Tab. 4.9), differs for the different blend compositions.

Prior the direct quantitative comparison of the experimental results with the theoretical models, we test these models aiming at obtaining the general tendencies (conditions) for the mutual miscibility of ethylene/norbornene copolymers. We first check the sensitivity of the parameters involved in the models and their effect on the miscibility (or immiscibility) regions. In the first example we explore the effect of the different models (fully flexible, stiff NB side groups, semiflexible NB bonds) on the values of the total interaction parameter χ. In the Figure 4.43 the blend interaction parameter for $N_x E_{1-x}/N_y E_{1-y}$ blends is plotted as a function of norbornene content (x)

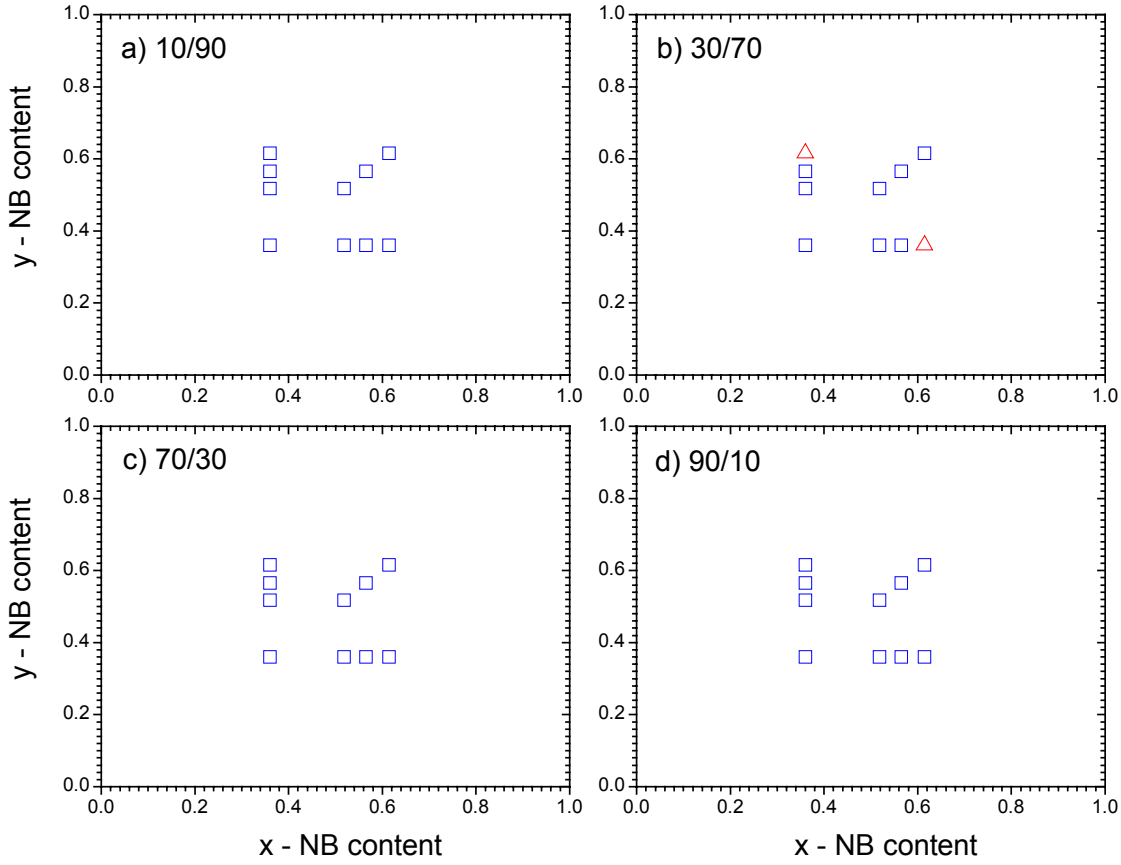

Fig. 4.40 Miscibility diagram of the different copolymers for various weight fraction blends obtained from DSC: (a) 10/90, (b) 30/70, (c) 70/30, (d) 90/10; the first component of each blend is the copolymer with 36 mol % in norbornene. Denotation is the same as in Fig. 4.39, i.e., □: miscible, Δ: immiscible.

for different compositions y of the second copolymer (y=0.36, 0.52, 0.62 and 0.75). The dimensionless exchange energy was taken $\varepsilon/kT=0.005$, while the dimensionless bending energy was chosen as $E_b/kT=0.7$ for the semiflexible model (the particular choice for these energies will be explained below). Notice the highly asymmetric shape of the $\chi(x)$ dependence that is independent of the particular model. This suggests that $N_x E_{1-x}/N_y E_{1-y}$ binary blends are more miscible for $y \geq x$ and are immiscible for $y < x$. For the same $|x-y|$ the result on blend miscibility may be very different depending on the actual values of x and y. As expected, the region of miscibility is not governed solely by $|x-y|$. Another finding, which is surprising, is that the miscibility in enhanced when rigidity is incorporated in the side-chain of NB monomer; indeed, the model with the rigid NB side groups shows the lowest χ, and hence, the highest ability of mixing.

As a second example we test the N – dependence on the miscibility of $N_x E_{1-x}/N_y E_{1-y}$ binary blends of within a particular model. Figure 4.44 shows the

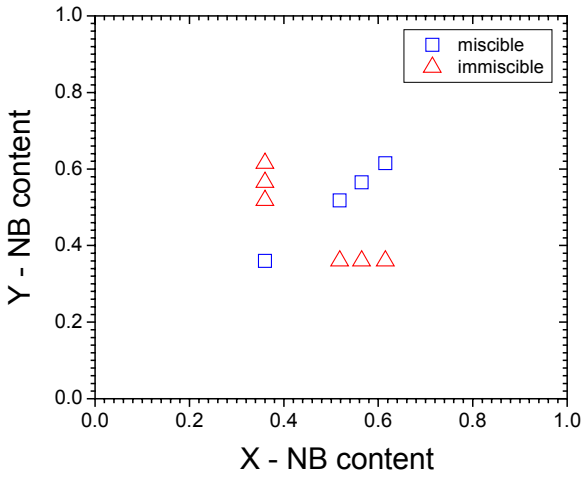

Fig. 4.41 Phase diagram of the different copolymers for equal weight fraction blends (symmetric) obtained from rheology. Denotation is the same as in Fig. 4.39. Notice that, in contrast to DSC, all symmetric blends are practically immiscible.

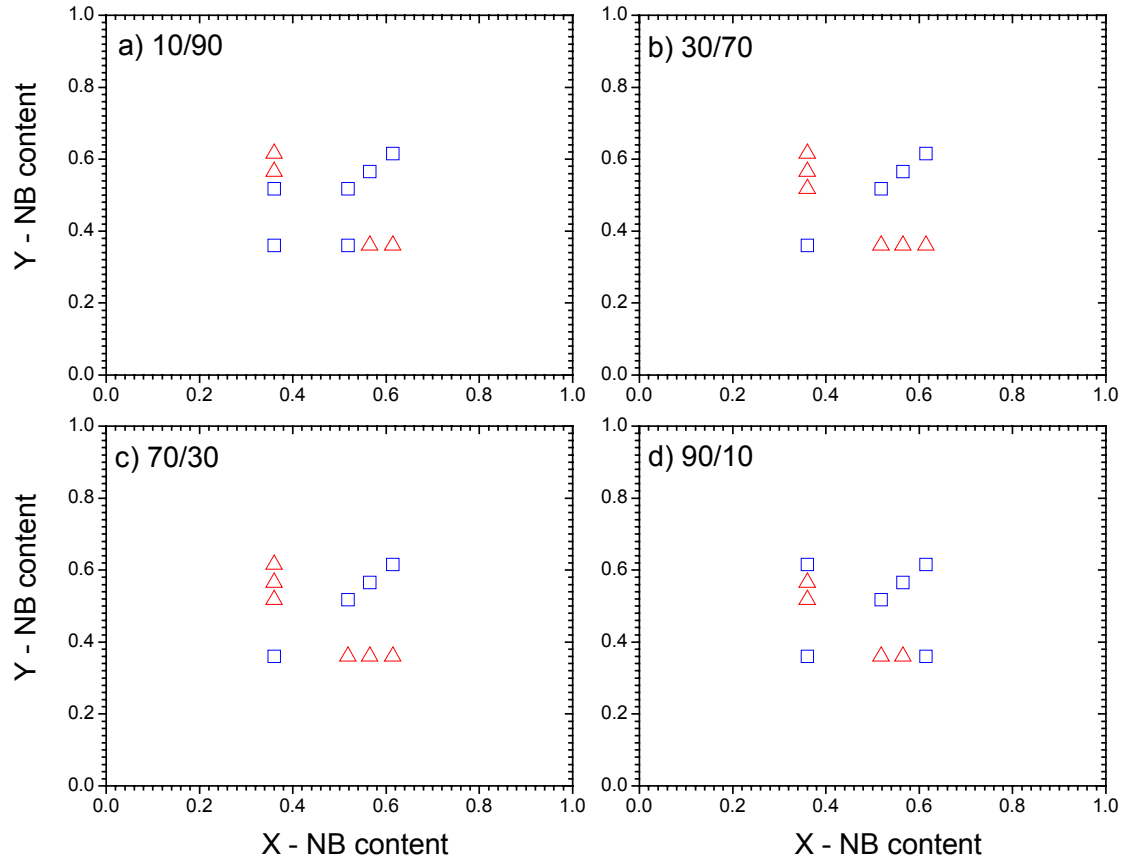

Fig. 4.42 Miscibility diagram of the different asymmetric blends for various weight fractions obtained from rheology: (a) 10/90, (b) 30/70, (c) 70/30, (d) 90/10; the first component of each blend is the copolymer with 36 mol% in norbornene. Denotation is the same as in Fig. 4.39. Notice the similarities of the diagrams for the 30/70 and 70/30 compositions with the symmetric case (Fig. 4.41).

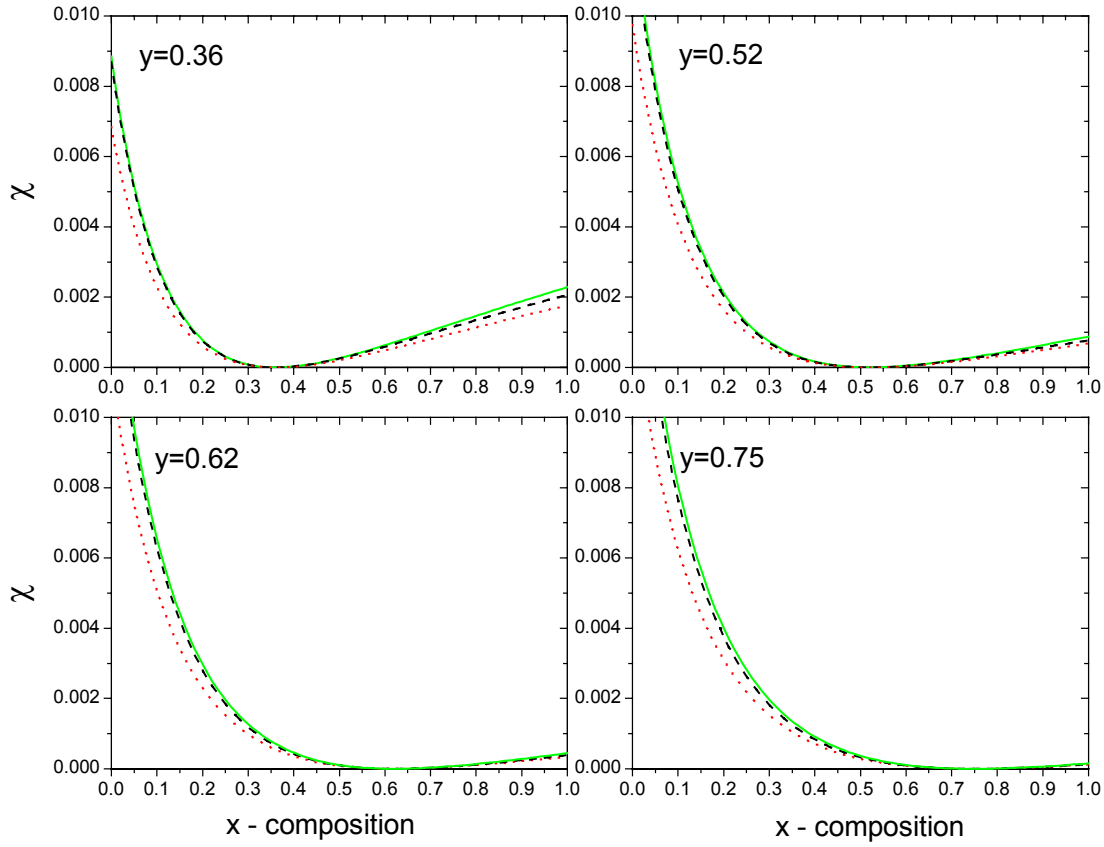

Fig. 4.43 Computed total interaction parameter χ, for $N_x E_{1-x}/N_y E_{1-y}$ *binary blends, from the three models and for four different compositions of the second copolymer (y=0.36, 52, 62 and 0.75); the dimensionless exchange energy is taken as* ε/kT *=0.005, while the dimensionless bending energy for the semiflexible model is chosen as* E_b/kT *= 0.7 (see text). Solid, dashed, and dotted lines refer to the models with fully flexible bonds, with semiflexible backbone, and with stiff norbornene side groups, respectively.*

phase boundaries for the different N's (N=1000, 2000 and 10000) for one of the models (with the stiff NB side groups). We mention here that this model gives the widest miscibility window and thus more effectively separates the miscible/immiscible regions. Therefore, it will be employed later to predict the miscibility for all asymmetric blend compositions. Notice in Figure 4.44 the large influence of the degree of polymerization on the phase boundaries, in particular between N=1000 and N=2000. Increasing N reduces the miscibility window, which is consistent with the experiment findings. The strong sensitivity of the phase boundaries on N made necessary its calculation for all the components of the blends (N=2664, 2261, 2160 and 2009 for COCs with 36, 52, 56, 62 mol % of NB, respectively). As a good approximation of these values we employ N_1= N_2=2500 for the subsequent analysis.

As a third example we test the influence of the dimensionless $b = E_b/kT$ term, associated with the chain backbone stiffness, i.e. with the bending energy of NB backbone bonds connecting adjacent norbornene units. The phase boundaries for the

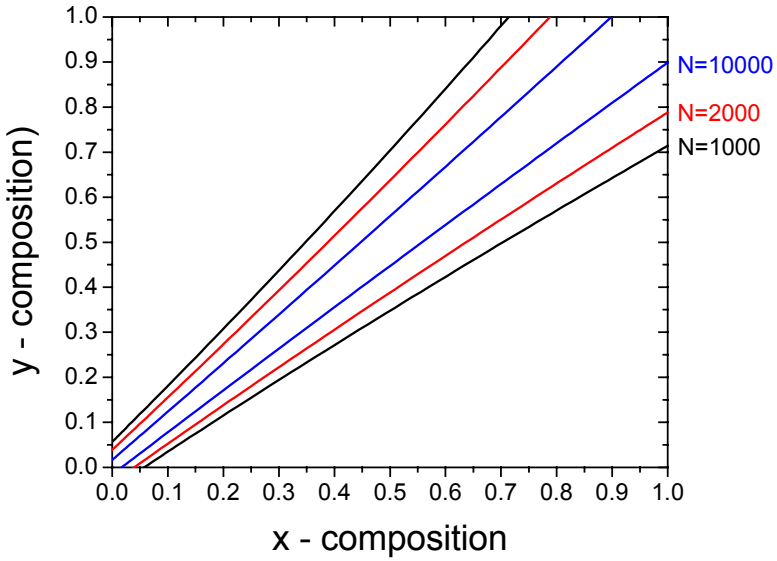

Fig. 4.44 Influence of the polymerization index (N) on the phase boundaries (spinodals) for the model with the stiff norbornene groups (rigid).

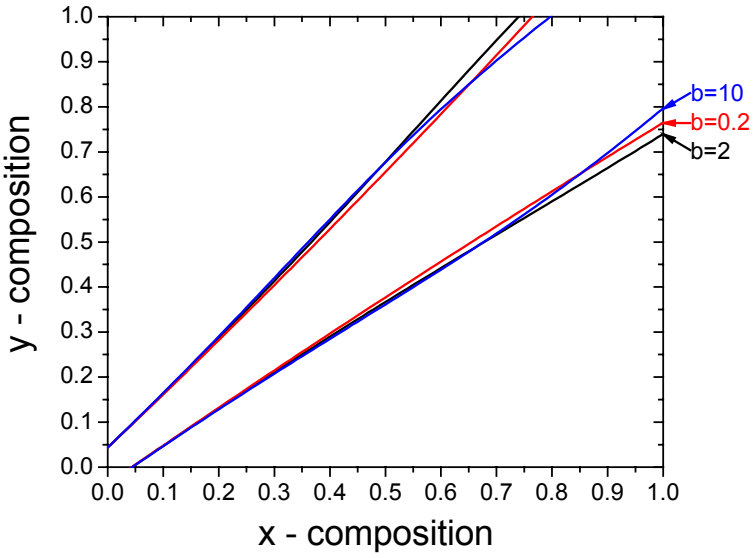

Fig. 4.45 The effect of the bending energy $b = E_b/kT$ on the phase boundaries. The polymerization indices $N_1 = N_2 = 2500$ and the exchange energy is taken as $a = \varepsilon/kT = 0.005$ (see text).

semiflexible model shown in Figure 4.45 were calculated for b=0.2, 2 and 10, and for $\varepsilon/kT = 0.005$ and $N_1 = N_2 = 2500$. The former b values are considered as representative of the real NB sequences (i.e. a value of $b \approx 10$, that is, $E_b \approx 25$ kJ/mol is very close to the calculated energy barriers for trans-to-gauche conformations (Fig. 1.4). Notice the insensitivity of the phase boundaries to the particular b values, especially for low x values. This suggests that backbone stiffness is not the major factor affecting the miscibility of $N_x E_{1-x}/N_y E_{1-y}$ binary blends. This is a rather surprising result, given the

fact that backbone stiffness, in many cases, plays an important role in polymer blend miscibility.

Testing the theoretical predictions against experimental data requires some control of the parameters involved, namely the polymerization indices, the bending and exchange energies. First, as we tested in Fig. 4.45, the miscibility window is not sensitive to the bending energy, therefore we employ $E_b/kT=0.7$, i.e. a value close to the thermal energy. Second, the phase boundaries are sensitive to the degrees of polymerization, therefore in calculating the exact phase boundaries we employ N values that are close to the experimental ones ($N_1= N_2=2500$). Third, the phase boundaries are very sensitive to the exchange energy reflecting the attractive van der Waals energies between united atom groups of the respective monomer pairs. Decreasing the exchange energy makes a wider miscibility region due to the smaller interaction between monomers. The maximal value of ε/kT for the model with the rigid NB side groups, being still in agreement with the experimental data, was found to be 0.005. This value of the exchange energy was chosen from the model with the rigid NB side groups due to its outermost phase boundaries. Notice, however, that the boundaries obtained for all the models lie relatively close to each other.

As a last step we applied the thus determined value of the exchange energy (0.005), the bending energy and degrees of polymerization from the symmetric blends, and critically tested the predictions of the model (rigid NB side groups) for the asymmetric blend compositions (Fig. 4.47). It was found that the model correctly predicts all the 70/30 and 30/70 compositions, together with the 10/90 in 36/52, 10/90 in 36/62, and 90/10 in 36/62 mol % NB blends. For the blends 10/90 in 36/56, 90/10 in 36/52 and 90/10 in 36/56 mol % NB the model failed. Notice that the model was successful for all the compositions of the 36/62 blend. From these results it can be concluded that the theoretical model works at best for the "middle" (70/30-30/70) compositions, and (partially) fails for the extreme ones. These results are shown in a tabulated form in Table 4.11.

It is surprising that, despite a number of approximations, such as blend incompressibility, lack of the dependence of the contact probabilities on monomer structure and simple structure for the NB monomer,[27] the model predicts correctly the miscibility of many (asymmetric) blends. On the other hand, there are also some experimental uncertainties, related to the polydispersity of chains (affecting the N values), and the value of the criterion set for tTs violation (eq. 4.9). Given the above, the overall the agreement between theory and experiment is reasonable.

Table 4.11 Prediction of the model (rigid) against the experimental data for the different asymmetric composition blends; (∨): successful and (x) unsuccessful prediction

Blend compositions	Prediction of the model
36/52 mol % NB	
10/90	∨
30/70	∨
70/30	∨
90/10	x
36/56 mol % NB	
10/90	x
30/70	∨
70/30	∨
90/10	x
36/62 mol % NB	
10/90	∨
30/70	∨
70/30	∨
90/10	∨

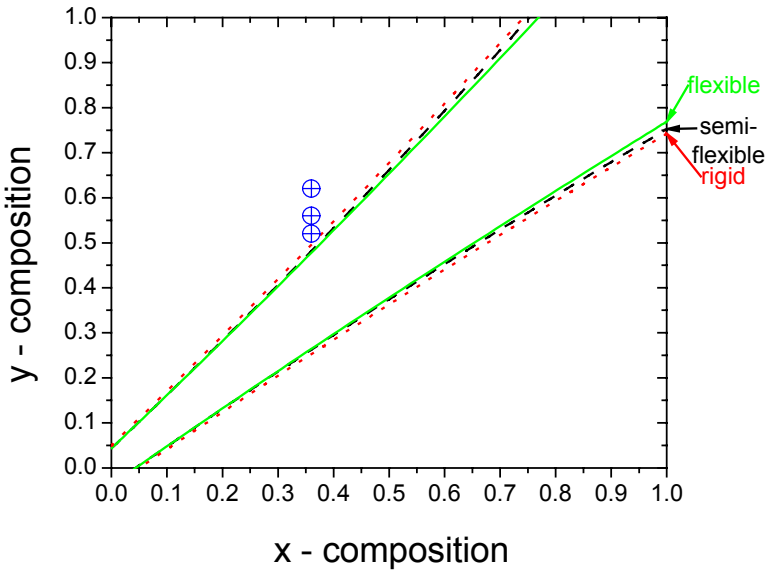

*Fig. 4.46 Determination of the maximal value of the exchange energy (*ε/kT*) applicable for the symmetric blends (see text). Comparison of the different models for the same set of parameters: ε/kT =0.005, N_1= N_2=2500, E_b/kT =0.7. The value of the exchange energy was adjusted so as to correctly predict the experimental data (circles (⊕) denote the different blend compositions). This value is then kept fixed in comparing the theoretical and experimental data for the asymmetric blends (see Fig.4.47 below). Solid, dashed, and dotted lines refer to the models with fully flexible bonds, with semiflexible backbone, and with stiff norbornene side groups, respectively.*

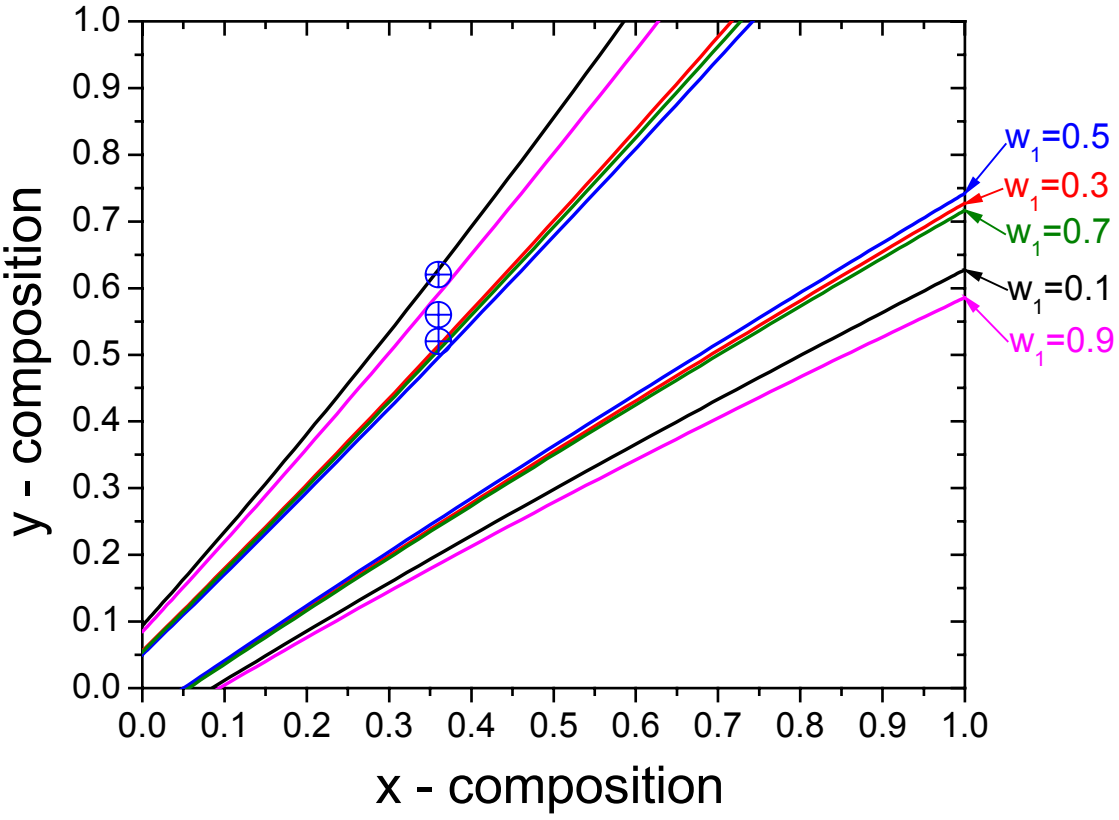

Fig. 4.47 Parameter – free test of the model with rigid NB side groups against the experimental data. Lines give the phase boundaries for the asymmetric blends (ε/kT =0.005, N_1= N_2=2500) and circles (⊕) denote the different blend compositions. There is reasonable agreement of the theoretical predictions with the experimental data (see also Tab. 4.11).

5. Conclusions

Cycloolefin copolymers of ethylene and norbornene exhibit several unique properties that make them suitable materials for a range of industrial applications. Understanding these properties is essential in the strive towards the design of new COCs, suitable for particular applications. Properties that are of fundamental importance in the design of these materials include: a control of the microstructure, knowledge of the thermorheological state (i.e. simplicity/complexity), relation between structural and dynamic heterogeneity, dynamics in the glassy state in relation to the free volume, the origin of the liquid-to-glass transition and finally criteria for miscibility when designing binary copolymer blends.

Herein, we have employed structural (NMR, X-rays), thermodynamic (pressure-volume-temperature, differential scanning calorimetry) and dynamic (rheology) probes to explore the issues above. The main results of the present work can be summarized as follows:

- Thermorheological simplicity/complexity of the copolymers.
  For this purpose a total of 17 copolymers were employed with compositions in the range from 36 to 68 mol % (5 copolymers were commercially available and 12 were made for the purpose of this study) and investigated the thermal and rheological properties of both the segmental and chain (terminal) processes. The thermorheological simplicity was tested by making use of the time-Temperature superposition (tTs) principle. To quantify the efficacy of tTs the temperature dependence of the minimum of loss tangent ($d\tan\delta_{min}/dT$) was employed. A weak T-dependence was found in all copolymers investigated suggesting that tTs is valid and that the systems are thermorheologically simple. Furthermore, both segmental and therminal dynamics in the copolymers could be well described by the Vogel-Fulcher-Tammann or the Williams-Landel-Ferry equations.

- The critical molecular weight for entanglements (M_c).
  The molecular weight dependence of the chain relaxation times (τ_c) was used in obtaining the critical molecular weight for entanglements. Two regimes were identified from a total of 17 copolymers with respective molecular weight dependencies as $\tau_c \sim M^{1.9}$ and $\tau_c \sim M^{3.9}$ for unentangled and entangled chains, respectively. From the crossover regime the critical molecular weight was estimated as $M_c \sim 31000$ g/mol.

- The origin of the liquid-to-glass transition in the copolymers.
  In order to explore the origin of the dynamic arrest at T_g we employed thermodynamic measurements (i.e., Pressure-Volume-Temperature) providing the equation of state in an effort in obtaining the ratio of the activation energy E_V^* to the enthalpy of activation H^*, E_V^*/H^*. This ratio is used to quantify the relative contribution of density and temperature on the segmental dynamics. From the value of this dynamic quantity we found that free-volume becomes increasingly important with increasing NB content. In contrast to this, in copolymers with low NB content

the segmental dynamics are largely determined by the thermal energy required to explore the energy landscape.

- Relation between structural and dynamic heterogeneity.
  The structural probes (NMR, X-rays) provided able evidence for increasing structural heterogeneity with increasing NB content. For example, the NMR investigation revealed that in copolymers with NB content above 50 mol % the structure consists of blocks of norbornene of varying lengths, linked in both stereogenic positions, together with some alternating norbornene/ethylene units. In contrast, in copolymers with low norbornene content (below 50 mol %) the structure consists mainly of alternating norbornene/ethylene sequences and of some ethylene sequences comprising two or more units. This microstructural heterogeneity was also revealed by the wide-angle X-ray diffraction patterns. We have investigated a possible connection between the structural and dynamic heterogeneity the latter based on the values of the activation ratio E_V^*/H^*, the pressure coefficient of T_g and the values of the dynamic fragility *m*. We found that the initial slope, $(dT_g/dP)_{P\to 0}$, exhibits a pronounced composition dependence with higher values for the copolymers with the higher NB content. Furthermore, the dynamic fragility *m*, being another sensitive quantity to the microstructural heterogeneity, increased with increasing NB content. These results suggested a coupling between the structural and dynamic heterogeneity in the copolymers.

- Relation of glassy dynamics to free volume.
  The positron annihilation lifetime spectroscopy allowed determining the *o*-Ps lifetime, τ_3, and thus the free volume in the bulk copolymer. It was found that the mean hole volume increases with increasing norbornene content, reaching the highest value for the pure polynorbornene. The *o*-Ps relative intensity I_3 (being proportional to the free volume hole density) exhibits a non-monotonous trend over the investigated composition range. This means that a lower number of free volume holes but of a larger size are present in polynorbornene. Free volume holes are probably located in the vicinity of ethylene units linking larger norbornene units. In addition, the existence of subglass relaxation processes in rheology was found to affect the PALS signal.

- Mutual miscibility of COC blends.
  Three different ethylene/norbornene copolymer blends were investigated by rheology and differential scanning calorimetry: 8007/6013 (36/52 mol % NB), 8007/6015 (36/56 mol % NB) and 8007/6017 (36/62 mol % NB) in five different compositions. The aim of the thermal investigation was to provide the T_g as well as the width, ΔT_g, as a function of blend composition; these results were compared with the pure components of the blends. The thermal analysis revealed a single – albeit broad – glass temperature for all the different (symmetric and asymmetric) compositions in the 36/52 mol % COC blends. On the other hand, the blends with the larger difference in norbornene content exhibited dual transition temperatures in the blends with 36/56 and 36/62 mol % of norbornene, respectively. Rheology, providing a very stringent test of miscibility, was employed in order to test the range of validity of the time-temperature superposition principle, i.e., thermorheological

simplicity. It was found that the vast majority of the various binary blends ($N_x E_{1-x}/N_y E_{1-y}$) violates the tTs, i.e. they are thermorheologically complex, and hence immiscible. The experimental data from rheology were compared to the lattice cluster theory (LCT), which demonstrated a dependence on the x and y compositions on top to the $|x-y|$ dependence. Prior to this comparison, we tested the effect of the various parameters involved in the theoretical model, such as the degree of polymerization (N), dimensionless bending ($b = E_b/kT$) and exchange ($a = \varepsilon/kT$) energies. We found a large influence of the degree of polymerization on the phase boundaries; an increase of N reduced the miscibility window. The b term, associated with the chain backbone stiffness, i.e., with the bending energy of norbornene backbone bonds connecting adjacent NB units, was insensitive to the phase boundaries, especially for low blend compositions. The exchange energy, a, reflecting the attractive van der Waals energies between united atom groups (representing the norbornene molecule) of the respective monomer pairs, had a large influence on the boundaries of the miscibility window. Moreover, the analysis of the interaction parameter showed that the norbornene/ethylene ($N_x E_{1-x}/N_y E_{1-y}$) binary blends were more miscible for $y \geq x$ and became immiscible for $y < x$. Eventually, a test of the theoretical model against the experimental data obtained from rheology was performed. We first adjusted the values of the above parameters in order to generate complete agreement with the experimental phase boundaries for the symmetric blends. We employed E_b/kT =0.7 and N_1= N_2=2500. The maximal value of ε/kT for the model with the rigid NB side groups, being still in agreement with the experimental data, was found to be 0.005. We applied the above values of the parameters from the symmetric blends and critically tested the predictive power of the model for the asymmetric blend compositions. The comparison of the rheological data with the model resulted in nine successful predictions and three failures. From these results it can be concluded that the theoretical model works at best for the "middle" (70/30-30/70) compositions, and (partially) fails for the extreme ones. Such success of the LTC theory with the experiment is appreciated, taking into account the number of approximations involved such as blend incompressibility, the oversimplified structure of the norbornene monomer, as well as experimental uncertainties originating from the polydispersity, and the value of the criterion set for tTs violation and thus of miscibility.

Overall our experimental results together with the theoretical predictions can be employed as recipes in designing new COC copolymers with desired compositions and hence controlled material properties

Appendix

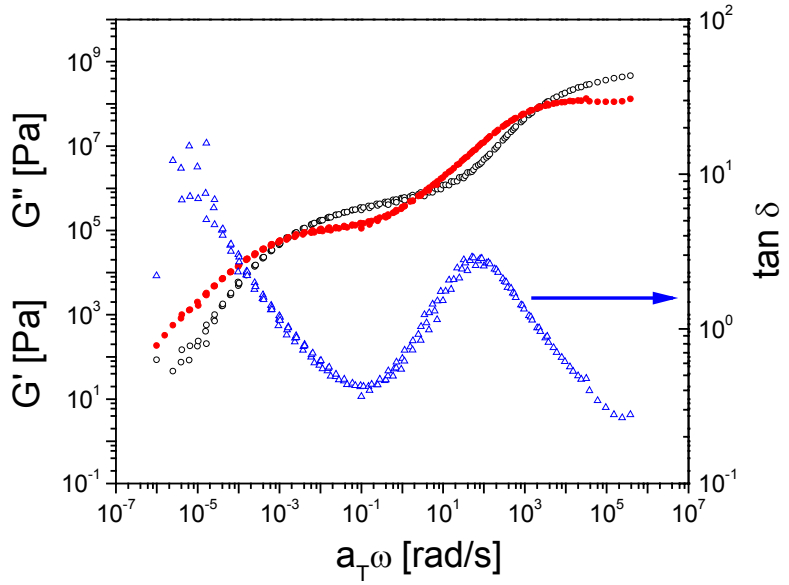

Fig. A.1 Master curve for the storage modulus (G', open circles), the loss modulus (G", filled circles) and the loss tangent (tanδ, triangles) for the 10/90 composition of the 8007/6013 blend using data in the T-range 135 <T< 240°C. The reference temperature was at 155°C.

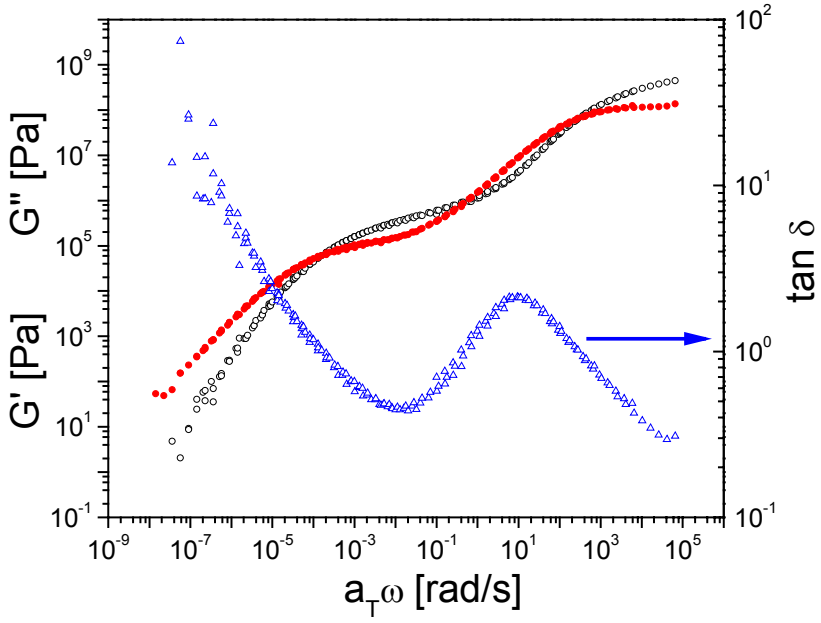

Fig. A.2 The same as in Fig. A.1 for the 30/70 composition of the 8007/6013 blend using data in the T-range 120 <T< 270°C. The reference temperature was at 135°C.

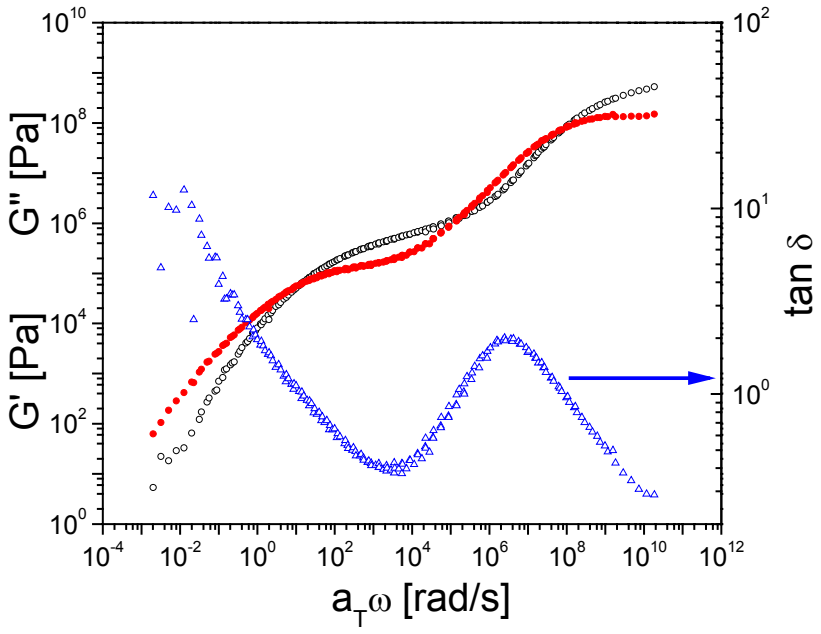

Fig. A.3 The same as in Fig. A.1 for the 70/30 composition of the 8007/6013 blend using data in the T-range 95 <T< 250°C. The reference temperature was at 180°C.

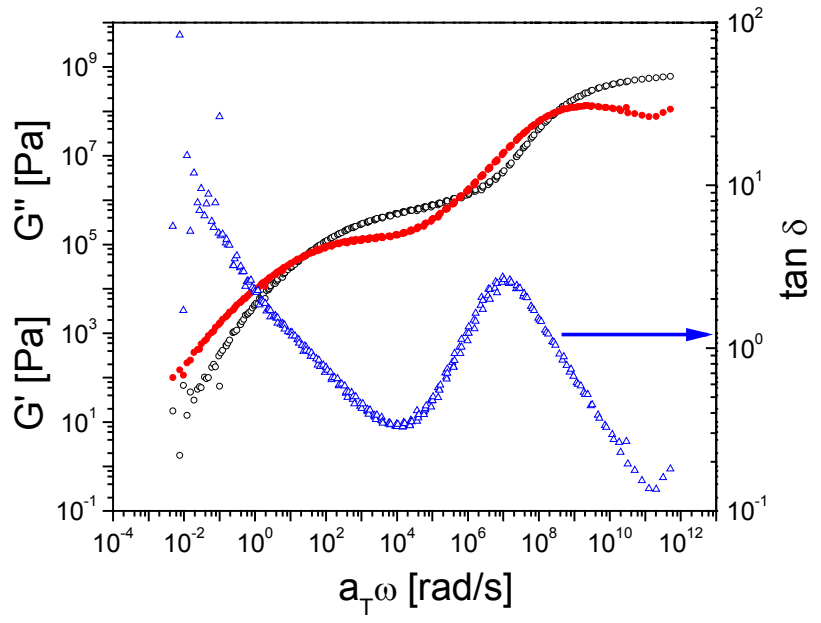

Fig. A.4 The same as in Fig. A.1 for the 90/10 composition of the 8007/6013 blend using data in the T-range 80 <T< 240°C. The reference temperature was at 180°C.

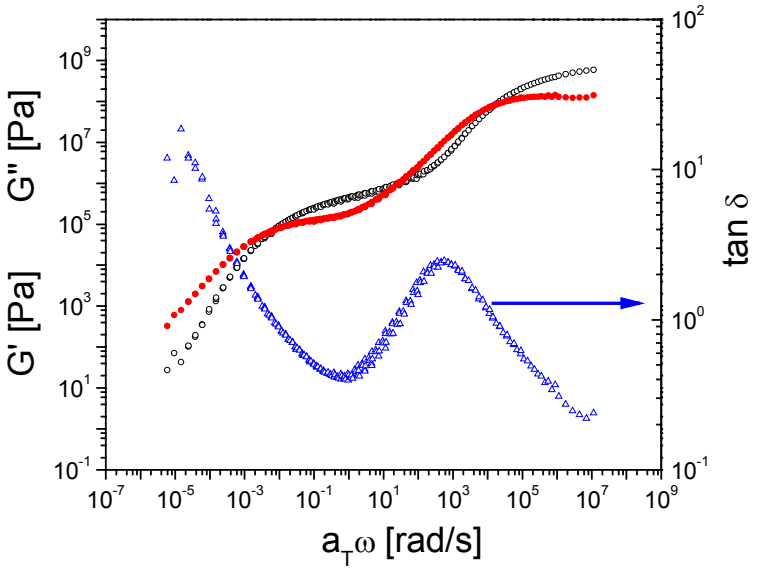

Fig. A.5 The same as in Fig. A.1 for the 10/90 composition of the 8007/6015 blend using data in the T-range 150 <T< 260°C. The reference temperature was at 180°C.

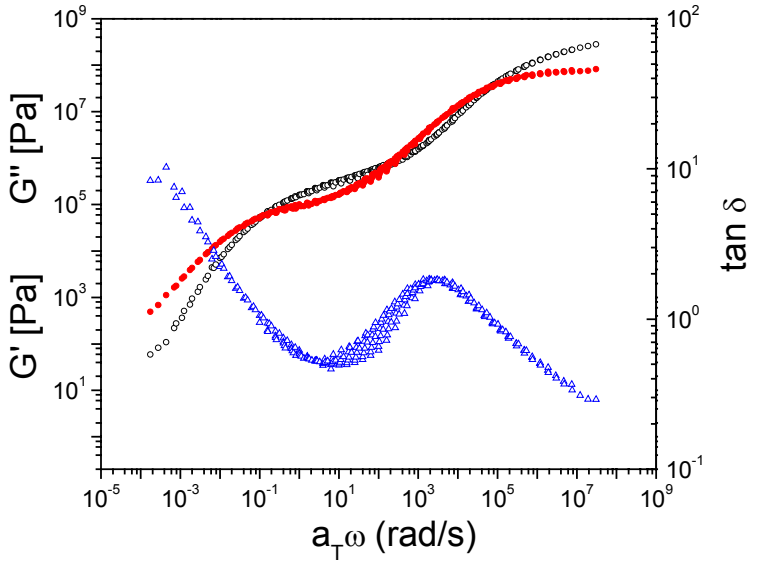

Fig. A.6 The same as in Fig. A.1 for the 30/70 composition of the 8007/6015 blend using data in the T-range 139 <T< 240°C. The reference temperature was at 180°C.

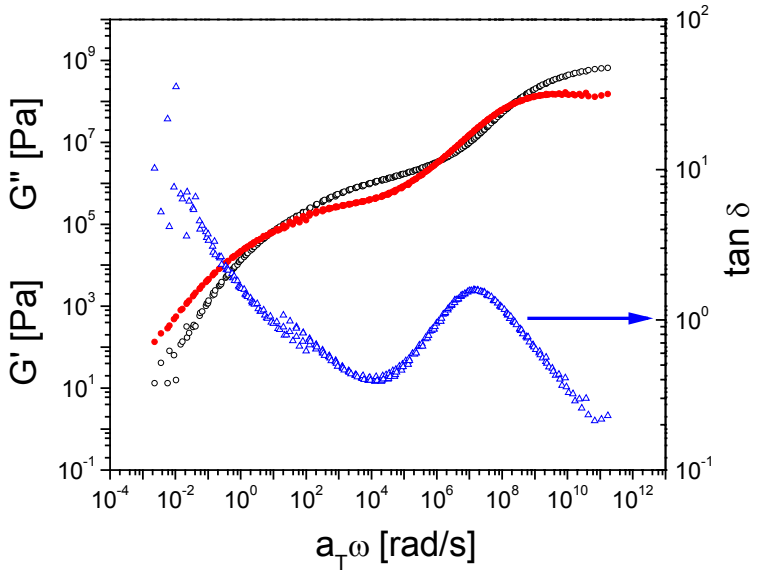

Fig. A.7 The same as in Fig. A.1 for the 70/30 composition of the 8007/6015 blend using data in the T-range 90 <T< 240°C. The reference temperature was at 180°C.

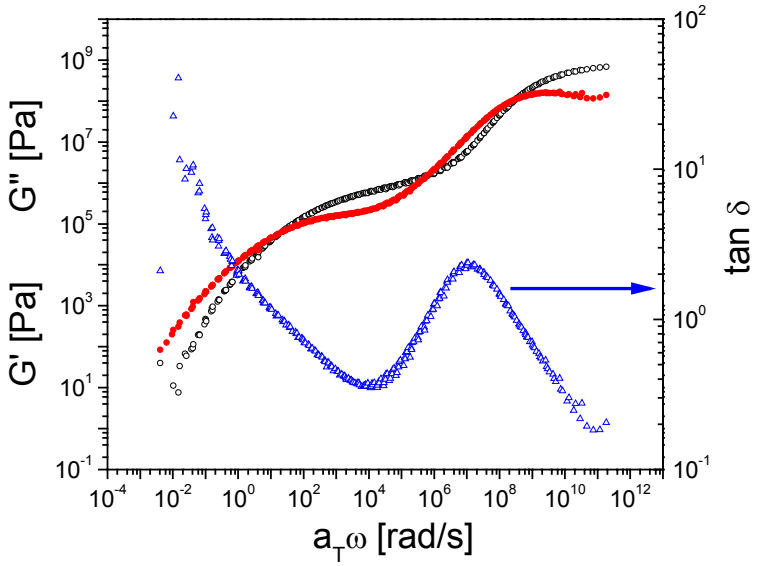

Fig. A.8 The same as in Fig. A.1 for the 90/10 composition of the 8007/6015 blend using data in the T-range 82 <T< 240°C. The reference temperature was at 180°C.

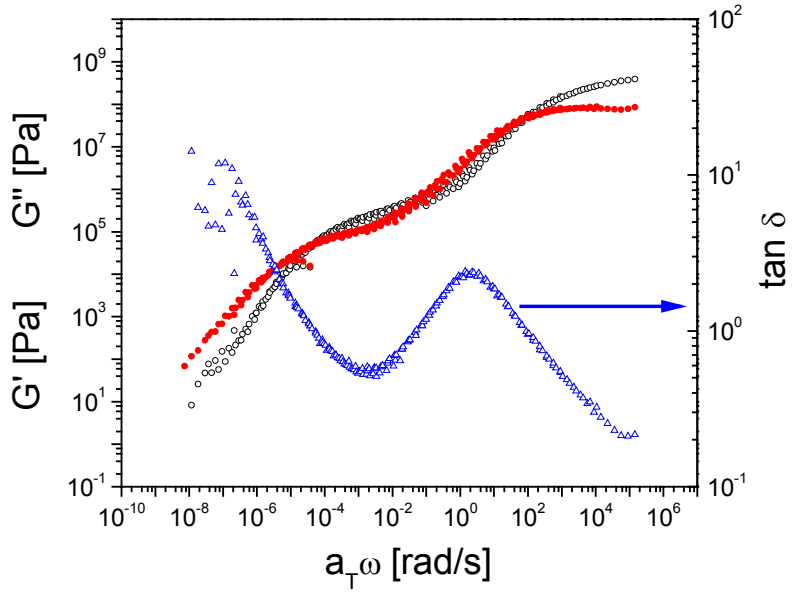

Fig. A.9 The same as in Fig. A.1 for the 10/90 composition of the 8007/6017 blend using data in the T-range 165<T< 290°C. The reference temperature was at 180°C.

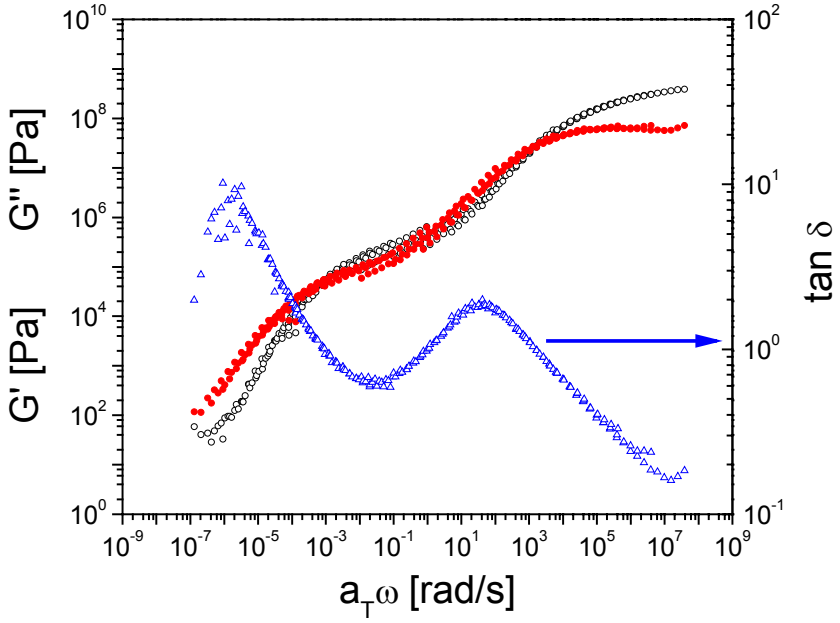

Fig. A.10 The same as in Fig. A.1 for the 30/70 composition of the 8007/6017 blend using data in the T-range 150<T< 250°C. The reference temperature was at 180°C.

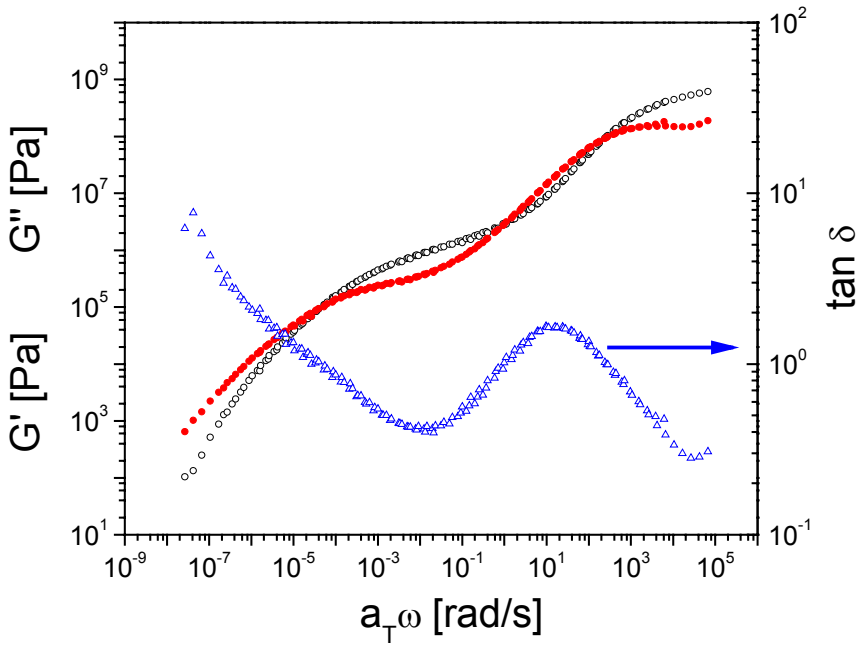

Fig. A.11 The same as in Fig. A.1 for the 70/30 composition of the 8007/6017 blend using data in the T-range 90<T< 210°C. The reference temperature was at 105°C.

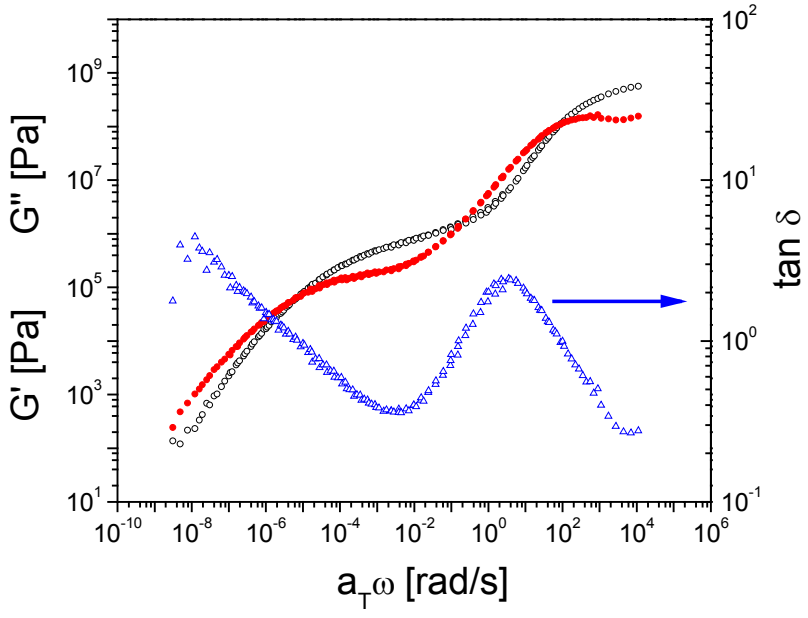

Fig. A.12 The same as in Fig. A.1 for the 90/10 composition of the 8007/6017 blend using data in the T-range 85<T< 220°C. The reference temperature was at 95°C.

References

1. Sullivan, V., Metallocene-Catalysed Cyclo-Olefin Copolymers. *Medical Device Technology,* October, **1998**.

2. Kaminsky, W.; Sinn, H., *Transition Metals and Organometallics as Catalysts for Olefin Polymerization*. Springer-Verlag, Berlin, **1988**.

3. Kaminsky, W.; Arndt, M., *Metalollocene based polyolefins. Preparation properties and technology*. J. Wiley, New York, **2000**.

4. Ruchatz, D.; Fink, G., Ethene-norbornene copolymerization using homogenous metallocene and half-sandwich catalysts: Kinetics and relationships between catalyst structure and polymer structure. 1. Kinetics of the ethene-norbornene copolymerization using the [(isopropylidene)(eta(5)-inden-l-ylidene-eta(5)-cyclopentadienyl)]zirconium dichloride methylaluminoxane catalyst. *Macromolecules* **1998,** 31, (15), 4669-4673.

5. Kaminsky, W., *Metalorganic Catalysts for Synthesis and Polymerization*. Springer, **1999**.

6. Tritto, I.; Boggioni, L.; Sacchi, M. C.; Locatelli, P.; Ferro, D. R.; Provasoli, A., Ethylene-norbornene copolymers prepared with metallocene-based catalysts: new sequence assignments by C-13 NMR. *Macromolecular Rapid Communications* **1999,** 20, (5), 279-283.

7. Sessler, G. M.; Yang, G. M.; Hatke, W. In *Electret Properties of Cycloolefin Copolymers*, Electrical Insulation and dielectric phenomena, Minneapolis, **1997**.

8. Rische, T.; Waddon, A. J.; Dickinson, L. C.; MacKnight, W. J., Microstructure and morphology of cycloolefin copolymers. *Macromolecules* **1998,** 31, (6), 1871-1874.

9. U.S. Patent 5, 087, 677. **1992**.

10. Scrivani, T.; Benavente, R.; Perez, E.; Perena, J. M., Stress-strain behaviour, microhardness, and dynamic mechanical properties of a series of ethylene-norbornene copolymers. *Macromolecular Chemistry and Physics* **2001,** 202, (12), 2547-2553.

11. Forsyth, J. F.; Scrivani, T.; Benavente, R.; Marestin, C.; Perena, J. M., Thermal and dynamic mechanical behavior of ethylene/norbornene copolymers with medium norbornene contents. *Journal of Applied Polymer Science* **2001,** 82, (9), 2159-2165.

12. Forsyth, J.; Perena, J. M.; Benavente, R.; Perez, E.; Tritto, I.; Boggioni, L.; Brintzinger, H. H., Influence of the polymer microstructure on the thermal properties of cycloolefin copolymers with high norbornene contents. *Macromolecular Chemistry and Physics* **2001,** 202, (5), 614-620.

13. Ekizoglou, N.; Thorshaug, K.; Cerrada, M. L.; Benavente, R.; Perez, E.; Perena, J. M., Influence of the molecular weight on the thermal and mechanical properties of

ethylene/norbornene copolymers. *Journal of Applied Polymer Science* **2003,** 89, (12), 3358-3363.

14. Harrington, B. A.; Crowther, D. J., Stereoregular, alternating ethylene-norbornene copolymers from monocyclopentadienyl catalysts activated with non-coordinating discrete anions. *Journal of Molecular Catalysis a-Chemical* **1998,** 128, (1-3), 79-84.

15. Huang, W. J.; Chang, F. C.; Chu, P. P. J., Solid-state NMR study of cyclo-olefin copolymer (COC). *Journal of Polymer Science Part B-Polymer Physics* **2000,** 38, (19), 2554-2563.

16. Arndt-Rosenau, M.; Beulich, I., Microstructure of ethene/norbornene copolymers. *Macromolecules* **1999,** 32, (22), 7335-7343.

17. Tritto, I.; Marestin, C.; Boggioni, L.; Zetta, L.; Provasoli, A.; Ferro, D. R., Ethylene-norbornene copolymer microstructure. assessment and advances based on assignments of C-13 NMR spectra. *Macromolecules* **2000,** 33, (24), 8931-8944.

18. Bergstrom, C. H.; Sperlich, B. R.; Ruotoistenmaki, J.; Seppala, J. V., Investigation of the Microstructure of Metallocene-Catalyzed Norbornene-Ethylene Copolymers Using Nmr Spectroscopy. *Journal of Polymer Science Part A-Polymer Chemistry* **1998,** 36, (10), 1633-1638.

19. Ruchatz, D.; Fink, G., Ethene-norbornene copolymerization with homogeneous metallocene and half-sandwich catalysts: Kinetics and relationships between catalyst structure and polymer structure. 3. Copolymerization parameters and copolymerization diagrams. *Macromolecules* **1998,** 31, (15), 4681-4683.

20. Wang, Q.; Weng, J. H.; Fan, Z. Q.; Feng, L. X., Influence of Mixed Aluminoxane Systems on Ethylene-Norbornene Copolymerization Catalyzed by Metallocene. *Macromolecular Rapid Communications* **1997,** 18, (12), 1101-1107.

21. Bergstrom, C. H.; Vaananen, T. L. J.; Seppala, J. V., Influence of Polymerization Conditions on Microstructure of Norbornene-Ethylene Copolymers Made Using Metallocene Catalysts and Mao. *Journal of Applied Polymer Science* **1997,** 63, (8), 1071-1076.

22. Haselwander, T. F. A.; Heitz, W.; Krugel, S. A.; Wendorff, J. H., Polynorbornene: Synthesis, properties and simulations. *Macromolecular Chemistry and Physics* **1996,** 197, (10), 3435-3453.

23. Cerrada, M. L.; Perena, J. M.; Benavente, R.; Perez, E., Viscoelastic processes in vinyl alcohol-ethylene copolymers. Influence of composition and thermal treatment. *Polymer* **2000,** 41, (17), 6655-6661.

24. Poulsen, L.; Zebger, I.; Klinger, M.; Eldrup, M.; Sommer-Larsen, P.; Ogilby, P. R., Oxygen diffusion in copolymers of ethylene and norbornene. *Macromolecules* **2003,** 36, (19), 7189-7198.

25. Djourelov, N.; Misheva, M.; Zamfirova, G.; Benavente, R.; Perez, E.; Perena, J. M., Positron annihilation in norbornene-ethylene copolymers. *Macromolecular Chemistry and Physics* **2003,** 204, (12), 1531-1538.

26. Zamfirova, G.; Misheva, M.; Perez, E.; Benavente, R.; Cerrada, M. L.; Djourelov, N.; Kresteva, M.; Perena, J. M., Norbornene-ethylene copolymers studied by non-destructive methods. *Polymer Journal* **2002,** 34, (11), 779-785.

27. Delfolie, C.; Dickinson, L. C.; Freed, K. F.; Dudowicz, J.; MacKnight, W. J., Molecular factors affecting the miscibility behavior of cycloolefin copolymers. *Macromolecules* **1999,** 32, (23), 7781-7789.

28. Pakula, T., Dielectric and Mechanical Spectroscopy - a Comparison. In *Broadband dielectric spectroscopy*, Ed(s). Kremer, F.; Schonhals, A., Springer-Verlag, Berlin and Heidelberg, **2003**.

29. Riande, E., *Polymer viscoelasticity: stress and strain in practice*. Marcel Dekker, **2000**.

30. Berry, G. C.; Fox , T. G., *Advances in Polymer Science* **1968,** 5, 261.

31. Ferry, J. D., *Viscoelastic Properties of Polymers*. Wiley, New York, **1980**.

32. Graessley, W. W., Some Phenomenological Consequences of the Doi-Edwards Theory of Viscoelasticity. *Journal of Polymer Science Part B-Polymer Physics* **1980,** 18, (1), 27-34.

33. Ward, I. M.; Sweeney, J., *An introduction to the mechanical properties of solid polymers*. Wiley, **2004**.

34. Hadjichristidis, N.; Pispas, S.; Floudas, G., *Block Copolymers: Synthetic Strategies, Physical Properties, and Applications*. J. Wiley & Sons, New York, **2003**.

35. Williams, M. L.; Landel, R. F.; Ferry, J. D., Mechanical Properties of Substances of High Molecular Weight .19. The Temperature Dependence of Relaxation Mechanisms in Amorphous Polymers and Other Glass-Forming Liquids. *Journal of the American Chemical Society* **1955,** 77, (14), 3701-3707.

36. Angell, C. A., Formation of Glasses from Liquids and Biopolymers. *Science* **1995,** 267, (5206), 1924-1935.

37. Stillinger, F. H., A Topographic View of Supercooled Liquids and Glass-Formation. *Science* **1995,** 267, (5206), 1935-1939.

38. Sokolov, A. P., Why the glass transition is still interesting. *Science* **1996,** 273, (5282), 1675-1676.

39. Grest, G. S., *Advances in Chemical Physics* **1981,** 48, (455).

40. Bendler, J. T.; Fontanella, J. J.; Shlesinger, M. F., A new Vogel-like law: Ionic conductivity, dielectric relaxation, and viscosity near the glass transition. *Physical Review Letters* **2001,** 8719, (19).

41. Pakula, T., Collective dynamics in simple supercooled and polymer liquids. *Journal of Molecular Liquids* **2000,** 86, (1-3), 109-121.

42. Doolittle, A. K., Studies in Newtonian Flow .2. The Dependence of the Viscosity of Liquids on Free-Space. *Journal of Applied Physics* **1951,** 22, (12), 1471-1475.

43. Fulcher, G. S., Analysis of recent measurements of the viscosity of glasses. *Journal of the American Ceramic Society* **1925,** 8, (6), 339-355.

44. Fulcher, G. S., Analysis of recent measurements of the viscosity of glasses. II. *Journal of the American Ceramic Society* **1925,** 8, (12), 789-794.

45. Tammann, G.; Hesse, W., The dependancy of viscosity on temperature in hypothermic liquids. *Zeitschrift Fur Anorganische Und Allgemeine Chemie* **1926,** 156, (4).

46. Naoki, M.; Endou, H.; Matsumoto, K., Pressure Effects on Dielectric-Relaxation of Supercooled Ortho-Terphenyl. *Journal of Physical Chemistry* **1987,** 91, (15), 4169-4174.

47. Dreyfus, C.; Aouadi, A.; Gapinski, J.; Matos-Lopes, M.; Steffen, W.; Patkowski, A.; Pick, R. M., Temperature and pressure study of Brillouin transverse modes in the organic glass-forming liquid orthoterphenyl. *Physical Review E* **2003,** 68, (1).

48. Papadopoulos, P.; Peristeraki, D.; Floudas, G.; Koutalas, G.; Hadjichristidis, N., Origin of glass transition of poly(2-vinylpyridine). A temperature- and pressure-dependent dielectric spectroscopy study. *Macromolecules* **2004,** 37, (21), 8116-8122.

49. Williams, G., Dipole Relaxation in Polyethyl Methacrylate and Polyethyl Acrylate as a Function of Frequency Temperature and Pressure - Alpha Beta and Alphabeta Relaxations. *Transactions of the Faraday Society* **1966,** 62, (524P), 2091.

50. Ferrer, M. L.; Lawrence, C.; Demirjian, B. G.; Kivelson, D.; Alba-Simionesco, C.; Tarjus, G., Supercooled liquids and the glass transition: Temperature as the control variable. *Journal of Chemical Physics* **1998,** 109, (18), 8010-8015.

51. Floudas G., Chapter 8. In *Broadband Dielectric Spectroscopy*, Ed(s). Kremer F., S. A., Springer, Berlin, **2002**.

52. Tolle, A.; Schober, H.; Wuttke, J.; Randl, O. G.; Fujara, F., Fast relaxation in a fragile liquid under pressure. *Physical Review Letters* **1998,** 80, (11), 2374-2377.

53. Mpoukouvalas, K.; Floudas, G.; Verdonck, B.; Du Prez, F. E., Pressure-enhanced dynamic heterogeneity in block copolymers of poly(methyl vinyl ether) and poly(isobutyl vinyl ether). *Physical Review E* **2005,** 72, (1), 011802.

54. Roland, C. M.; Paluch, M.; Pakula, T.; Casalini, R., Volume and temperature as control parameters for the dielectric a relaxation of polymers and molecular glass formers. *Philosophical Magazine* **2004,** 84, (13-16), 1573-1581.

55. Floudas, G.; Mpoukouvalas, K.; Papadopoulos, P., The role of temperature and density on the glass-transition dynamics of glass formers. *Journal of Chemical Physics* **2006,** 124, (7), 074905.

56. Casalini, R.; Roland, C. M., Thermodynamical scaling of the glass transition dynamics. *Physical Review E* **2004,** 69, (6).

57. Alba-Simionesco, C.; Cailliaux, A.; Alegria, A.; Tarjus, G., Scaling out the density dependence of the a relaxation in glass-forming polymers. *Europhysics Letters* **2004,** 68, (1), 58-64.

58. Tarjus, G.; Kivelson, D.; Mossa, S.; Alba-Simionesco, C., Disentangling density and temperature effects in the viscous slowing down of glassforming liquids. *Journal of Chemical Physics* **2004,** 120, (13), 6135-6141.

59. Roland, C. M.; Casalini, R., Comment on: "Disentangling density and temperature effects in the viscous slowing down of glass forming liquids" [J. Chem. Phys. 120, 6135 (2004)]. *Journal of Chemical Physics* **2004,** 121, (22), 11503-11504.

60. Tarjus, G.; Mossa, S.; Alba-Simionesco, C., Response to: "Comment on 'Disentangling density and temperature effects in the viscous slowing down of glassforming liquids' " [J. Chem. Phys. 121, 11503 (2004)]. *Journal of Chemical Physics* **2004,** 121, (22), 11505-11506.

61. Kroschowitz, J. I., *Encyclopedia of Polymer Science and Engeeniring*. Wiley, **1986**.

62. Quach, A.; Simha, R., Pressure Volume Temperature Properties and Transition of Amorphous Polymers Polystyrene and Poly (Orthomethylstyrene). *Journal of Applied Physics* **1971,** 42, (12), 4592-&.

63. Van Krevelen, D. W., *Properties of Polymers*. Elsevier Science, Amsterdam, **1997**.

64. Andersson, S. P.; Andersson, O., Relaxation studies of poly(propylene glycol) under high pressure. *Macromolecules* **1998,** 31, (9), 2999-3006.

65. Floudas, G., Effects of pressure on systems with intrinsic orientational order. *Progress in Polymer Science* **2004,** 29, (11), 1143-1171.

66. Bartos, J., Positron Annihilation Spectroscopy of Polymers and Rubbers. In *Encyclopedia of Analitical Chemistry*, Ed(s). Meyers, R. A., Wiley, Chichester, **2000**.

67. Hill, A. J., Positron Annihilation Lifetime Spectroscopy. In *Polymer Characterization Techniques and Their Application to Blends*, Ed(s). Simon, G. P., Oxford University Press, Washington, D.C., **2003**.

68. Brandt, W.; Berko, S.; Walker, W. W., Positronium Decay in Molecular Substances. *Physical Review* **1960,** 120, (4), 1289-1295.

69. Tao, S. J., Positronium Annihilation in Molecular Substances. *Journal of Chemical Physics* **1972,** 56, (11), 5499.

70. Eldrup, M.; Lightbody, D.; Sherwood, J. N., The Temperature-Dependence of Positron Lifetimes in Solid Pivalic Acid. *Chemical Physics* **1981,** 63, (1-2), 51-58.

71. Nakanishi, H.; Wang, S. J.; Jean, Y. C., *Positron Annihilation Studies of Fluids*. World Scientific, Singapore, **1988**.

72. Kobayashi, Y.; Zheng, W.; Meyer, E. F.; Mcgervey, J. D.; Jamieson, A. M.; Simha, R., Free-Volume and Physical Aging of Polyvinyl Acetate) Studied by Positron-Annihilation. *Macromolecules* **1989,** 22, (5), 2302-2306.

73. Kirkegaard, P.; Eldrup, M.; Mogensen, O. E.; Pedersen, N. J., *Comput. Phys. Comm.* **1989,** 23, (307).

74. Richards, R. W., *Scattering Methods in Polymer Science*. Ellis Horwood, **1995**.

75. Floudas, G.; Stepanek, P., Structure and dynamics of poly(n-decyl methacrylate) below and above the glass transition. *Macromolecules* **1998,** 31, (20), 6951-6957.

76. U.S. Patent 5, 698, 645. **1997**.

77. Blochowiak, M.; Pakula, T.; Butt, H. J.; Bruch, M.; Floudas, G., Thermodynamics and rheology of cycloolefin copolymers. *Journal of Chemical Physics* **2006,** 124, (13), 134903.

78. Zoller, P.; Walsh, D., *Standard pressure-volume-temperature data for polymers*. Technomic Publishing, **1995**.

79. Bartos, J., *Encyclopedia of Analytical Chemistry*. Wiley&Sons, Chichester, **2000**.

80. Schneider, H. A., Polymer class specificity of the glass temperature. *Polymer* **2005,** 46, (7), 2230-2237.

81. Dimarzio, E. A., The Glass Temperature of Polymer Blends. *Polymer* **1990,** 31, (12), 2294-2298.

82. Bharadwaj, R. K.; Boyd, R. H., Conformational dynamics in polyethylene under isochoric conditions: A molecular dynamics simulation study. *Journal of Chemical Physics* **2001,** 114, (11), 5061-5068.

83. Plazek, D. J.; Schlosser, E.; Schonhals, A.; Ngai, K. L., Breakdown of the Rouse Model for Polymers near the Glass-Transition Temperature. *Journal of Chemical Physics* **1993,** 98, (8), 6488-6491.

84. Schonhals, A., Relation between Main and Normal Mode Relaxations for Polyisoprene Studied by Dielectric-Spectroscopy. *Macromolecules* **1993,** 26, (6), 1309-1312.

85. Nicolai, T.; Floudas, G., Dynamics of linear and star poly(oxypropylene) studied by dielectric spectroscopy and rheology. *Macromolecules* **1998,** 31, (8), 2578-2585.

86. Floudas, G.; Reisinger, T., Pressure dependence of the local and global dynamics of polyisoprene. *Journal of Chemical Physics* **1999,** 111, (11), 5201-5204.

87. Bohmer, R.; Angell, C. A., Correlations of the Nonexponentiality and State Dependence of Mechanical Relaxations with Bond Connectivity in Ge-as-Se Supercooled Liquids. *Physical Review B* **1992,** 45, (17), 10091-10094.

88. Plazek, D. J.; Ngai, K. L., Correlation of Polymer Segmental Chain Dynamics with Temperature-Dependent Time-Scale Shifts. *Macromolecules* **1991,** 24, (5), 1222-1224.

89. Wang, L. M.; Angell, C. A., Response to "Comment on 'Direct determination of the fragility indices of glassforming liquids by differential scanning calorimetry: Kinetic versus thermodynamic fragilities'" - [J. Chem. Phys. 118, 10351 (2003)]. *Journal of Chemical Physics* **2003,** 118, (22), 10353-10355.

90. Roland, C. M.; Santangelo, P. G.; Ngai, K. L., The application of the energy landscape model to polymers. *Journal of Chemical Physics* **1999,** 111, (12), 5593-5598.

91. Pathak, J. A.; Colby, R. H.; Kamath, S. Y.; Kumar, S. K.; Stadler, R., Rheology of miscible blends: SAN and PMMA. *Macromolecules* **1998,** 31, (25), 8988-8997.

92. Pathak, J. A.; Colby, R. H.; Kumar, S. K.; Krishnamoorti, R.; Floudas, G., Floudas, Miscible Polyolefin Blend Dynamics: Head-to-Head Polypropylene/Poly(ethylene-propylene) and Head-to-Head Polypropylene/Polyisobutylene Blends. *in preparation*.

93. Paul, D. R.; Barlow, J. W., A Binary Interaction-Model for Miscibility of Copolymers in Blends. *Polymer* **1984,** 25, (4), 487-494.

94. Tenbrinke, G.; Karasz, F. E.; Macknight, W. J., Phase-Behavior in Co-Polymer Blends - Poly(2,6-Dimethyl-1,4-Phenylene Oxide) and Halogen-Substituted Styrene Co-Polymers. *Macromolecules* **1983,** 16, (12), 1827-1832.

95. Scott, R. L., Thermodynamics of High Polymer Solutions .6. The Compatibility of Copolymers. *Journal of Polymer Science* **1952,** 9, (5), 423-432.

96. Freed, K. F.; Dudowicz, J., A Lattice-Model Molecular Theory for the Properties of Polymer Blends. *Trends in Polymer Science* **1995,** 3, (8), 248-255.

97. Dudowicz, J.; Freed, K. F., Effect of Monomer Structure and Compressibility on the Properties of Multicomponent Polymer Blends and Solutions .1. Lattice Cluster Theory of Compressible Systems. *Macromolecules* **1991,** 24, (18), 5076-5095.

98. Nemirovsky, A. M.; Bawendi, M. G.; Freed, K. F., Lattice Models of Polymer-Solutions - Monomers Occupying Several Lattice Sites. *Journal of Chemical Physics* **1987,** 87, (12), 7272-7284.

99. Dudowicz, J.; Freed, K. F., Molecular influences on miscibility patterns in random copolymer/homopolymer binary blends. *Macromolecules* **1998,** 31, (15), 5094-5104.

100. Foreman, K. W.; Freed, K. F., Influence of stiffness, monomer structure, and energetic asymmetries on polymer blend miscibilities: Applications to polyolefins. *Macromolecules* **1997,** 30, (23), 7279-7295.

Abstract

Commercial as well as tailored-made cycloolefin copolymers of ethylene and norbornene were studied with respect to the structural, thermal, thermodynamic, and rheological properties using NMR, wide-angle X-ray scattering, positron annihilation lifetime spectroscopy (PALS), differential scanning calorimetry, pressure-volume-temperature, and dynamic mechanical techniques in view of the increasing industrial interest. The structural analysis provided evidence for increasing structural heterogeneity with increasing norbornene content. The NMR investigation revealed that in copolymers with NB content above 50 mol % the structure consists of blocks of norbornene of varying lengths, linked in both stereogenic positions, together with some alternating norbornene/ethylene units. In contrast, in copolymers with low norbornene content (below 50 mol %) the structure consists mainly of alternating norbornene/ethylene sequences and of some ethylene sequences comprising two or more units. In addition, the microstructural heterogeneity was also revealed by the wide-angle X-ray diffraction investigation; the copolymers with less than 50 mol% in norbornene displayed a single broad peak in the wide-angle region characteristic of all amorphous polymers, while the copolymers with higher norbornene content (above 50 mol%) showed increasing intensity at a position characteristic of the bulk polynorbornene. The PALS study revealed the size and density of cavities within the glassy state; it was found that the size of free volume holes increases with increasing norbornene content. On the other hand, increasing norbornene content causes worse packing and reduces the density of the cavities. All copolymers obey the principle of time-temperature superposition, i.e, they can be considered as thermorheologically simple. Despite this, the results on (i) the ratio of activation energies E_V^*/H^* used to quantify the origin of the liquid-to-glass transition, (ii) the pressure coefficient of the glass temperature $T_g(P)$ and (iii) the dynamic fragility *m,* suggest increasing dynamic heterogeneity with increasing norbornene content that is driven by the structural heterogeneity along the backbone.

In addition, the mutual miscibility of ethylene/norbornene copolymers (symmetric and asymmetric binary blends) was investigated by rheology and differential scanning calorimetry aiming at testing the range of validity of the time-temperature superposition principle, i.e. the thermorheological simplicity, and to provide the glass temperature T_g as well as the width, ΔT_g, as a function of blend composition. The thermal analysis revealed a single (albeit broad) or dual glass temperatures, depending on the difference in norbornene content of the blend components. On the other hand, rheology provides a more stringent test of miscibility. It was found that the vast majority of the various binary blends ($N_x E_{1-x}/N_y E_{1-y}$) violates the tTs, i.e. they are thermorheologically complex, and hence immiscible. The experimental data from rheology were compared to the lattice cluster theory (LCT), which demonstrated a dependence on the x and y compositions on top to the $|x-y|$ dependence. This comparison resulted in nine successful predictions and three failures. From these results it can be concluded that the theoretical model works at best for the “middle” (70/30-30/70) compositions, and (partially) fails for the extreme ones.

Streszczenie (abstract in polish)

Kopolimery cykloolefinowe etylenu (E) i norbornenu (NB) zawierają elementy wywodzące się z liniowych i cyklicznych olefin. Badania przedstawione w niniejszej pracy zostały przeprowadzone dla kopolimerów o nazwie handlowej Topas®. Materiały te wykazują użyteczną kombinację właściwości, takich jak, na przykład, bardzo wysoka przezroczystość, niska gęstość, bardzo niska absorpcja wody, nieprzepuszczalność pary wodnej i niska dwójłomność. Właściwości te, wraz z unikatową charakterystyką mechaniczną, taką jak duża sztywność, wytrzymałość i twardość, oraz znakomita odporność na rozpuszczalniki organiczne sprawia, że kopolimery cykloolefinowe znajdują zastosowanie m.in. w urządzeniach medycznych, optyce, czy farmacji. Właściwosci kopolimerów etylenu i norbornenu, w szczególności ich temperaturę przejścia szklistego, można zmieniać w szerokim zakresie. Wynika to z obecności elementu struktury pochodzącego z monomeru norbornenu, która nadaje sztywność łańcuchowi i tym samym zwiększa temperaturę przejścia szklistego.

Statystyka i stereoselektywność fragmentów pochodzących z norbornenu w łańcuchu może być kontrolowana przez użycie odpowiednich katalizatorów. Mikrostruktura kopolimerów cykloolefinowych zależy od katalizatorów metalocenowych, a dokładnie od ich symetrii i rodzaju ligandu. Metalocenowe podstawniki i ich symetria stanowią o taktyczności i rozkładzie (blokowym, statystycznym, czy przemiennym) sekwencji wywodzących się z etylenu i norbornenu. Monomery kopolimeru Topas® są kopolimeryzowane również przy użyciu katalizatorów metalocenowych, aczkolwiek dokładne dane objęte są tajemnicą.

W niniejszej pracy przeprowadzono badania kopolimerów etylenu i norbornenu w celu uzyskania informacji o ich strukturze (z zastosowaniem magnetycznego rezonansu jądrowego (NMR), szerokokątowego rozpraszania rentgenowskiego (WAXS), spektroskopii anihilacji pozytronów (PALS), skaningowej kalorymetrii różnicowej (DSC), badań termodynamicznych (PVT: Pressure-Volume-Temperature) i dynamice (z zastosowaniem dynamicznej analizy mechanicznej (DMA)).

Badania strukturalne (NMR, WAXS) dowiodły wzrostu niejednorodności strukturalnych wraz ze wzrostem udziału fragmentów wywodzących sie z norbornenu w kopolimerze. Badania NMR wykazały, że w kopolimerach o zawartości „fragmentów norboronenowych" powyżej 50 % molowych, łańcuchy składają się z bloków norbornenu o zmiennej długości, połączonych w stereogenicznych pozycjach 2 i 3, oraz częściowo z przemiennych sekwencji pochodnych norbornenu i etylenu. Natomiast w kopolimerach z niską zawartością „fragmentów norboronenowych" (poniżej 50 % molowych), struktura składa się głównie z przemiennych sekwencji wywodzących się z norbornenu i etylenu, i częściowo z sekwencji wywodzacych się z etylenu zawierających dwie lub więcej jednostek. Niejednorodność strukturalna została rownież zaobserwowana w dyfraktogramach WAXS. Ponadto zbadano potencjalną zależność między strukturalną i dynamiczną niejednorodnością. Niejednorodność dynamiczna została oceniona na podstawie stosunku energii aktywacji (E_V^*/H^*), zależności od ciśnienia temperatury przejścia szklistego $T_g(P)$ i wartości tzw. parametru kruchości dynamicznej *m*. Analizując zależności $T_g(P)$ stwierdzono, że początkowe nachylenie, $(dT_g/dP)_{P\to 0}$, wykazuje znaczną zależność od składu kopolimeru, przy czym największe wartości przyjmuje dla kopolimerów o największej zawartości norbornenu. Ponadto dynamiczna kruchość *m*, która jest rownież wielkością czułą na

niejednorodność strukturalną, wzrasta wraz ze wzrostem zawartości norbornenu. Wyniki te sugerują związek pomiędzy niejednorodnością strukturalną i dynamiczną w badanych kopolimerach.

Kopolimery etylenu i norbornenu badane były pod kątem ich termiczno-reologicznej prostoty/złożoności przy użyciu DMA. W tym celu użyto 17 kopolimerow o zawartości norbornenu od 36 do 68 % molowych (5 kopolimerów jest dostępnych komercyjnie, a 12 zostało przygotowane specjalnie dla celów niniejszych badań) i poddano badaniom ich właściwości termiczne i reologiczne w odniesieniu do procesów relaksacji segmentalnych i terminalnych (łańcuchowych). Prostota termiczno-reologiczna była określana przy użyciu zasady superpozycji czasowo-temperaturowej (*tTs*). W celu oceny ilościowej zasady *tTs* poddano analizie zależność temperaturową minimum tangensa stratności ($d\tan\delta_{min}/dT$). Analiza ta wykazała słabą zależność tej wielkości od temperatury dla wszystkich kopolimerów, potwierdzając ważność zasady superpozycji czasowo-temperaturowej, i tym samym wskazując, że badane kopolimery są materiałami termiczno-reologicznie prostymi. Zarówno dynamika segmentalna, jak i terminalna, mogły zostać dobrze opisane przez równania Vogela-Fulchera-Tammanna, czy Williamsa-Landela-Ferry'ego.

Zależność łańcuchowego czasu relaksacji (τ_c) od masy molekularnej zastosowano w celu wyznaczenia krytycznej masy molekularnej dla splątań M_c. Znaleziono dwa rodzaje zależności dla 17 kopolimerów o różnych masach molekularnych: $\tau_c \sim M^{1.9}$ i $\tau_c \sim M^{3.9}$ dla odpowiednio nie splątanych i splątanych łaćuchów. Z punktu przecięcia tych dwóch zależności wyznaczono krytyczną masę molekularną dla splątań równą $M_c \sim 31000$ g/mol.

Aby zbadać naturę przejścia ze stanu płynnego do szklistego, poddano kopolimery badaniom termodynamicznym (pomiary dylatometryczne metodą PVT), które pozwoliły na całościowy opis układu przy pomocy równania stanu. To zaś pozwoliło uzyskać stosunek energii aktywacji (E_V^*) do entalpii aktywacji (H^*), E_V^*/H^*. Wielkości tej użyto do ilościowego wyznaczenia względnego wpływu gęstości i temperatury na dynamikę segmentalną. Z wartości tej wielkości dynamicznej wynika, ze objętość swobodna odgrywa tym większą rolę, im większy jest udział norbornenu w kopolimerze. Z dugiej strony, dla kopolimerów z niską zawartością norbornenu, dynamika segmentlna jest w dużm stopniu zdominowana przez energię termiczną potrzebną do pokonania barier energetycznych.

Spektroskopia anihilacji pozytronowej (PALS) pozwoliła na określenie czasu życia (τ_3) orto pozytronium (*o*-Ps), a tym samym na wyznacznie objętości swobodnej w kopolimerach. Stwierdzono, ze średnia objętość dziur wzrasta wraz ze wzrostem norbornenu, osiągając najwyższą wartość dla czystego polinorbornenu. Natomiast względna intensywność I_3, która jest proporcjonalna do gęstości dziur objętości swobodnej, wykazuje niemonotoniczną zależność w badanym zakresie składu kopolimerów. Oznacza to, że w czystym polinorbornenie występuje mniejsza liczba dziur. Dziury zlokalizowane są prawdopodobnie w otoczeniu jednostek etylenu łączących większe jednostki norbornenu.

Druga część niniejszej pracy poświęcona jest wzajemnej mieszalności kopolimerów etylenu i norbornenu. Mieszaniny trzech różnych par kopolimerów zbadano przy użyciu technik DSC i DMA: 8007/6013 (36/52 mol % NB), 8007/6015 (36/56 mol % NB) i 8007/6017 (36/62 mol % NB). Badane mieszaniny miały pięć różnych składów. Celem badań termicznych było uzyskanie informacji zarówno o temperaturze przejścia szklistego (T_g), jak i jego szerokości (ΔT_g), jako funkcji składu mieszaniny; wyniki te porównano z danymi dla wyjściowych składników mieszanin. Analiza termiczna

wykazała pojedynczą, aczkolwiek szeroką, temperaturę przejścia dla wszystkich składów mieszaniny 8007/6013. Z drugiej strony, w mieszaninach kopolimerów o większej różnicy składu (8007/6015, 8007/6017) pojawiły się dwie temperatury przejścia. Badania reologiczne, wykazujące dużą zdolność do określania stopnia mieszalności polimerów, zostały przeprowadzone w celu zbadania obszaru ważności zasady superpozycji czasowo-temperaturowej, tzn. prostoty termiczno-reologicznej. Stwierdzono, że przeważająca większość binarnych mieszanin ($N_x E_{1-x}/N_y E_{1-y}$) nie spełnia zasady superpozycji czasowo-temperaturowej, tzn. są one termiczno-reologicznie złożone, a zatem niemieszalne. Dane eksperymentalne uzyskane z badań reologicznych porównano do teorii klasterów sieciowych LCT (ang. lattice cluster theory) która, według doniesień literaturowych, uzależnia mieszalność zarówno od składów x i y, jak i ich różnicy $|x-y|$. Przetestowano wpływ różnych parametrów obecnych w modelu teoretycznym takich, jak stopień polimeryzacji (N), czy bezwymiarowa energia zginania ($b = E_b/kT$) i bezwymiarowa energia oddziaływań ($a = \varepsilon/kT$). Stwierdzono duży wpływ stopnia polimeryzacji na granice fazy; wzrost N prowadził do redukcji obszaru mieszalności. Parametr b natomiast, związany ze sztywnością łańcucha, tzn. z energią zginania wiązań łączących przyległe do siebie jednostki norbornenu, nie miał wpływu na granice diagramu fazowego, w szczególności dla mieszanin o niskich zawartościach norbornenu w komponentach wyjściowych. Energia oddziaływania a, odzwierciedlająca energię przyciągania van der Waalsa między tzw. united atom groups (reprezentującymi molekułę norbornenu), wykazywała duży wpływ na granice okna mieszalności. Ponadto, analiza parametru Flory-Huggins'a χ pokazała, że binarne mieszaniny norbornenu i etylenu ($N_x E_{1-x}/N_y E_{1-y}$) są bardziej mieszalne dla składów $y \geq x$, a stają się niemieszalne dla składów $y < x$. Ostatecznie porównano wyniki modelu teoretycznego z danymi eksperymentalnymi uzyskanymi z badań reologicznych. Następujące wartości parametrów zostały zastosowane w modelu: $E_b/kT = 0.7$ i $N_1 = N_2 = 2500$. Maksymalna wartość ε/kT dla modelu ze sztywnymi grupami bocznymi norbornenu, zgodna z danymi eksperymentalnymi, wyniosła 0.005. Powyższe wartości parametrów zostały tak dobrane, aby odpowiadały danym eksperymentalnym dla mieszanin symetrycznych. Przy tych samych wartościach parametrów sprawdzono zgodność przewidywań modelu z wynikami badań reologicznych dla mieszanin asymetrycznych. Uzyskano dziewięć trafnych przewidywań i trzy niepowodzenia. Reasumując, z porównania teorii z eksperymentem wynika, ze model teoretyczny sprawdza się najlepiej dla „środkowych" (70/30-30/70) mieszanin, a zawodzi (częściowo) dla mieszanin skrajnych. Zważywszy na fakt, ze teoria ta posługuje się przybliżeniami takimi, jak nieściśliwość mieszanin i uproszczona struktura molekuły norbornenu, można więc mówić o sukcesie teorii LCT w odniesieniu do kopolimerów norbornenu i etylenu. Ponadto, pewna nieokreśloność wynika z polidyspersyjnosci i wartości kryterium ważności zasady *tTs*, a tym samym mieszalności.

Podsumowując, eksperymentalne wyniki badań wraz z przewidywaniami teoretycznymi, mogą posłużyć do zaprojektowania nowych kopolimerów cykloolefinowych o żądanym składzie, a zatem o pożądanych własnościach materiałowych.

List of Figures

List of Tables

Acknowledgements

I would like to thank all the people that contributed to formation of this work, especially

- Prof. Tadeusz Pakula[†], who was my first supervisor, for his leadership and the possibility of doing research in Max Planck Institute for Polymer Research. In addition, I express my thanks for his great scientific and not scientific help as well
- Prof. Georg Floudas for his leadership, a lot of help and engagement concerning my research and writing the thesis
- Prof. Hans-Jürgen Butt for discussions, help and kindness during my PhD work.
- Dr. Matthias Bruch and Dr. Udo Stehling from Topas Advanced Polymers (former Ticona) for a lot of scientific help including discussions, providing information and samples.
- Prof. Jacek Ulański for enabling me to conduct the PhD procedure at the Faculty of Chemistry of Technical University of Lodz, for his kind help during the entire PhD work and his agreement to be the referee of my thesis
- Prof. Adam Patkowski that he agreed to be the referee as well
- Andreas Best for a lot of help, especially concerning technical matters like building equipment, writing a program and solving computer problems
- Andreas Hanewald for introducing me into rheology measurements and his help in the mechanical lab
- Christine Herrmann for DSC and stretching measurements
- Dr. Hans-Jodef Beauvisage for his help with *Mathematica*
- Marek Majtyka, Leszek Jakuczek, Arek Ptak, Wojtek Pisula for interesting discussions, however, mainly not on the scientific topics ☺
- Markus Wolkenhauer for scientific and not scientific discussions, and for our common whiskey and vodka tasting
- colleagues from my office, i.e. Olga Priadilova and Rüdiger Stark for a good sense of humour and nice atmosphere

- I acknowledge the Marie Curie Fellowship Association for the financial support during the first year (contract number: HPMT-CT-2000-00015)

- I thank the Ticona company (Topas Advanced Polymers now) for the financial support as well

Thanks to Maciej Cierpka and Michał Lewandowski for introducing me into the Dupa theory (still being developed), which brought me to higher state of conscious.

Thank you Cathrine for the many dances we had together during my stay in Mainz.

I thank all my friends from Poland and Mainz for their support, talks and meetings.

Thank you Agnieszka for your support, especially in the pre-exam and the pre-defense time!☺

I am grateful to my perents for their contionus support and the delicious food ☺

[†] Deceased June 7, 2005